UNIVERSIDADE ESTADUAL PAULISTA
"JÚLIO DE MESQUITA FILHO"
CAMPUS DE GUARATINGUETÁ

André Felipe Moraes Luiz Lucchini

Probing Gravitational Fluctuations in Spherically Symmetric Black Holes and Extreme Mass Ratios Systems

Guaratinguetá/Brazil

2024

André Felipe Moraes Luiz Lucchini

Probing Gravitational Fluctuations in Spherically Symmetric Black Holes and Extreme Mass Ratios Systems

Master Thesis presented to the Graduate Program in 2024 of the Sao Paolo State University "Júlio de Mesquita Filho" as a partial requirement to obtain the degree of Master in Physics and Astronomy

Universidade Estadual Paulista "Júlio de Mesquita Filho"

Graduate Program in 2024

Supervisor: Prof. Dr. Rogério Teixeira Cavalcanti

Guaratinguetá/Brazil

2024

Lucchini, André Felipe Moraes Luiz
L934p Probing gravitational fluctuations in spherically symmetric black holes and extreme mass ratios systems / André Felipe Moraes Luiz Lucchini. - Guaratinguetá, 2024.
91 f : il.
Bibliografia: f. 80-82

Dissertação (Mestrado) – Universidade Estadual Paulista, Faculdade de Engenharia e Ciências de Guaratinguetá, 2024.
Orientador: Prof. Dr. Rogério Teixeira Cavalcanti

1. Buracos negros (Astronomia). 2. Perturbação (Astronomia). 3. Ondas gravitacionais. 4. Massa (Física). I. Título.

CDU 531.5:043

Pâmella Benevides Gonçalves
Bibliotecária/CRB-8 9203

unesp

UNIVERSIDADE ESTADUAL PAULISTA
CAMPUS DE GUARATINGUETÁ

ANDRÉ FELIPE MORAES LUIZ LUCCHINI

ESTA DISSERTAÇÃO FOI JULGADA ADEQUADA PARA A OBTENÇÃO DO TÍTULO DE
"MESTRE EM FÍSICA"

PROGRAMA: FÍSICA E ASTRONOMIA
CURSO: MESTRADO

APROVADA EM SUA FORMA FINAL PELO PROGRAMA DE PÓS-GRADUAÇÃO

Prof. Dr. Ernesto Vieira Neto
Coordenador

B A N C A E X A M I N A D O R A:

Prof. Dr. ROGÉRIO TEIXEIRA CAVALCANTI
Orientador - UNESP

Prof. Dr. MÁRCIO EDUARDO DA SILVA ALVES
UNESP

Prof. Dr. RODOLFO JOSÉ BUENO ROGÉRIO
UNIFEI

***OUTUBRO* de 2024**

CURRICULAR DATA

FULL NAME

BIRTH	02/07/1999 - São Paulo / SP
PARENTAGE	Andréa Luiz
2014 / 2016	Academic Background (High School) Technical College Opção
2014 / 2016	Additional Education (Technician in Mechatronics) Technical College Opção
2018 / 2022	Academic Background (Bachelor's Degree in Physics) São Paulo State University "Júlio de Mesquita Filho"

The present work, as well as all my past and future achievements,
is dedicated to my grandmother, Nancy. Without her none of
this would be possible and/or imaginable.

Acknowledgements

First of all, I would like to thank my family, who has always been a constant pillar in my life. I would like to thank my three mothers, Andréa, Nancy, and Biza Max, for raising me with unconditional support, showing me what love and affection are, and teaching me that family consists of those around you who want the best for you. A special thank you goes to my grandmother, Nancy, for being my grandmother, mother, great-grandmother, and father. For making me who I am and making me proud of it. For showing me how strong a person can be, and that love leads us to the extremes of kindness and generosity. For these reasons, I will never be able to thank you enough.

To my siblings and cousin, Carol, João, and Maitê, for always being my family and friends and showing me that even from afar, we always have someone to turn to. Your support has always been and will always be a safe harbor.

To my friends, Mosquim and Lorena, for putting up with my absences and always welcoming me with open arms every chance they get. A special thank you to Mosquim, my brother from another mother, for the late-night talks on your balcony. Our conversations helped me through difficult times in my academic and life journey, especially during the Covid-19 pandemic. I know our friendship and brotherhood will only grow stronger every day.

To my friends from the República Babilônia, Maguá, Murta, Especial, and Julius. Since the beginning of my undergraduate studies, you have given me the best stories, parties, and laughs that I had the pleasure of sharing. Without your daily support, both my undergraduate and master's journeys would have been much harder, and for that, I will be eternally grateful. A special thank you to Maguá, my inseparable brother since day one of undergrad. I hope our conversations and laughter last for the rest of our lives.

To my advisor, Dr. Rogério Teixeira Cavalcanti, for his support from the very first moment I expressed interest in Relativity and Gravitation in his postdoc office. I thank you for showing me what the academic world is like and how incredible this career is, even though it is also demanding. I appreciate your understanding of my anxiety issues and supporting me, even in projects that were not part of my research. I hope our partnership continues to be long-lasting and prosperous.

Finally, but certainly not least, I would like to thank the woman with whom I share all aspects of my life, Millena. Thank you for your unconditional support, especially during my master's degree; it has been and continues to be essential. I thank you for choosing to share your day-to-day life with me and for finding in me a friend and confidant. You are the love of my life, and there is nothing in this world I wouldn't do for you. I also thank

you for agreeing to adopt with me our feline son, Aroldo, who is another source of joy in our home. I love you so much, and I hope to spend every day of my life making you as happy as you make me.

This study was financially supported by:

Coordenação de Aperfeiçoamento de Pessoal de Nível Superior – Brasil (CAPES)

Conselho Nacional de Desenvolvimento Científico e Tecnológico - Brasil (CNPq)

"There are more things in Heaven and Earth, Horatio, than are dreamt of in your philosophy." - Hamlet, Act 1 Scene 5

William Shakespeare

Abstract

Einstein's theory of General Relativity transformed our understanding of gravity by predicting the existence of black holes—astrophysical objects with gravitational fields so strong that not even light can escape. Over time, theoretical developments and astronomical observations have established black holes as key phenomena in modern astrophysics, particularly in the study of Extreme Mass Ratio Inspirals (EMRs), where a supermassive black hole interacts with a much smaller compact object. These systems are vital for testing the predictions of General Relativity, as they generate gravitational waves that encode detailed information about the properties of the black hole and the surrounding spacetime. This master thesis reviews the literature on gravitational perturbations emitted by black holes, examining the emergence of quasi-normal modes (QNMs) and their role in dissipating energy via gravitational waves. Furthermore, it shows the dynamics of radial infall in Schwarzschild black holes and the application of perturbative methods in Kerr spacetime to explore gravitational self-force effects in EMRIs, reviewing into it orbital evolution and dissipative mechanisms.

KEYWORDS: black-holes. gravitational perturbation. quasi-normal modes. radial infall. extreme-mass-ratio inspiral.

Resumo

A teoria da Relatividade Geral de Einstein transformou nossa compreensão da gravidade, prevendo a existência de buracos negros — objetos astrofísicos com campos gravitacionais tão intensos que nem mesmo a luz consegue escapar. Com o tempo, desenvolvimentos teóricos e observações astronômicas estabeleceram buracos negros como fenômenos-chave na astrofísica moderna, particularmente no estudo de Inspirais de Razão de Massa Extrema (EMRIs), onde um buraco negro supermassivo interage com um objeto compacto muito menor. Esses sistemas são vitais para testar as previsões da Relatividade Geral, pois geram ondas gravitacionais que codificam informações detalhadas sobre as propriedades do buraco negro e o espaço-tempo circundante. Esta dissertação de mestrado faz uma revisão bibliográfica das perturbações gravitacionais emitidas por buracos negros, examinando o surgimento de modos quasi-normais (QNMs) e seu papel na dissipação de energia por meio de ondas gravitacionais. Além disso, ele mostra a dinâmica da queda radial em buracos negros de Schwarzschild e a aplicação de métodos perturbativos no espaço-tempo de Kerr para explorar efeitos de *self-force* gravitacional em EMRIs, revisando sua evolução orbital e seus mecanismos dissipativos.

PALAVRAS-CHAVE: buraco negro. perturbaçõegravitacionais. modos quasi-normais. queda radial. inspiral de razão de massa extrema.

List of Figures

Figure 1 – Potential $V_l^{RW}(r)$, where r is in units of GM/c^2, with the horizon at $r = 2$. 34

Figure 2 – Potential $V_l^{RW}(r_*)$, where r_* is in units of GM/c^2, with the horizon at $r_* = -\infty$. 34

Figure 3 – The Zerilli potential, V_l^Z (solid lines), and the RW potential, V_l^{RW} (dashed lines), as functions of r_* for three different values of l. The potential is measured in units of $(GM/c^2)^{-2}$. 42

Figure 4 – Representation of the superposition of plane waves for $Z_{lm}(t, r_*)$ only for $r_* \to \infty$, with the RW potential. 45

Figure 5 – Representation of the superposition of plane waves for $Z_{lm}(t, r_*)$ only for $r_* \to \infty$, after the assumption of the asymptotic behavior, with the RW potential. 45

Figure 6 – Representation of the superposition of plane waves for $Z_{lm}(t, r_*)$ only for $r_* \to -\infty$, with the RW potential. 47

Figure 7 – Representation of the superposition of plane waves for $Z_{lm}(t, r_*)$ only for $r_* \to -\infty$, after the assumption of the asymptotic behavior, with the RW potential. 47

Figure 8 – The integration contour in the complex s-plane. 56

Figure 9 – Comparison of the numerical integration of the scalar wave equation with the approximate contribution from the first QNMs. 62

Figure 10 – The energy spectrum $(c/Gm^2)dE_l/d\omega$ as a function of $\omega R_S/c$, for $l = 2, 3, 4$.(Mitsou, 2011). 68

Figure 11 – The energy spectrum $(c/Gm^2)dE_l/d\omega$ as a function of $\omega R_S/c$, for $l = 2, 3, 4, 5, 6$, on a logarithmic vertical scale.(Mitsou, 2011). 69

Figure 12 – The gravitational waveform $u_l(t)$ with $l = 2$ (in units $G = c = 1$). . . . 69

Figure 13 – The gravitational waveform $u_l(t)$ with $l = 3$ (in units $G = c = 1$). . . . 70

Figure 14 – The gravitational waveform $u_l(t)$ with $l = 4$ (in units $G = c = 1$). . . . 70

Figure 15 – Sample inspiral orbits around a Schwarzschild black hole, as calculated by Osburn et al. (2016) for a mass ratio $\eta = 10^{-5}$. 76

Figure 16 – Sample output from van de Meent's code (van de Meent, 2016), showing the first-order GSF along eccentric geodesic orbits in the equatorial plane of a Kerr black hole. 76

Figure 17 – Central hole spinning at 99% of the maximal allowable rate. 77

Contents

1 INTRODUCTION 14

2 SPHERICAL PERTURBATIONS 16
2.1 Spherical harmonics 17
2.1.1 Spin-2 tensor spherical harmonics 18
2.2 Zerilli tensor 19
2.2.1 Polar and axial perturbations 24
2.2.2 Energy-momentum tensor 25
2.3 Regge-Wheeler gauge 26
2.3.1 Regge-Wheeler equation 31
2.3.2 Zerilli equation 35

3 QUASI-NORMAL MODES 43
3.1 Boundary Conditions 43
3.2 Waveform 46
3.2.1 Laplace transformation 51

4 RADIAL INFALL INTO A SPHERICALLY SYMMETRIC BLACK HOLE 63
4.1 Energy-momentum tensor 63
4.2 Integration of the Zerilli Equation 66
4.3 The energy spectrum 67

5 GAVITATIONAL SELF-FORCE IN GENERAL RELATIVITY 71
5.1 Perturbative approaches in extreme-mass-ratio-inspiral 71
5.1.1 Geodesic Orbits Around a Kerr Black Hole 72
5.1.2 Long-term orbital evolution 72
5.1.3 Transient resonances 73
5.2 Dissipative effects and orbital evolution 74
5.2.1 Balance laws and adiabatic evolution 74
5.3 Inspiral Orbits with Gravitational Self-Force 75
5.4 Research in progress 77

6 CONCLUSIONS 79

References 80

APPENDIX A – COEFFICIENTS OF PURE-SPIN $\mathrm{s} = 2$ SPHERICAL HARMONICS 83

APPENDIX B – NON-ZERO TERMS OF THE CHRISTOFFEL SYMBOLS IN THE SCHWARZSCHILD METRIC 84

APPENDIX C – LAPLACE TRANSFORM FOR ZERILLI AND REGGE-WHEELER HOMOGENEOUS EQUATIONS . . . 85

APPENDIX D – THE GREEN'S FUNCTION AND THE HOMOGENEOUS EQUATION OF $\hat{\phi}(\mathrm{s}, \mathrm{x})$ 87

APPENDIX E – TRAJECTORY EQUATIONS IN THE KERR SPACETIME 90

1 Introduction

Einstein's theory of General Relativity revolutionized our understanding of gravity, predicting the existence of extraordinary objects such as black holes. Black holes are astrophysical entities with gravitational fields so intense that even light cannot escape, making them invisible to direct observation. The existence of these entities was initially proposed through mathematical derivations before any empirical observations were made. Schwarzschild (1916) formulated the solution for the spacetime surrounding a non-rotating object, while Reissner (1916) and Nordström (1918) extended this to incorporate electromagnetic fields. These solutions, though not fully understood for many years, exposed curvature singularities—regions where the equations of relativity break down—enclosed by the so called event horizon.
The concept of black holes as real phenomena was highly debated until Oppenheimer and Snyder (1939) demonstrated that the collapse of dust clouds could lead to their formation. In the 1960s, improvements in astronomical instruments provided indirect evidence, such as quasars powered by the accretion of matter onto supermassive black holes and X-ray sources in binary systems too massive to be neutron stars, leading to the acknowledgment of black holes as plausible candidates. Kerr's solution for rotating spacetime on (Kerr, 1963), later expanded by Newman et al. (1965) to include electromagnetic fields, showed that all previous solutions, including Schwarzschild's, could be viewed as specific instances. This reinforced the theory of black holes as singular entities, yet surrounded by event horizons, a critical feature that shields the external universe from the singularities within. These advancements underscore the paradoxical nature of black holes: although their formation is highly complex, their mathematical characterization is relatively simple, relying on just a few physical parameters, such as mass and angular momentum. According to general relativity, the gravitational properties of astrophysical black holes should be fully described by the Kerr metric. Any deviations observed could necessitate a reevaluation of general relativity or suggest the presence of new physics, such as naked singularities or solid surfaces in the massive objects observed in the universe.

That said, black holes also play a significant practical role in modern astrophysics, particularly in the study of binary systems with extreme mass ratios, known as Extreme Mass-Ratio Inspirals (EMRIs). These systems consist of a supermassive black hole and a much smaller compact object, such as a white dwarf, neutron star, or stellar-mass black hole, which orbits and gradually spirals toward the larger black hole. The interaction between these bodies induces strong perturbations in spacetime, resulting in the emission of gravitational waves (Barack and Sago, 2007).
The analysis of EMRIs is crucial for studying the gravitational properties of black holes,

as these interactions provide detailed insights into the Kerr metric and allow direct tests of the predictions of general relativity in strong-field regimes, as mentioned above. In particular, EMRIs represent one of the best opportunities for detecting gravitational waves with future observatories such as the Laser Interferometer Space Antenna (LISA), which will be capable of observing low-frequency gravitational wave signals generated by these systems (Katz and Larson, 2019; Barack and Cutler, 2007). Also, the study of EMRIs offers a unique opportunity to investigate fundamental questions regarding the nature of black holes, such as the gravitational self-force (Barack and Pound, 2018) produced these systems.

This master thesis revisits the foundational concepts of gravitational perturbations in the context of spherically symmetric black holes. Specifically, we explore how such perturbations give rise to quasi-normal modes (QNMs) that, similar to damped oscillations in elastic bodies, dissipate energy but in the form of gravitational waves. Using the formalism developed by (Regge and Wheeler, 1957) and Zerilli (1970), we will analyze the behavior of these perturbations through their corresponding equations, delving into the resulting waveforms and the emergence of QNMs. The analysis is extended to the scenario of radial infall of matter into a Schwarzschild black hole, where the Zerilli equation will be integrated to derive the energy spectrum of the system. This provides a natural transition into the study of EMRIs, where perturbative methods are applied within the framework of Kerr spacetime to examine gravitational self-force effects. We will discuss how geodesic orbits evolve under these perturbations and the role of dissipative effects, including balance laws and adiabatic evolution. Finally, the penultimate chapter will present ongoing research, highlighting the latest advances in the theoretical study of these phenomena, and exploring novel methodologies aimed at refining our understanding of gravitational self-force and waveform modeling in EMRI systems.

2 Spherical Perturbations

The purpose of this work is to investigate the gravitational perturbations of a Schwarzschild Black Hole. To achieve this, it is possible to express the metric that characterizes it in the following form

$$g_{\alpha\beta}(x) = \bar{g}_{\alpha\beta}(x) + h_{\alpha\beta}(x), \tag{2.0.1}$$

where $\bar{g}_{\mu\nu}$ denotes the Schwarzschild metric, given by

$$\bar{g}_{\alpha\beta}dx^{\alpha\beta} = -A(r)(cdt)^2 + B(r)dr^2 + r^2(d\theta^2 + \sin^2\theta d\phi^2), \tag{2.0.2}$$

and

$$A(r) = 1 - \frac{R_S}{r}, \qquad B(r) = \frac{1}{A(r)}, \tag{2.0.3}$$

$R_S = 2GM/c^2$ is the Schwarzschild radius and $h_{\mu\nu}$ represents the metric perturbation, which satisfies $|h_{\mu\nu}| \ll 1$. This condition indicates that the perturbation is small enough to be treated within the linear perturbation theory framework. The expansion of the Einstein tensor for the perturbation case can be represented as follows

$$G_{\alpha\beta}[g_{\alpha\beta}] = \bar{G}_{\alpha\beta}[\bar{g}_{\alpha\beta}] + \Delta G_{\alpha\beta}[h_{\alpha\beta}] = \frac{8\pi G}{c^4} T_{\alpha\beta}[g_{\alpha\beta}], \tag{2.0.4}$$

where $\bar{G}_{\alpha\beta} = 0$, once that the background Schwarzschild metric is a vacuum solution of the Einstein equations, subject to the conditions of spherical symmetry. $\Delta G_{\alpha\beta}$ represents the Einstein's tensor of the perturbation $h_{\mu\nu}$, and $T_{\alpha\beta}[g_{\alpha\beta}] = \bar{T}_{\alpha\beta}[\bar{g}_{\alpha\beta}] + \Delta T_{\alpha\beta}[h_{\alpha\beta}]$ is the total energy-momentum tensor. Accordingly, the Einstein equation for the perturbation case reads

$$\Delta G_{\alpha\beta}[h_{\alpha\beta}] = \frac{8\pi G}{c^4} \Delta T_{\alpha\beta}[h_{\alpha\beta}], \tag{2.0.5}$$

assuming $\Delta T_{\alpha\beta}$ - following the same procedure that $\Delta G_{\alpha\beta}$ - represents an external matter

that perturbs the black hole. At this stage, will be investigated all the ten components of $h_{\alpha\beta}$. As the background metric is spherically symmetric, it can be separated into the radial and angular dependence of the metric perturbation. Therefore, it requires a basis of ten independent tensor harmonics that correspond to the ten components of $h_{\alpha\beta}$.

2.1 Spherical harmonics

The tensor spherical harmonics play a crucial role in the construction of the multipole expansion formalism. While scalar spherical harmonics are useful for describing the angular dependence of a scalar field, tensor spherical harmonics are essential for the description of the angular dependence of a spin field (Maggiore, 2007).

In this context, it will be used the notation $\mathbf{J} = \mathbf{L} + \mathbf{S}$ to represent the total angular momentum, where $\mathbf{L}$ denotes the orbital angular momentum operator and $\mathbf{S}$ represents the spin operator. All units will be measured in terms of $\hbar$, such that the action of the operator on functions can be expressed as $\mathbf{L} = \mathbf{r} \times (-i\boldsymbol{\nabla})$. Since the operators $\mathbf{J}^2$, J_z^2, $\mathbf{L}^2$ and $\mathbf{S}^2$ mutually commute, they can be simultaneously diagonalized. The resulting eigenfunctions are the tensor spherical harmonics, denoted as $Y^{ls}_{jj_z}(\theta, \phi)$. By definition, these functions satisfy the following equation

$$\mathbf{J}^2 Y^{ls}_{jj_z} = j(j+1) Y^{ls}_{jj_z}, \tag{2.1.1}$$

$$J_z Y^{ls}_{jj_z} = j_z Y^{ls}_{jj_z}, \tag{2.1.2}$$

$$\mathbf{L}^2 Y^{ls}_{jj_z} = l(l+1) Y^{ls}_{jj_z}, \tag{2.1.3}$$

$$\mathbf{S}^2 Y^{ls}_{jj_z} = s(s+1) Y^{ls}_{jj_z}. \tag{2.1.4}$$

The explicit forms of the tensor spherical harmonics can be obtained through the coupling of spherical harmonics Y_{lm} with spin functions χ_{s,s_z}, utilizing the appropriate Clebsch-Gordan coefficients. This yields a state with total angular momentum $|j, j_z\rangle$. So

$$Y^{ls}_{jj_z}(\theta, \phi) = \sum_{l_z=-l}^{l} \sum_{s_z=-s}^{s} \langle s\, l\, s_z\, l_z | j\, j_z \rangle Y_{jj_z}(\theta, \phi) \chi_{s\, s_z}. \tag{2.1.5}$$

The validity of the expression given above in satisfying equations (2.1.1)-(2.1.4) can be established with ease. As such, the Clebsch-Gordan coefficients $\langle s, l, s_z, l_z | j, j_z \rangle$ couple a state with orbital angular momentum $|l, l_z\rangle$ to a state with spin $|s, s_z\rangle$, resulting in a state with total angular momentum $|j, j_z\rangle$.

Tensor spherical harmonics provide a description of the angular distribution and polarization of spin particles in a state with well-defined values of total angular momentum

j, j_z, and orbital angular momentum l. In the context of gravitational waves, the focus of this work will be on spin-2 tensor spherical harmonics.

2.1.1 Spin-2 tensor spherical harmonics

The introduction of spin-2 tensor spherical harmonics requires the spin wave function for $s = 2$ with well-defined values of s_z. These wave functions are both symmetric and traceless and are denoted by $t_{ik}^{(s_z)}$. They can be obtained by combining two spin-1 wave functions, $\xi_i^{(m_1)}$ and $\xi_k^{(m_2)}$, with an appropriate Clebsch-Gordan coefficient, resulting

$$t_{ik}^{(s_z)} = \sum_{m_1,m_2=-1}^{1} \langle 1, m_1, 1, m_2 | 2, s_z \rangle \xi_i^{(m_1)} \, \xi_k^{(m_2)}. \tag{2.1.6}$$

The five tensors $t_{ik}^{(s_z)}$ corresponding to the values $s_z = 0$, $s_z = \pm 1$, and $s_z = \pm 2$, are all symmetric and traceless. These tensors perform the same role as the three vectors $\xi_i^{(s_z)}$, where $s_z = 0$ and $s_z = \pm 1$, for vector spherical harmonics. Specifically, when combined with scalar spherical harmonics, the spin-2 tensor spherical harmonics are obtained,

$$(\mathbf{T}^l_{jj_z})_{ik} \equiv (Y^{l2}_{jj_z})_{ik} = \sum_{l_z=-l}^{l} \sum_{s_z=-2}^{2} \langle 2\, l\, s_z\, l_z | j\, j_z \rangle Y_{ll_z}(\theta, \phi) t_{ik}^{(s_z)}. \tag{2.1.7}$$

The tensor $(\mathbf{T}^l_{j,j_z})_{ik}$ is an eigenfunction of the operator $\mathbf{L}^2$ by construction. However, it does not possess any particular properties with respect to the unit radial vector $\hat{\mathbf{n}}$. It can be observed that the complete set of tensors $\mathbf{T}^l_{j,j_z}$ can be expressed in terms of combinations, which are called pure-spin $s = 2$ tensor spherical harmonics. These harmonics have defined properties under rotation along the radial direction. For $j \geq 2$, the spherical harmonics can be expressed as

$$\mathbf{T}^{\mathrm{S0}}_{jj_z} = a_{11}\mathbf{T}^{j+2}_{jj_z} + a_{12}\mathbf{T}^{j}_{jj_z} + a_{13}\mathbf{T}^{j-2}_{jj_z}, \tag{2.1.8}$$

$$\mathbf{T}^{\mathrm{E1}}_{jj_z} = a_{21}\mathbf{T}^{j+2}_{jj_z} + a_{22}\mathbf{T}^{j}_{jj_z} + a_{23}\mathbf{T}^{j-2}_{jj_z}, \tag{2.1.9}$$

$$\mathbf{T}^{\mathrm{E2}}_{jj_z} = a_{31}\mathbf{T}^{j+2}_{jj_z} + a_{32}\mathbf{T}^{j}_{jj_z} + a_{33}\mathbf{T}^{j-2}_{jj_z}, \tag{2.1.10}$$

$$\mathbf{T}^{\mathrm{B1}}_{jj_z} = b_{11}i\mathbf{T}^{j+1}_{jj_z} + b_{12}i\mathbf{T}^{j-1}_{jj_z}, \tag{2.1.11}$$

$$\mathbf{T}^{\mathrm{B2}}_{jj_z} = b_{21}i\mathbf{T}^{j+1}_{jj_z} + b_{22}i\mathbf{T}^{j-1}_{jj_z}, \tag{2.1.12}$$

where the above coefficients are expressed in Appendix A. The above tensors can be expressed in terms of the scalar spherical harmonics as below[1]

[1] Here, the notation l, m will be used instead of j, j_z to represent the total angular momentum, since i, j will be used to represent the spatial indices of vectors.

$$(\mathbf{T}^{\mathrm{S0}}_{lm})_{ij} = [n_i n_j - (1/3)\delta_{ij}]Y_{lm}, \tag{2.1.13}$$
$$(\mathbf{T}^{\mathrm{E1}}_{lm})_{ij} = c_l^{(1)}(r/2)(n_i\partial_j - n_j\partial_i)Y_{lm}, \tag{2.1.14}$$
$$(\mathbf{T}^{\mathrm{E2}}_{lm})_{ij} = c_l^{(2)}r^2\Lambda_{ij,i'j'}(\hat{\mathbf{n}})\partial_{i'}\partial_{j'}Y_{lm}, \tag{2.1.15}$$
$$(\mathbf{T}^{\mathrm{B1}}_{lm})_{ij} = c_l^{(1)}(i/2)(n_i L_j - n_j L_i)Y_{lm}, \tag{2.1.16}$$
$$(\mathbf{T}^{\mathrm{B2}}_{lm})_{ij} = c_l^{(2)}r\Lambda_{ij,i'j'}(\hat{\mathbf{n}})(i/2)(\partial_{i'}L_{j'} - \partial_{j'}L_{i'})Y_{lm}. \tag{2.1.17}$$

The tensors $\Lambda_{ij,i'j'}$ are the tensors responsible for implementing the TT projections (transverse and traceless)

$$\Lambda_{ij,i'j'} = P_{ii'}P_{jj'} - \frac{1}{2}P_{ij}P_{i'j'}, \qquad P_{ij}(\hat{\boldsymbol{n}}) = \delta_{ij} - n_i n_j,$$

and the other coefficients will be expressed by

$$c_l^{(1)} = \left(\frac{2}{l(l+1)}\right)^{1/2}, \tag{2.1.18}$$
$$c_l^{(2)} = \left(2\frac{(l-2)!}{(l+2)!}\right)^{1/2}. \tag{2.1.19}$$

It is important to note that all tensors above are transverse and traceless by construction.

2.2 Zerilli tensor

The Zerilli harmonic tensors represent a set of mathematical entities employed in the examination of gravitational waves in the context of General Relativity. They bear the name of Frank Zerilli, the scholar who initially presented them in Zerilli (1970). In the General Theory of Relativity, gravitational waves indicate undulations within the space-time fabric that extend outward from locations of potent gravitational fields, such as the fusion of black holes or the contraction of colossal stars. Zerilli harmonic tensors offer a means to break down these gravitational waves into various modes, each characterized by its own frequency and polarization.

Zerilli harmonic tensors constitute solutions to a group of partial differential equations referred to as the Zerilli equation, which delineates the dynamics of gravitational waves in the presence of a rotating black hole. Through the decomposition of gravitational waves into diverse modes, their properties can be more readily analyzed, and information about

the underlying source that produced them can be extracted. Apart from their applications in the study of gravitational waves, Zerilli harmonic tensors have also been applied in other realms of physics and mathematics, such as black hole thermodynamics and the theory of harmonic functions (Monteiro, 2010).

These tensors constitute a collection of six linearly independent functions that depict the behavior of gravitational waves within the Schwarzschild space-time, i.e., in the absence of rotation. They are employed to break down the gravitational wave field into its odd-parity and even-parity modes, corresponding to the two polarization states of the gravitational wave. Despite originating from distinct concepts and applications, there exists a correlation between spin-2-tensor harmonics and the Zerilli tensors. Specifically, the Zerilli tensors can be expressed as linear combinations of spin-2-tensor harmonics, having specific coefficients contingent upon the properties of the Schwarzschild space-time. This connection between the Zerilli tensors and spin-2-tensor harmonics is referred to as the Zerilli-Moncrief formalism, named after Zerilli and his collaborator, Barry Moncrief. The Zerilli-Moncrief formalism is an influential tool for investigating gravitational waves in Schwarzschild space-time and is extensively used in numerical simulations of black hole mergers (Martel and Poisson, 2005).

The six tensorial spherical harmonics necessary for separating the angular dependence in the spatial coordinates of h_{ij} for a spin-2 field are the ones expressed by (2.1.14) - (2.1.17), and (2.1.13) can be combined with the function $\delta_{ij}Y_{lm}$ to give a purely longitudinal and a purely transverse (but not traceless) tensor harmonics, such as

$$(\boldsymbol{T}^{L0}_{lm})_{ij} = n_i n_j Y_{lm}, \tag{2.2.1}$$

$$(\boldsymbol{T}^{T0}_{lm})_{ij} = \frac{1}{\sqrt{2}}(\delta_{ij} - n_i n_j)Y_{lm}. \tag{2.2.2}$$

Will also be necessary four independent harmonic tensors, which will allow to expression of the components $h_{0\mu}$. Since h_{00} is a scalar under rotation, it can be expressed in terms of any scalar spherical harmonic. Therefore, defining $(\boldsymbol{T}^{tt}_{lm})_{\mu\nu}$, in the BH's inertial frame, as

$$(\boldsymbol{T}^{tt}_{lm})_{\mu\nu} = \delta^0_\mu \delta^0_\nu Y_{lm}.$$

From the point of view of rotations, h_{0i} is a vector, so it can be expressed in terms of vector spherical harmonics

$$\boldsymbol{Y}^E_{lm} = [l(l+1)]^{-1/2}\, r\boldsymbol{\nabla} Y_{lm}, \tag{2.2.3}$$
$$\boldsymbol{Y}^B_{lm} = [l(l+1)]^{-1/2}\, i\boldsymbol{L} Y_{lm}, \tag{2.2.4}$$
$$\boldsymbol{Y}^R_{lm} = Y_{lm}\hat{\boldsymbol{n}}. \tag{2.2.5}$$

If one defines the harmonic tensors $(\boldsymbol{T}^{Rt}_{lm})_{\mu\nu}$, $(\boldsymbol{T}^{Et}_{lm})_{\mu\nu}$ and $(\boldsymbol{T}^{Bt}_{lm})_{\mu\nu}$ assuming that, in the BH's inertial frame, they are nonzero only when $\mu = 0$ and $\nu = i$ - and vice versa - it will result

$$(\boldsymbol{T}^{Et}_{lm})_{0i} = \frac{1}{\sqrt{2}}(\boldsymbol{Y}^E_{lm})i, \tag{2.2.6}$$
$$(\boldsymbol{T}^{Bt}_{lm})_{0i} = \frac{1}{\sqrt{2}}(\boldsymbol{Y}^B_{lm})i, \tag{2.2.7}$$
$$(\boldsymbol{T}^{Rt}_{lm})_{0i} = \frac{1}{\sqrt{2}}(\boldsymbol{Y}^R_{lm})_i. \tag{2.2.8}$$

Or, explicitly

$$(\boldsymbol{T}^{Et}_{lm})_{0i} = [2l(l+1)]^{-1/2}\, r\partial_i Y_{lm}, \tag{2.2.9}$$
$$(\boldsymbol{T}^{Bt}_{lm})_{0i} = i\,[2l(l+1)]^{-1/2}\, L_i Y_{lm}, \tag{2.2.10}$$
$$(\boldsymbol{T}^{Rt}_{lm})_{0i} = \frac{1}{\sqrt{2}} n_i Y_{lm}. \tag{2.2.11}$$

Where $\boldsymbol{L} = -i\boldsymbol{r}\times\boldsymbol{\nabla}$ and $\hat{\boldsymbol{n}}$ is the unit vector in the radial direction, normalized with respect to the metric, $\delta_{ij}n_i n_j = 1$.
The factor i in the definition of the terms $\boldsymbol{T}^{Bt}_{lm}$, $\boldsymbol{T}^{B1}_{lm}$, and $\boldsymbol{T}^{B2}_{lm}$ was inserted to ensure that these tensors satisfy the relation

$$(\boldsymbol{T}^a_{lm})^*_{\mu\nu} = (-1)^m(\boldsymbol{T}^a_{lm})_{\mu\nu},$$

which is derived by observing that $i\boldsymbol{L} = \boldsymbol{r}\times\boldsymbol{\nabla}$ is real.
Thus, a complete basis for the expansion of h_{ij} is provided by the six spherical harmonics when T^{L0}_{lm} and T^{T0}_{lm} exist for $l \geq 0$, T^{E1}_{lm} and T^{B1}_{lm} for $l \geq 1$[2], and T^{E2}_{lm} and T^{B2}_{lm} for $l \geq 2$.

[2] For the papers of Regge and Wheeler (1957) and Zerilli (1970), for these 10 tensor harmonics the following notation is $a_{lm} = \boldsymbol{T}^{L0}_{lm}$, $a^{(0)}_{lm} = \boldsymbol{T}^{L0}_{lm}$, $a^{(1)}_{lm} = \boldsymbol{T}^{L0}_{lm}$, $b_{lm} = \boldsymbol{T}^{E1}_{lm}$, $b^{(0)}_{lm} = i\boldsymbol{T}^{Et}_{lm}$, $c_{lm} = -i\boldsymbol{T}^{B1}_{lm}$, $c^{(0)}_{lm} = -\boldsymbol{T}^{Bt}_{lm}$, $d_{lm} = -i\boldsymbol{T}^{B2}_{lm}$, $f_{lm} = \boldsymbol{T}^{E2}_{lm}$, $g_{lm} = \boldsymbol{T}^{T0}_{lm}$.

Similarly, for h_{0i}, T^{Rt}_{lm} is defined for $l \geq 0$, while T^{Et}_{lm} and T^{Bt}_{lm} are defined for $l \geq 1$. If these 10 harmonic tensors are already normalized, so

$$\int d\Omega\, \eta^{\mu\rho}\eta^{\nu\sigma}(\boldsymbol{T}^{a}_{l'm'})^{*}_{\mu\nu}(\boldsymbol{T}^{b}_{lm})_{\rho\sigma} = \epsilon_a \delta^{ab}\delta_{ll'}\delta_{mm'}, \tag{2.2.12}$$

where the indices a and b run over the set $\{L0, T0, E1, B1, E2, B2, tt, Rt, Et, Bt\}$, and the coefficient ϵ_a has a value of -1 when $a = Rt, Et, Bt$, and $+1$ for its other values. If then separates $h_{\mu\nu}$ into a part dependent on the angular variables (θ, ϕ) and another part dependent on (t, r)

$$h_{\mu\nu}(t, \boldsymbol{x}) = \sum_a \sum_{lm} H^{a}_{lm}(t, r)(\boldsymbol{T}^{a}_{lm})_{\mu\nu}(\theta, \phi), \tag{2.2.13}$$

where $(\boldsymbol{T}^{a}_{lm})_{\mu\nu}$ is known as the *spherical harmonics of the Zerilli tensor*. It is important to note that $(\boldsymbol{T}^{a}_{lm})_{\mu\nu}$ describes the expansion of the perturbation in Cartesian coordinates, $x^\mu = (ct, x, y, z)$. However, the Schwarzschild background metric is much simpler in polar coordinates, $x^\alpha = (ct, r, \theta, \phi)$, so the perturbation in polar coordinates will be needed. By definition, the polar components $h_{\alpha\beta}$ are related to the Cartesian components of $h_{\mu\nu}$ as follows

$$h_{\alpha\beta}dx^\alpha dx^\beta = h_{\mu\nu}dx^\mu dx^\nu.$$

It can also write the same relationship for the Zerilli harmonic tensors

$$(\boldsymbol{T}^{a}_{lm})_{\alpha\beta}dx^\alpha dx^\beta = (\boldsymbol{T}^{a}_{lm})_{\mu\nu}dx^\mu dx^\nu.$$

Therefore,

$$h_{\alpha\beta}(t, r, \theta, \phi) = \sum_a \sum_{lm} H^{a}_{lm}(t, r)(\boldsymbol{T}^{a}_{lm})_{\alpha\beta}(\theta, \phi). \tag{2.2.14}$$

Since the temporal variable is the same in both coordinate systems, the transformation is only in the spatial variables, so it is useful to define the matrix

$$A_a{}^i = \frac{\partial x^i}{\partial x^a} = \begin{pmatrix} \sin\theta\cos\phi & \sin\theta\sin\phi & \cos\theta \\ r\cos\theta\cos\phi & r\cos\theta\sin\phi & -r\sin\theta \\ -r\sin\theta\sin\phi & r\sin\theta\cos\phi & 0 \end{pmatrix}, \tag{2.2.15}$$

where $x^a = (r, \theta, \phi)$ and $x^i = (x, y, z)$. Thus, for a generic tensor, $T_{ab} = A_a{}^i A_b{}^i T_{ij}$, while $T_{0a} = A_a{}^i T_{0i}$. Therefore, for the expression of angular momentum, there is

$$L_a \equiv A_a{}^k L_k = ir\left(0, \frac{1}{\sin\theta}\partial_\phi, -\sin\theta\partial_\theta\right)_a . \tag{2.2.16}$$

Using these results, the calculation of explicit expressions for all harmonic tensors in polar coordinates becomes relatively simple. The result can be conveniently written as

$$(\boldsymbol{T}^a_{lm})_{\alpha\beta} = c^a(r)(\boldsymbol{t}^a_{lm})_{\alpha\beta}, \tag{2.2.17}$$

where $c^a(r)$ are given by

$$c^{L0} = c^{tt} = 1, \qquad c^{T0} = \frac{r^2}{\sqrt{2}}, \qquad c^{Rt} = \frac{1}{\sqrt{2}},$$

$$c^{Et} = c^{E1} = -c^{Bt} = -c^{B1} = \frac{r}{[2l(l+1)]^{1/2}},$$

$$c^{E2} = c^{B2} = r^2\left[\frac{1}{2}\frac{(l-2)!}{(l+2)!}\right]^{1/2}.$$

And, the tensor harmonics $(\boldsymbol{t}^a_{lm})_{\alpha\beta}$ are, with (α, β) indices

$$\boldsymbol{t}^{tt}_{lm} = \begin{pmatrix} 1 & 0 & 0 & 0 \\ 0 & 0 & 0 & 0 \\ 0 & 0 & 0 & 0 \\ 0 & 0 & 0 & 0 \end{pmatrix} Y_{lm}, \qquad \boldsymbol{t}^{Rt}_{lm} = \begin{pmatrix} 0 & 1 & 0 & 0 \\ 1 & 0 & 0 & 0 \\ 0 & 0 & 0 & 0 \\ 0 & 0 & 0 & 0 \end{pmatrix} Y_{lm}, \qquad \boldsymbol{t}^{L0}_{lm} = \begin{pmatrix} 0 & 0 & 0 & 0 \\ 0 & 1 & 0 & 0 \\ 0 & 0 & 0 & 0 \\ 0 & 0 & 0 & 0 \end{pmatrix} Y_{lm},$$

$$\boldsymbol{t}^{T0}_{lm} = \begin{pmatrix} 0 & 0 & 0 & 0 \\ 0 & 0 & 0 & 0 \\ 0 & 0 & 1 & 0 \\ 0 & 0 & 0 & \sin^2\theta \end{pmatrix} Y_{lm}, \qquad \boldsymbol{t}^{Et}_{lm} = \begin{pmatrix} 0 & 0 & \partial_\theta & \partial_\phi \\ 0 & 0 & 0 & 0 \\ \star & 0 & 0 & 0 \\ \star & 0 & 0 & 0 \end{pmatrix} Y_{lm}, \qquad \boldsymbol{t}^{E1}_{lm} = \begin{pmatrix} 0 & 0 & 0 & 0 \\ 0 & 0 & \partial_\theta & \partial_\phi \\ 0 & \star & 0 & 0 \\ 0 & \star & 0 & 0 \end{pmatrix} Y_{lm},$$

$$\boldsymbol{t}^{Bt}_{lm} = \begin{pmatrix} 0 & 0 & (1/\sin\theta)\partial_\phi & -\sin\theta\partial_\theta \\ 0 & 0 & 0 & 0 \\ \star & 0 & 0 & 0 \\ \star & 0 & 0 & 0 \end{pmatrix} Y_{lm}, \qquad \boldsymbol{t}^{B1}_{lm} = \begin{pmatrix} 0 & 0 & 0 & 0 \\ 0 & 0 & (1/\sin\theta)\partial_\phi & -\sin\theta\partial_\theta \\ 0 & \star & 0 & 0 \\ 0 & \star & 0 & 0 \end{pmatrix} Y_{lm},$$

$$\boldsymbol{t}^{E2}_{lm} = \begin{pmatrix} 0 & 0 & 0 & 0 \\ 0 & 0 & 0 & 0 \\ 0 & 0 & W & X \\ 0 & 0 & \star & -\sin^2\theta W \end{pmatrix} Y_{lm}, \qquad \boldsymbol{t}^{B2}_{lm} = \begin{pmatrix} 0 & 0 & 0 & 0 \\ 0 & 0 & 0 & 0 \\ 0 & 0 & -(1/\sin\theta)X & \sin\theta W \\ 0 & 0 & \star & \sin\theta X \end{pmatrix} Y_{lm},$$

where rows and columns correspond to t, r, θ and ϕ, respectively, and the star denotes components obtained by the symmetry of the matrix. Defining the following operators

$$X = 2\partial_\theta\partial_\phi - 2\theta\partial_\phi \tag{2.2.18}$$

$$W = \partial^2_\theta - \theta\partial_\theta - \frac{1}{\sin^2\theta}\partial^2_\phi. \tag{2.2.19}$$

Thus, it can be written the expansion of the metric perturbation as

$$h_{\alpha\beta}(x) = \sum_a \sum_{lm} h^a_{lm}(t,r)(\boldsymbol{t}^a_{lm})_{\alpha\beta}(\theta,\phi), \tag{2.2.20}$$

where the factor $c^a(r)$ has been reabsorbed, when defining

$$h^a_{lm}(t,r) = c^a(r)H^a_{lm}(t,r)$$

2.2.1 Polar and axial perturbations

Under a parity transformation, $\theta \to \pi - \theta$ and $\phi \to \phi + \pi$, the harmonic tensors with $a = L0, T0, E1, E2, tt, Rt$ and Et receive a factor of $(-1)^l$ and are thus called polar. Meanwhile, the harmonic tensors with $a = B1, B2$ and Bt receive a factor of $(-1)^{l+1}$ and are called axial. Furthermore, since the Schwarzschild metric is invariant under parity - when linearized - the perturbations do not mix. Thus, it is useful to separate these two parts.

$$h_{\alpha\beta}(x) = h^{\rm pol}_{\alpha\beta}(x) + h^{\rm ax}_{\alpha\beta}(x). \tag{2.2.21}$$

Explicitly, the components of $h^{\text{pol}}_{\alpha\beta}$ are

$$\begin{aligned} h^{\text{pol}}_{\alpha\beta}(t,\boldsymbol{x}) =& \sum_{l=0}^{\infty}\sum_{m=-l}^{l}\left[h^{tt}_{lm}(\boldsymbol{t}^{tt}_{lm})_{\alpha\beta} + h^{Rt}_{lm}(\boldsymbol{t}^{Rt}_{lm})_{\alpha\beta}\right] \\ &+ \sum_{l=0}^{\infty}\sum_{m=-l}^{l}\left[h^{L0}_{tt}(\boldsymbol{t}^{L0}_{tt})_{\alpha\beta} + h^{T0}_{lm}(\boldsymbol{t}^{T0}_{lm})_{\alpha\beta}\right] \\ &+ \sum_{l=1}^{\infty}\sum_{m=-l}^{l}\left[h^{Et}_{lm}(\boldsymbol{t}^{Et}_{lm})_{\alpha\beta} + h^{E1}_{lm}(\boldsymbol{t}^{E1}_{lm})_{\alpha\beta}\right] \\ &+ \sum_{l=2}^{\infty}\sum_{m=-l}^{l} h^{E2}_{lm}(\boldsymbol{t}^{E2}_{lm})_{\alpha\beta}. \end{aligned} \tag{2.2.22}$$

And for $h^{\text{ax}}_{\alpha\beta}$,

$$\begin{aligned} h^{\text{ax}}_{\alpha\beta}(t,\boldsymbol{x}) =& \sum_{l=1}^{\infty}\sum_{m=-l}^{l}\left[h^{Bt}_{lm}(\boldsymbol{t}^{Bt}_{lm})_{\alpha\beta} + h^{B1}_{lm}(\boldsymbol{t}^{B1}_{lm})_{\alpha\beta}\right] \\ &+ \sum_{l=2}^{\infty}\sum_{m=-l}^{l} h^{B2}_{lm}(\boldsymbol{t}^{B2}_{lm})_{\alpha\beta}. \end{aligned} \tag{2.2.23}$$

2.2.2 Energy-momentum tensor

Once in possession of the perturbation $h_{\alpha\beta}$ in terms of the harmonic tensors $(\boldsymbol{t}^{a}_{lm})_{\alpha\beta}$, it is convenient to do the same for the energy-momentum tensor $T_{\mu\nu}$. In the form

$$T_{\alpha\beta}(x) = T^{\text{pol}}_{\alpha\beta}(x) + T^{\text{ax}}_{\alpha\beta}(x). \tag{2.2.24}$$

Thus, similarly to the case of the perturbation, equations (2.2.22) and (2.2.23), for $T^{\text{pol}}_{\alpha\beta}$

$$\begin{aligned} T^{\text{pol}}_{\alpha\beta}(t,\boldsymbol{x}) =& \sum_{l=0}^{\infty}\sum_{m=-l}^{l}\left[s^{tt}_{lm}(\boldsymbol{t}^{tt}_{lm})_{\alpha\beta} + s^{Rt}_{lm}(\boldsymbol{t}^{Rt}_{lm})_{\alpha\beta}\right] \\ &+ \sum_{l=0}^{\infty}\sum_{m=-l}^{l}\left[s^{L0}_{tt}(\boldsymbol{t}^{L0}_{tt})_{\alpha\beta} + s^{T0}_{lm}(\boldsymbol{t}^{T0}_{lm})_{\alpha\beta}\right] \\ &+ \sum_{l=1}^{\infty}\sum_{m=-l}^{l}\left[s^{Et}_{lm}(\boldsymbol{t}^{Et}_{lm})_{\alpha\beta} + s^{E1}_{lm}(\boldsymbol{t}^{E1}_{lm})_{\alpha\beta}\right] \\ &+ \sum_{l=2}^{\infty}\sum_{m=-l}^{l} s^{E2}_{lm}(\boldsymbol{t}^{E2}_{lm})_{\alpha\beta}. \end{aligned} \tag{2.2.25}$$

And for $T^{\rm ax}_{\alpha\beta}$

$$T^{\rm ax}_{\alpha\beta}(t,\boldsymbol{x}) = \sum_{l=1}^{\infty}\sum_{m=-l}^{l}\left[s^{Bt}_{lm}(\boldsymbol{t}^{Bt}_{lm})_{\alpha\beta} + s^{B1}_{lm}(\boldsymbol{t}^{B1}_{lm})_{\alpha\beta}\right] + \sum_{l=2}^{\infty}\sum_{m=-l}^{l} s^{B2}_{lm}(\boldsymbol{t}^{B2}_{lm})_{\alpha\beta}, \tag{2.2.26}$$

where $s^{a}_{lm}(t,r)$ denotes the expansion coefficients of the energy-momentum tensor in spherical harmonics.

2.3 Regge-Wheeler gauge

Considering an infinitesimal coordinate transformation

$$x^{\mu} \to x^{'\mu} = x^{\mu} + \xi^{\mu}(x),$$

by choosing ξ_{μ} such that $\bar{D}_{\mu}\xi_{\mu}$ is of the same order as $h_{\alpha\beta}$, will have a background metric $\bar{g}_{\alpha\beta}$ invariant under this transformation. So, $h_{\alpha\beta}$ will transform as follows

$$h_{\alpha\beta}(x) \to h'_{\alpha\beta}(x) = h_{\alpha\beta}(x) - (\bar{D}_{\alpha}\xi_{\beta} + \bar{D}_{\beta}\xi_{\alpha}). \tag{2.3.1}$$

This generalizes the gauge transformation of flat space to curved space. The definition of the property $\bar{D}_{\mu}$ is that it transforms covariantly under coordinate transformations. It can be explored now the gauge freedom to simplify the expansions of $h^{\rm pol}_{\alpha\beta}(t,\boldsymbol{x})$ and $h^{\rm ax}_{\alpha\beta}(t,\boldsymbol{x})$. Firstly, it can be observed that the generic four-vector field $\xi_{\alpha}(x) = (\xi_0(x), \xi_a(x))$ can be expanded in scalar and vector spherical harmonics as

$$\xi_0(x) = \sum_{l=0}^{\infty}\sum_{m=-l}^{l}\xi^{(t)}_{lm}(t,r)Y_{lm}(\theta,\phi), \tag{2.3.2}$$

and also

$$\xi_a(x) = \sum_{l=0}^{\infty}\sum_{m=-l}^{l}\xi^{(R)}_{lm}(t,r)Y_{lm}(\theta,\phi)n_a + \sum_{l=1}^{\infty}\sum_{m=-l}^{l}\left[\xi^{(E)}_{lm}(t,r)\partial_a Y_{lm}(\theta,\phi) + \xi^{(B)}_{lm}(t,r)\frac{i}{r}L_a Y_{lm}(\theta,\phi)\right] \tag{2.3.3}$$

In the above expressions, $\xi^{(B)}_{lm}$ generates an axial term in the metric, while $\xi^{(t)}_{lm}$, $\xi^{(R)}_{lm}$ and $\xi^{(E)}_{lm}$ generate a polar term. For the first transformation, it is considered an axial gauge transformation, where $\xi^{(t)}_{lm} = \xi^{(R)}_{lm} = \xi^{(E)}_{lm} = 0$. By denoting $\xi^{(B)}_{lm} = \Lambda_{lm}$, there is

$$\xi^{\text{ax}}_0(x) = 0, \qquad \xi^{\text{ax}}_a(x) = \sum_{l=1}^{\infty}\sum_{m=-l}^{l} \Lambda_{lm}(t,r)\frac{i}{r}L_j Y_{lm}. \tag{2.3.4}$$

If one uses the definition of L_a, shown previously,

$$\xi^{\text{ax}}_\alpha(x) = \sum_{l=1}^{\infty}\sum_{m=-l}^{l} \Lambda_{lm}(t,r)\left(0, 0, -\frac{1}{\sin\theta}\partial_\phi Y_{lm}, \sin\theta\partial_\theta Y_{lm}\right). \tag{2.3.5}$$

Now, it can be calculated the covariant derivative

$$\bar{D}_\alpha \xi^{\text{ax}}_\beta = \partial_\alpha \xi^{\text{ax}}_\beta - \bar{\Gamma}^\gamma_{\alpha\beta}\xi^{\text{ax}}_\gamma,$$

where $\bar{\Gamma}^\gamma_{\alpha\beta}$ is the Christoffel symbol of the Schwarzschild metric, see Appendix B. If $\bar{D}_\alpha \xi^{\text{ax}}_\beta + \bar{D}_\beta \xi^{\text{ax}}_\alpha$ is expressed in the basis $(\boldsymbol{t}^a_{lm})_{\alpha\beta}$ (in matrix form), it becomes

$$\begin{aligned}\bar{D}_\alpha \xi^{\text{ax}}_\beta + \bar{D}_\beta \xi^{\text{ax}}_\alpha = &-\sum_{l=1}^{\infty}\sum_{m=-l}^{l} (\partial_0 \Lambda_{lm})(\boldsymbol{t}^{Bt}_{lm})_{\alpha\beta} \\ &-\sum_{l=1}^{\infty}\sum_{m=-l}^{l}\left(\partial_r\Lambda_{lm} - \frac{2}{r}\Lambda_{lm}\right)(\boldsymbol{t}^{B1}_{lm})_{\alpha\beta} \\ &+\sum_{l=2}^{\infty}\sum_{m=-l}^{l}\Lambda_{lm}(\boldsymbol{t}^{B2}_{lm})_{\alpha\beta}.\end{aligned} \tag{2.3.6}$$

The first thing to note in the previous result is that, as expected, ξ^{ax} induces a transformation on $h_{\alpha\beta}$ that can be expressed in terms of the axial harmonic tensors $\boldsymbol{t}^{Bt}_{lm}$, $\boldsymbol{t}^{B1}_{lm}$, and $\boldsymbol{t}^{B2}_{lm}$.Therefore, $h^{\text{pol}}_{\alpha\beta}$ is invariant, and the transformation only affects $h^{\text{ax}}_{\alpha\beta}$, and the notation $\partial_0 \equiv \partial_t/c$. Thus,

$$h^{Bt}_{lm} \to h^{Bt}_{lm} + \partial_0\Lambda_{lm}, \qquad (l \geq 1), \tag{2.3.7}$$

$$h^{B1}_{lm} \to h^{B1}_{lm} + \left(\partial_r - \frac{2}{r}\right)\Lambda_{lm}, \qquad (l \geq 1), \tag{2.3.8}$$

$$h^{B2}_{lm} \to h^{B2}_{lm} - \Lambda_{lm}, \qquad (l \geq 2). \tag{2.3.9}$$

In these transformations, is possible to see that h^{Bt}_{lm} and h^{B1}_{lm} acquire additional terms involving derivatives of Λ_{lm}, while h^{B2}_{lm} undergoes a simple shift by $-\Lambda_{lm}$. This shows how the axial gauge transformation affects the individual components of $h_{\alpha\beta}$ and provides the specific transformations for the axial harmonics h^{Bt}_{lm}, h^{B1}_{lm}, and h^{B2}_{lm}.
The choice of the Regge-Wheeler (RW) gauge for an axial perturbation consists of choosing Λ_{lm} in such a way that $h^{B2}_{lm} = 0$ for all $l \geq 2$. Thus, after fixing the gauge - the RW gauge - for the axial perturbation $h^{\text{ax}}_{\alpha\beta}$, it has no degrees of freedom with $l = 0$, one degree of freedom with $l = 1$ given by the perturbation h^{B1}_{1m}, and two degrees of freedom for each $l \geq 2$, h^{Bt}_{lm} and h^{B1}_{lm}. Therefore, for $h^{\text{ax}}_{\alpha\beta}$,

$$h^{\text{ax}}_{\alpha\beta}(t, \boldsymbol{x}) = \sum_{l=2}^{\infty} \sum_{m=-l}^{l} h^{Bt}_{lm} (\boldsymbol{t}^{Bt}_{lm})_{\alpha\beta} + \sum_{l=1}^{\infty} \sum_{m=-l}^{l} h^{B1}_{lm} (\boldsymbol{t}^{B1}_{lm})_{\alpha\beta}. \tag{2.3.10}$$

For the polar transformation, it can follow the same procedure as before. Using the previous expression for ξ_α,

$$\begin{aligned} \xi^{\text{pol}}_{\alpha} = &\sum_{l=0}^{\infty} \sum_{m=-l}^{l} (\xi^{(t)}_{lm}(t, r) Y_{lm}, \xi^{(R)}_{lm}(t, r) Y_{lm}, 0, 0) \\ &+ \sum_{l=1}^{\infty} \sum_{m=-l}^{l} \xi^{(E)}_{lm}(t, r)(0, 0, \partial_\theta Y_{lm}, \partial_\phi Y_{lm}) \end{aligned} \tag{2.3.11}$$

This expression shows the components of $\xi^{\text{pol}}_{\alpha}$ in the RW gauge, where $\xi^{(t)}_{lm}$ and $\xi^{(R)}_{lm}$ generate polar perturbations, and $\xi^{(E)}_{lm}$ generates an electric-type perturbation. Which gives

$$\begin{aligned} h^{tt}_{lm} &\to h^{tt}_{lm} - \left[2\partial_0 \xi^{(t)}_{lm} - \frac{A(r) R_S}{r^2} \xi^{(R)}_{lm} \right], \\ h^{Rt}_{lm} &\to h^{Rt}_{lm} - \left[\partial_0 \xi^{(R)}_{lm} + \partial_r \xi^{(t)}_{lm} - \frac{R_S}{r^2 A(r)} \xi^{(t)}_{lm} \right], \\ h^{L0}_{lm} &\to h^{L0}_{lm} - \left[2\partial_0 \xi^{(R)}_{lm} + \frac{R_S}{r^2 A(r)} \xi^{(R)}_{lm} \right], \\ h^{T0}_{lm} &\to h^{T0}_{lm} - \left[2rA(r) \xi^{(R)}_{lm} - l(l+1) \xi^{(E)}_{lm} \right], \end{aligned}$$

as well as

$$\begin{aligned} h^{Et}_{lm} &\to h^{Et}_{lm} - \left[\xi^{(t)}_{lm} + \partial_0 \xi^{(E)}_{lm} \right], \\ h^{E1}_{lm} &\to h^{E1}_{lm} - \left[\left(\partial_r - \frac{2}{r} \right) \xi^{(E)}_{lm} + \partial_0 \xi^{(R)}_{lm} \right], \\ h^{E2}_{lm} &\to h^{E2}_{lm} - \xi^{(E)}_{lm}. \end{aligned}$$

For the polar perturbation, the RW gauge consists of first choosing ξ^E_{lm} with $l \geq 2$ such that $h^{E2}_{lm} = 0$. Then, it can choose ξ^R_{lm} with $l \geq 1$ so that $h^{E1}_{lm} = 0$, and similarly for $\xi^{(t)}_{lm}$ with $l \geq 1$, which gives $h^{Et}_{lm} = 0$. However, there remains the freedom to choose $\xi^{(t)}_{00}$, $\xi^{(R)}_{00}$, and $\xi^{(E)}_{1m}$. The gauge function $\xi^{(E)}_{1m}$ can be used to set $h^{T0}_{1m} = 0$, $\xi^{(R)}_{00}$ can be chosen such that $h^{T0}_{00} = 0$, and $\xi^{(t)}_{00}$ allows us to adjust $h^{Rt}_{00} = 0$. These choices will completely specify the RW gauge, so that the polar perturbation takes the form

$$h^{\text{pol}}_{\alpha\beta}(t, \boldsymbol{x}) = \sum_{l=0}^{\infty} \sum_{m=-l}^{l} \left[h^{tt}_{lm} (\boldsymbol{t}^{tt}_{lm})_{\alpha\beta} + h^{L0}_{lm} (\boldsymbol{t}^{L0}_{lm})_{\alpha\beta} \right] + \sum_{l=1}^{\infty} \sum_{m=-l}^{l} h^{Rt}_{lm} (\boldsymbol{t}^{Rt}_{lm})_{\alpha\beta} + \sum_{l=2}^{\infty} \sum_{m=-l}^{l} h^{T0}_{lm} (\boldsymbol{t}^{T0}_{lm})_{\alpha\beta}. \tag{2.3.12}$$

In this expression, $h^{\text{pol}}_{\alpha\beta}$ is decomposed into different components, each associated with a specific harmonic tensor $\boldsymbol{t}$. The terms h^{tt}_{lm}, h^{L0}_{lm}, h^{Rt}_{lm}, and h^{T0}_{lm} correspond to different physical modes of the gravitational wave in the RW gauge. Using the explicit matrix form of the harmonic tensors $\boldsymbol{t}^a_{lm}$, the polar perturbation in the RW gauge, at a given level (l, m) with $l \geq 2$, takes the form

$$h^{\text{pol}}_{\alpha\beta} = \begin{pmatrix} h^{tt}_{lm} & h^{Rt}_{lm} & 0 & 0 \\ h^{Rt}_{lm} & h^{L0}_{lm} & 0 & 0 \\ 0 & 0 & h^{T0}_{lm} & 0 \\ 0 & 0 & 0 & h^{T0}_{lm} \sin^2\theta \end{pmatrix} Y_{lm}. \tag{2.3.13}$$

In order to compare the above perturbation with the Schwarzschild background metric, after choosing the RW gauge, it is convenient to define new functions $H^{(0)}_{lm}$, $H^{(1)}_{lm}$, $H^{(2)}_{lm}$, and K_{lm} as follows

$$h^{tt}_{lm}(t, r) = A(r) H^{(0)}_{lm}, \tag{2.3.14}$$
$$h^{L0}_{lm}(t, r) = B(r) H^{(2)}_{lm}, \tag{2.3.15}$$
$$h^{T0}_{lm}(t, r) = r^2 K_{lm}, \tag{2.3.16}$$
$$h^{Rt}_{lm}(t, r) = H^{(1)}_{lm}, \tag{2.3.17}$$
$$h^{Bt}_{lm}(t, r) = -h^{(0)}_{lm}, \tag{2.3.18}$$
$$h^{B1}_{lm}(t, r) = -h^{(1)}_{lm}. \tag{2.3.19}$$

In this notation, $A(r)$, $B(r)$, $H^{(0)}_{lm}$, $H^{(1)}_{lm}$, $H^{(2)}_{lm}$, and K_{lm} are functions that depend on the radial coordinate r and time t, and $h^{(0)}_{lm}$ and $h^{(1)}_{lm}$ are additional gauge freedom functions.

In conclusion, in the RW gauge, the most general metric of a perturbed Schwarzschild black hole, $g_{\alpha\beta} = \bar{g}_{\alpha\beta} + h_{\alpha\beta}$, can be expressed as follows

$$\begin{aligned} g_{\alpha\beta}dx^\alpha dx^\beta = &-A(r)(cdt)^2\left[1-\sum_{l=0}^{\infty}\sum_{m=-l}^{l}H_{lm}^{(0)}Y_{lm}\right] + 2cdtdr\left[\sum_{l=1}^{\infty}\sum_{m=-l}^{l}H_{lm}^{(1)}Y_{lm}\right] \\ &+ B(r)dr^2\left[1+\sum_{l=0}^{\infty}\sum_{m=-l}^{l}H_{lm}^{(2)}Y_{lm}\right] + r^2(d\theta^2+\sin^2\theta d\phi^2)\left[\sum_{l=2}^{\infty}\sum_{m=-l}^{l}K_{lm}Y_{lm}\right] \\ &- 2cdtd\theta\frac{1}{\sin\theta}\left[\sum_{l=2}^{\infty}\sum_{m=-l}^{l}h_{lm}^{(0)}\partial_\phi Y_{lm}\right] + 2cdtd\phi\sin\theta\left[\sum_{l=2}^{\infty}\sum_{m=-l}^{l}h_{lm}^{(0)}\partial_\theta Y_{lm}\right] \\ &- 2drd\theta\frac{1}{\sin\theta}\left[\sum_{l=1}^{\infty}\sum_{m=-l}^{l}h_{lm}^{(1)}\partial_\phi Y_{lm}\right] + 2drd\phi\sin\theta\left[\sum_{l=1}^{\infty}\sum_{m=-l}^{l}h_{lm}^{(1)}\partial_\theta Y_{lm}\right]. \quad (2.3.20) \end{aligned}$$

The functions $H^{(0)}$, $H^{(1)}$, $H^{(2)}$, and K describe the polar perturbation, while $h^{(0)}$ and $h^{(1)}$ describe the axial perturbation. From the previous explicit expression, it can be deduced that the perturbation $h_{\alpha\beta}$ in the RW gauge satisfies

$$h_{\theta\phi} = 0, \quad (2.3.21)$$

$$h_{\phi\phi} = h_{\theta\theta}\sin^2\theta, \quad (2.3.22)$$

$$\partial_\phi h_{t\phi} = -\sin\theta\partial_\theta(h_{t\theta}\sin\theta), \quad (2.3.23)$$

$$\partial_\phi h_{r\phi} = -\sin\theta\partial_\theta(h_{r\theta}\sin\theta). \quad (2.3.24)$$

These equations represent the specific relations between the components of the perturbation tensor $h_{\alpha\beta}$ in the RW gauge. They indicate that the perturbation components $h_{\theta\phi}$, $h_{\phi\phi}$, $\partial_\phi h_{t\phi}$, and $\partial_\phi h_{r\phi}$ are determined by the other components through these expressions.

In other words, in the RW gauge, the four gauge functions $\xi_{lm}^{(t)}$, $\xi_{lm}^{(R)}$, $\xi_{lm}^{(E)}$, and $\xi_{lm}^{(B)}$ are chosen in such a way that the four gauge conditions are satisfied. Therefore, by using the four conditions mentioned earlier, it is possible to immediately verify whether a given perturbation is in the RW gauge without the need to first decompose it into tensor harmonics. The choice of these gauge functions allows for a convenient and straightforward analysis of the perturbation in the RW gauge, facilitating the study of the effects on the metric and the properties of the Schwarzschild black hole.

Summarizing, the imposition of the RW gauge has led to the elimination of terms with the highest derivatives in the angles θ and ϕ, specifically, the terms associated with $\boldsymbol{t}_{lm}^{E2}$ and $\boldsymbol{t}_{lm}^{B2}$. These terms correspond to the tensor harmonics that describe GWs at infinity in the TT gauge. However, in order to extract the waveform of the GWs radiated at infinity

by a perturbed black hole, it is necessary to solve the linearized equations in the RW gauge and then transform the solution (or at least its expression in the far zone) back to the TT gauge. This transformation allows to recovery the GW waveform in the TT gauge, where the description of GWs at infinity is more natural and straightforward. Therefore, although the RW gauge simplifies the equations for perturbations and facilitates their analysis, the final step of transforming the solution back to the TT gauge is essential to obtain the accurate waveform of the GWs that are radiated by the perturbed black hole at infinity.

2.3.1 Regge-Wheeler equation

By imposing the RW gauge conditions, equations (2.3.21) - (2.3.24), and using equation (2.3.20), it is possible to simplify the equations governing the perturbation $\Delta G_{\alpha\beta}$ in a black hole space-time, given by equation (2.0.5). Focusing on the axial perturbations, which arise from the components $(\alpha\beta) = (t\phi)$, $(r\phi)$, and $(\theta\phi)$, it arrives at the following set of equations (Regge and Wheeler, 1957; Chandrasekhar and Detweiler, 1975)

$$\partial_r^2 h_{lm}^{(0)} - \left(\partial_r + \frac{2}{r}\right)\partial_0 h_{lm}^{(1)} + \frac{1}{A}\left[\frac{2}{r}\frac{dA}{dr} - \frac{l(l+1)}{r^2}\right] h_{lm}^{(0)} = \frac{16\pi G}{c^4 A} s_{lm}^{Bt}, \tag{2.3.25}$$

$$\partial_0^2 h_{lm}^{(1)} - \left(\partial_r - \frac{2}{r}\right)\partial_0 h_{lm}^{(0)} + A\frac{(l-1)(l+2)}{r^2} h_{lm}^{(1)} = -\frac{16\pi G}{c^4} A\, s_{lm}^{B1}, \tag{2.3.26}$$

$$\frac{1}{A}\partial_0 h_{lm}^{(0)} - \partial_r(A h_{lm}^{(1)}) = -\frac{16\pi G}{c^4} s_{lm}^{B2}. \tag{2.3.27}$$

Here, the first two equations hold for $l \geq 1$, and the last one hold for $l \geq 2$. In the RW gauge, it has the freedom to set the axial function s_{lm}^{B2} to zero, which leads to three equations for two unknowns, $h_{lm}^{(0)}$ and $h_{lm}^{(1)}$. It is important to notice that the gauge invariance of the perturbation equations implies that the three equations for the axial perturbations are not independent. In the case of vacuum equations, where the right-hand sides are set to zero, consistency is guaranteed by the Bianchi identities. These identities, specifically the equation $\bar{D}_\alpha \bar{G}^{\alpha\beta} = 0$, where $\bar{D}_\alpha$ represents the covariant derivative with respect to the Schwarzschild metric and $\bar{G}^{\alpha\beta}$ is the Einstein tensor in the Schwarzschild metric, ensure the preservation of the underlying geometry and the validity of the perturbation equations within the framework of general relativity. The functions s_{lm}^{Bt}, s_{lm}^{B1}, and s_{lm}^{B2} are sourced by matter distributions, and $A(r)$ is the radial component of the metric tensor. Sets these three terms of matter to zero, the time derivative of the equation (2.3.25) is automatically verified, this is easily obtained by using equation (2.3.27) to eliminate $\partial_0 h_{lm}^{(0)}$ from equation (2.3.26) and from the time derivative of equation (2.3.25), and then using equation (2.3.26) to eliminate $\partial_0^2 h_{lm}^{(0)}$. Thus, for the vacuum case, the three equations above imply that

$$\partial_r^2 h_{lm}^{(0)} - \left(\partial_r + \frac{2}{r}\right)\partial_0 h_{lm}^{(1)} + \frac{1}{A}\left[\frac{2}{r}\frac{dA}{dr} - \frac{l(l+1)}{r^2}\right] h_{lm}^{(0)} = f_{lm}(r), \tag{2.3.28}$$

where $f_{lm}(r)$ is a arbitrary function of r and independent of t. Therefore, equations (2.3.26) and (2.3.27) imply equation (2.3.25), except for the freedom of adding a time-independent part to $h_{lm}^{(0)}$. This is evident from the presence of $\partial_0 h_{lm}$ in equations (2.3.26) and (2.3.27), while $h_{lm}^{(0)}$ itself does not appear. The presence of this time-independent part can be fixed by imposing the boundary condition that the black hole is unperturbed as t approaches $-\infty$. In the presence of a non-zero source term, such as matter or energy-momentum, the consistency between the three equations is ensured by the covariant conservation of the matter energy-momentum tensor, expressed as $\bar{D}_\alpha \bar{T}^{\alpha\beta} = 0$. This conservation law guarantees that the matter distribution remains consistent with the gravitational perturbations. Additionally, it ensures the overall consistency between the Einstein equations and the Bianchi identity. This means that the matter source must move along the geodesics of the Schwarzschild metric (Maggiore, 2018).

After eliminating $\partial_0 h_{lm}^{(0)}$, it i possible to obtain a equation only dependent of $h_{lm}^{(1)}$. So, here, is useful to introduce the RW function $Q_{lm}(t,r)$, defined as (Maggiore, 2018; Chandrasekhar and Detweiler, 1975)

$$Q_{lm}(t,r) = \frac{1}{r}A(r)h_{lm}^{(1)}(t,r). \tag{2.3.29}$$

Substituting this expression into the equations, it is possible to obtain a single equation known as the Regge-Wheeler equation, as follows

$$\left[(\partial_*^2 - \partial_0^2) - V_l^{RW}(r)\right] Q_{lm} = S_{lm}^{ax}(t,r), \tag{2.3.30}$$

where $\partial_* \equiv \partial/\partial r_*$, and r_* represents the tortoise coordinate. It is convenient to introduce this coordinate because, unlike r that contains a singularity at $r = 2M$, r_* covers the entire spectrum of the potential from $-\infty$ to $+\infty$. In this way, one can study the entire potential without having to deal with the event horizon, the difference between the potential in both coordinates will be shown below. So, the new coordinate can be defined as

$$r_* = r + R_S \log\frac{r - R_R}{R_S} \tag{2.3.31}$$

In summary, by imposing the gauge conditions of RW and defining the RW function, it simplifies the equations for the axial perturbations in a black hole space-time, leading to the Regge-Wheeler equation, which characterizes the dynamics of these perturbations. The source term will be expressed by

$$S_{lm}^{ax}(t,r) = \frac{16\pi G}{c^4}\frac{A(r)}{r}\left\{A(r)s_{lm}^{B1}(t,r) + \left(\partial_r - \frac{2}{r}\right)\left[A(r)s_{lm}^{B2}(t,r)\right]\right\}, \tag{2.3.32}$$

and $V_l^{RW}(r)$ is the RW potential, express by

$$V_l^{RW}(r) = A(r)\left[\frac{l(l+1)}{r^2} - \frac{3R_S}{r^3}\right]. \tag{2.3.33}$$

This potential also can be expressed in a unified way, such as

$$V_l^{RW}(r) = A(r)\left[\frac{l(l+1)}{r^2} + (1-\sigma^2)\frac{R_S}{r^3}\right]. \tag{2.3.34}$$

The potential $V_l^{RW}(r)$ incorporates the influence of the black hole's gravitational field, given by the term $l(l+1)/r^2$, and the effect of its mass M, represented by the term $3GM/c^2r^3$.The specific value of σ characterizes the nature of the perturbations and reflects the behavior of the corresponding fields under certain transformations. Scalar perturbations have no preferred direction and are invariant under rotations (hence $\sigma = 0$), while axial gravitational perturbations exhibit a preferred direction along the axis of rotation ($\sigma = 2$). Electromagnetic perturbations, on the other hand, have a preferred direction associated with the polarization of the electromagnetic field ($\sigma = 1$). Indeed, it is quite remarkable that the equation for electromagnetic perturbations can also be written in the same form as the equations for scalar and axial gravitational perturbations, albeit with a different value of σ.

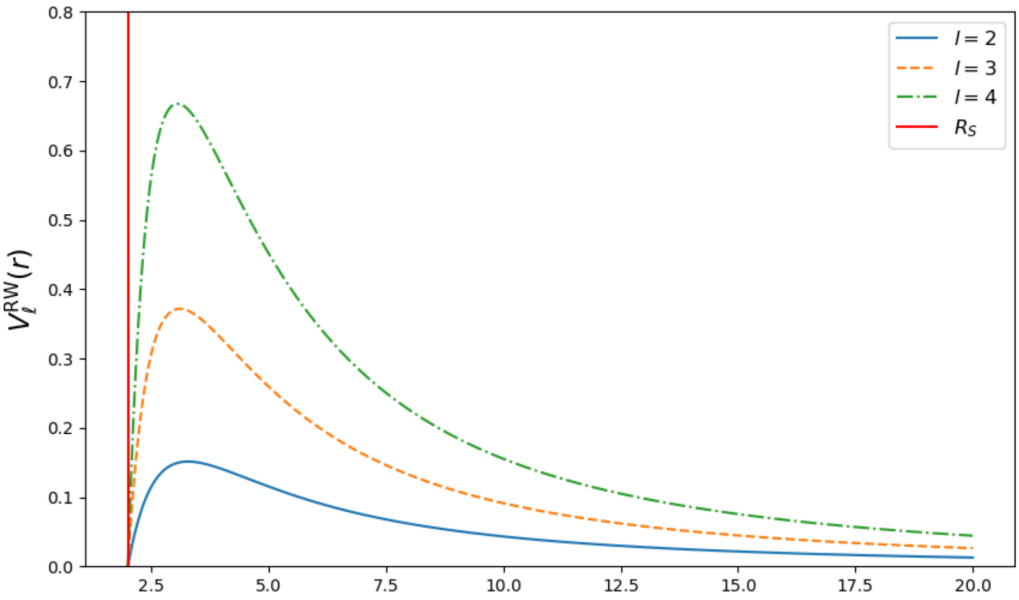
For convenience, it is useful to perform a Fourier transform on the Regge-Wheeler function Q_{lm}, given by

$$Q_{lm}(t,r) = \frac{1}{2\pi}\int_{-\infty}^{\infty} d\omega \tilde{Q}_{lm}(\omega,r)e^{-i\omega t}. \tag{2.3.35}$$

In this representation, $\tilde{Q}_{lm}(\omega,r)$ also satisfies a Schrödinger-like equation, equation (2.3.30). To visualize the potential $V_l^{RW}(r)$, it can be plotted as a function of r and r_*, this potential

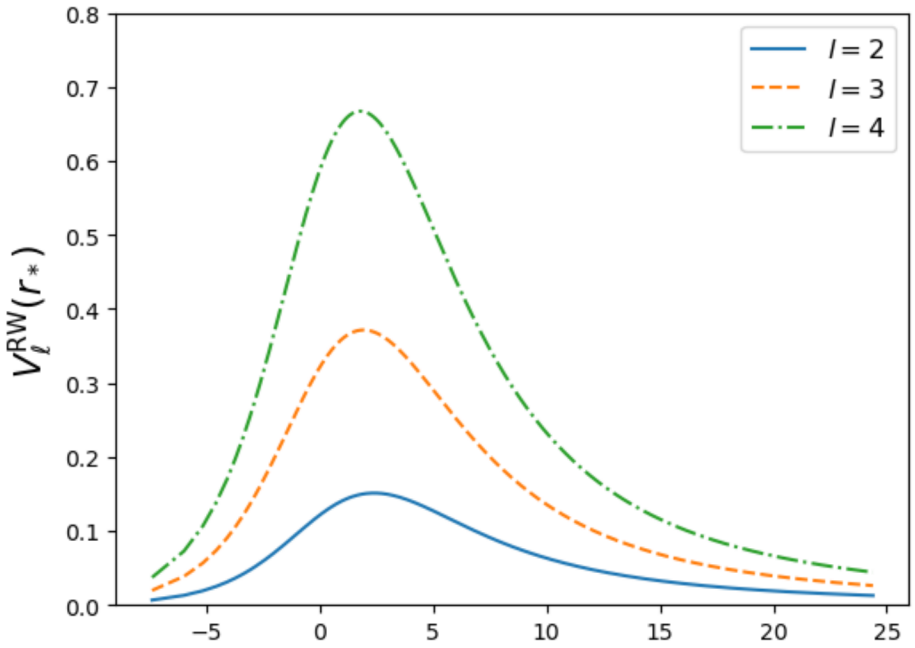
determines the behavior of the perturbation wavefunction for different angular modes l. In Figure 1 it is expressed the $V_l^{RW}(r)$, as a function of r, for $l = 2, 3, 4$, and in Figure 2 it is plotted as a function of r_* .

Figure 1 – Potential $V_l^{RW}(r)$, where r is in units of GM/c^2, with the horizon at $r = 2$.



Source: plotted by the author

Figure 2 – Potential $V_l^{RW}(r_*)$, where r_* is in units of GM/c^2, with the horizon at $r_* = -\infty$.



Source: plotted by the author

A similar process made in equation (2.3.35) can be done with (2.3.32). So, equation (2.3.30) can be express as

$$\frac{d^2}{dr_*^2}\tilde{Q}_{lm} + \left[\frac{\omega^2}{c^2} - V_l^{RW}(r)\right]\tilde{Q}_{lm} = \tilde{S}_{lm}^{ax}(\omega, r), \tag{2.3.36}$$

in the following sections, c^2 will be assumed to be 1 and the above expression will be studied with only the term ω^2 as the energy term.

2.3.2 Zerilli equation

When linearizing the Einstein equations around the Schwarzschild metric, additional equations involving the four polar perturbations $H_{lm}^{(0)}$, $H_{lm}^{(1)}$, $H_{lm}^{(2)}$ e K_{lm} are obtained. However, the derivation of these equations is more involved compared to the axial perturbations. In total, there are seven equations, with some being dynamical equations and others serving as constraints on the initial data. To simplify the equations, the gravitational constant G and the speed of light c will be equal to 1. Additionally, it is convenient to perform a Fourier transform with respect to time to obtain a frequency-domain representation. This can be achieved by defining the Fourier transform of a function $f(t)$ as

$$\tilde{f}_{lm}(\omega, r) = \int_{-\infty}^{\infty} dt\, f_{lm}(t, r)e^{i\omega t}, \tag{2.3.37}$$

for all four polar perturbations as the Source term of the Zerilli equation,

$$\tilde{s}_{lm}^{a}(\omega, r) = \int_{-\infty}^{\infty} dt\, s_{lm}^{a}(t, r)e^{i\omega t}. \tag{2.3.38}$$

By applying this Fourier transform to the perturbation variables, they can be expressed in terms of their frequency-domain counterparts, denoted by a tilde symbol. The Fourier-transformed equations for the polar perturbations involve both dynamical equations and constraint equations that determine the initial data. The details of these equations and their derivation are not that simply and require thorough treatment, the explicit derivation will be done next. However, it is worth noting that these equations provide a description of the gravitational field perturbations in terms of the polar perturbation variables. These perturbations capture the gravitational field fluctuations in different angular directions and contribute to the overall characterization of the perturbed space-time.

As said before, for polar perturbations in a black hole space-time, there are in principle seven equations. However, when expanded in tensor harmonics, these equations

can be grouped into different categories based on their angular dependence and the corresponding coefficients of the energy-momentum tensor. When expanded in tensor harmonics, four of them involve polar perturbations that start from $l = 0$, while two equations involve quantities with $l > 1$ and one involve quantities whose expansion starts from $l = 2$. To begin, the four equations that hold for $l \geq 0$ are

$$A^2\partial_r^2 K + A\left(3 - \frac{5M}{r}\right)\frac{1}{r}\partial_r K - A^2\frac{1}{r}\partial_r H^{(2)} + \frac{A}{r^2}(K - H^{(2)}) - A\frac{l(l+1)}{2r^2}(K + H^{(2)}) = -8\pi s^{tt}, \tag{2.3.39}$$

$$\partial_t\left(\partial_r K + \frac{1}{r}(K - H^{(2)}) - \frac{M}{r^2 A}\right) - \frac{l(l+1)}{2r^2}H^{(1)} = -8\pi s^{Rt}, \tag{2.3.40}$$

$$\frac{1}{A^2}\partial_t^2 K - \frac{1 - M/r}{rA}\partial_r K - \frac{2}{rA}\partial_t H^{(1)} + \frac{1}{2}\partial_r H^{(0)} - \frac{1}{r^2 A}(K - H^{(2)}) + \frac{l(l+1)}{2r^2 A}(K - H^{(0)}) = -8\pi s^{L0}, \tag{2.3.41}$$

and

$$-\frac{1}{A}\partial_t^2(K + H^{(2)}) + A\partial_r^2(K - H^{(0)}) + \left(1 - \frac{M}{r}\right)\frac{2}{r}\partial_r K + 2\partial_r\partial_t H^{(1)} + \frac{2}{rA}\left(1 - \frac{M}{r}\right)\partial_t H^{(1)} - \frac{1}{r}\left(1 - \frac{M}{r}\right)\partial_r H^{(2)} - \frac{1}{r}\left(1 + \frac{M}{r}\right)\partial_r H^{(0)} - \frac{l(l+1)}{2r^2}(H^{(2)} - H^{(0)}) = \frac{16\pi s^{T0}}{r^2}. \tag{2.3.42}$$

Where $H_{lm}^{(1)}$ vanishes for $l = 0$, and K_{lm} vanishes for $l = 0, 1$. The two equations that hold for $l \geq 1$ are

$$\partial_r(AH^{(1)}) - \partial_t(K + H^{(2)}) = 16\pi s^{Et}, \tag{2.3.43}$$

$$\frac{1}{A}\partial_t H^{(1)} + \partial_t(K - H^{(0)}) - \frac{2M}{Ar^2}H^{(0)} - \frac{1 - M/r}{Ar}(H^{(2)} - H^{(0)}) = -16\pi s^{E1}. \tag{2.3.44}$$

And, the last one, which holds for $l \geq 2$ is

$$H^{(0)} - H^{(2)} = 32\pi s^{E2}. \tag{2.3.45}$$

Here, the case being considered is that of $l \geq 2$, a choice that corresponds to the radiative degrees of freedom in the system. The equations corresponding to $l = 0$ and $l = 1$ capture the evolution of the non-radiative degrees of freedom in the system, which include mass, momentum, and angular momentum. These perturbations describe the changes in

these physical quantities as the system evolves. For example, in the case of the infall of a particle with mass m into a black hole of mass M, the $l = 0$ perturbation accounts for the change in the Schwarzschild mass of the system from M to $M + m$. This perturbation characterizes the variation in the total mass of the system due to the presence of the infalling particle. Regarding the $l = 1$ axial perturbation, it exhibits interesting properties in different scenarios. For a test particle following a trajectory $R(t)$, this perturbation vanishes for $r < R(t)$, indicating that it does not have an effect within the region inside the particle's trajectory. However, for $r > R(t)$, the $l = 1$ axial perturbation carries an angular momentum that is equal to the angular momentum of the orbiting particle. This perturbation captures the rotational effects associated with the motion of the particle in the gravitational field of the black hole. On the other hand, the $l = 1$ polar perturbations can be eliminated through a gauge transformation. This transformation corresponds to a translation of the center of mass of the system (Zerilli, 1970).

For each (l, m) with $l > 2$, there are seven equations involving four unknown functions $H_{lm}^{(0)}$, $H_{lm}^{(1)}$, $H_{lm}^{(2)}$ e K_{lm}. This apparent mismatch in the number of equations and unknowns is a result of gauge invariance. Gauge invariance allows us to reduce the number of independent functions in the polar perturbations from seven to four. Similarly to the axial case, gauge invariance implies that the equations are not independent, and a solution exists. Therefore, even though there are more equations than unknowns, the system is still solvable due to the underlying gauge symmetry.
Equation (2.3.45) allows to eliminate of $H_{lm}^{(0)}$ immediately, resulting in six equations involving three functions. The presence of an algebraic relation like (2.3.45) might seem surprising at first. However, let t_0 be the initial time at which one assigns the initial conditions for the system of differential equations. At $t = t_0$, one has the freedom to choose the values of the energy-momentum tensor, and consequently, the value of s_{lm}^{E2}. It might also be expected that one has the freedom to choose the initial conditions for $H_{lm}^{(0)}$ and $H_{lm}^{(2)}$. Equation (2.3.45) reveals that the initial condition for $H_{lm}^{(0)}$ uniquely determines the initial condition for $H_{lm}^{(2)}$ in the presence of an external perturbation. This result arises from the fundamental structure of the Einstein equations. As it is known, the Einstein equations consist of 10 components, with some serving as dynamic equations and others as constraints on the initial data. Equation (2.3.45) represents a constraint on the initial data, indicating that the choice of initial condition for $H_{lm}^{(0)}$ imposes a specific requirement on the initial condition for $H_{lm}^{(2)}$ in order to satisfy the equations of general relativity. For example, if s_{lm}^{E2} vanishes at the initial time, it implies that $H_{lm}^{(0)}$ and $H_{lm}^{(2)}$ must be equal at the initial time. On the other hand, if s_{lm}^{E2} is non-zero and specified at the initial time, it uniquely determines the value of $H_{lm}^{(0)}$ at all subsequent times in terms of $H_{lm}^{(0)}$. In essence, equation (2.3.45) acts as a constraint on the initial data, which remains satisfied throughout the evolution of the system according to the equations of motion. This constraint ensures the consistency and self-conservation of the gravitational perturbations.

To simplify the remaining six equations, it is convenient to perform a Fourier transform with respect to the time variable, as described in equation (2.3.35). Here, will be denoted the Fourier transforms of $K(t,r)$, ..., $H^{(2)}(t,r)$ as $\tilde{K}(\omega,r)$, ..., $\tilde{H}^{(2)}(\omega,r)$, respectively, and the Fourier transforms of $s^a(t,r)$ as $\tilde{s}^a(\omega,r)$. In this Fourier space, the time derivative in equation (2.3.40) introduces a factor of $(-i\omega)$, leading to

$$\left(\partial_r + \frac{r-3M}{r^2A}\right)\tilde{K} - \frac{1}{r}\tilde{H}^{(2)} + \frac{l(l+1)}{2i\omega r^2}\tilde{H}^{(1)} = \frac{8\pi}{i\omega}\tilde{s}^{Rt}. \tag{2.3.46}$$

Equation (2.3.44) can be solved for $\partial_r\tilde{H}^{(2)}$ by eliminating $\partial_r\tilde{K}$ using equation (2.3.46) and eliminating $\tilde{H}^{(0)}$ using equation (2.3.45). Which gives

$$\begin{aligned}&\left(\partial_r - \frac{r-4M}{r^2A}\right)\tilde{H}^{(2)} + \frac{r-3M}{r^2A}\tilde{K} + \left[\frac{i\omega}{A} + \frac{l(l+1)}{2i\omega r^2}\right]\tilde{H}^{(1)} \\ &= \frac{8\pi}{i\omega}\tilde{s}^{Rt} + 32\pi\left[\frac{r-3M}{r^2A} - \partial_r\right]\tilde{s}^{E2} + 16\pi\tilde{s}^{E1}.\end{aligned} \tag{2.3.47}$$

The derivative of $\partial_r\tilde{H}^{(1)}$ can be obtained from equation (2.3.43), as follow

$$\left(\partial_r + \frac{2M}{r^2A}\right)\tilde{H}^{(1)} + \frac{i\omega}{A}(\tilde{K} + \tilde{H}^{(2)}) = \frac{16\pi}{A}\tilde{s}^{Et}. \tag{2.3.48}$$

It is evident that once specified the external source and set the initial conditions for $\tilde{K}$, $\tilde{H}^{(1)}$, and $\tilde{H}^{(2)}$, equations (2.3.46), (2.3.47), and (2.3.48) uniquely determine the solution. Therefore, the remaining equations of motion must either be redundant or serve as constraints on the initial values. In fact, by utilizing equations (2.3.46)–(2.3.48) and the covariant conservation of the energy-momentum tensor, it can be easily verified that equations (2.3.39) and (2.3.42), which are the only second-order equations in ∂_r, are automatically satisfied. By performing the Fourier transform, and substituting $\partial_r\tilde{K}$ from equation (2.3.46) and $\partial_r\tilde{H}^{(0)}$ from equations (2.3.45) and (2.3.47), it finds that equation (2.3.41) provides an algebraic relation among $\tilde{K}$, $\tilde{H}^{(1)}$, $\tilde{H}^{(2)}$, and the external source, expressed by

$$\begin{aligned}&\frac{\lambda r^2A + Mr - 3M^2 - \omega^2r^4}{rA}\tilde{K} + \frac{(\lambda+1)M - \omega^2r^3}{i\omega r}\tilde{H}^{(1)} - (\lambda r + 3M)\tilde{H}^{(1)} \\ &= \frac{8\pi Mr}{i\omega}\tilde{s}^{Rt} + 32\pi(\lambda r + 3M)\tilde{s}^{E2} - 8\pi r^2A(r\tilde{s}^{L0} + 2\tilde{s}^{E1}),\end{aligned} \tag{2.3.49}$$

where it was defined

$$\lambda = \frac{(l-1)(l+2)}{2}. \tag{2.3.50}$$

Just like equation (2.3.45), this algebraic relation serves as a constraint on the initial data. Alternatively, it can be interpreted as a first integral of the equations of motion (2.3.46)-(2.3.48). To ensure consistency between these two equations, it can use the equation (2.3.49) to eliminate, for example, $\tilde{H}^{(2)}$ from two of the first-order equations (2.3.46)-(2.3.48). By verifying that the third equation is automatically satisfied (taking into account the right-hand side using the covariant conservation of $T^{\mu\nu}$), it confirms the validity of this algebraic relation.

Using equation (2.3.49), it can eliminate one of the functions $\tilde{K}$, $\tilde{H}^{(1)}$, $\tilde{H}^{(2)}$ from equations (2.3.46)-(2.3.48), resulting in two first-order equations for two functions. If eliminate, for example, $\tilde{H}^{(2)}$, equations (2.3.46) and (2.3.48) become

$$\partial_r \tilde{K} + a_1(r)\tilde{K} + a_2(r)\tilde{H}^{(1)} = j_1, \tag{2.3.51}$$

$$\partial_r \tilde{H}^{(1)} + b_1(r)\tilde{K} + b_2(r)\tilde{H}^{(1)} = j_2, \tag{2.3.52}$$

where

$$a_1(r) = \frac{2Mr - \lambda Mr - 6M^2 + \omega^2 r^4}{r(r-2M)(\lambda r + 3M)}, \tag{2.3.53}$$

$$a_2(r) = \frac{\lambda(\lambda+1)r + 2(\lambda+1)M + \omega^2 r^3}{i\omega r(\lambda r + 3M)}, \tag{2.3.54}$$

and

$$b_1(r) = i\omega r \frac{2\lambda r^2 + 4Mr - 4\lambda Mr - 9M^2 - \omega^2 r^4}{(r-2M)^2(\lambda r + 3M)}, \tag{2.3.55}$$

$$b_2(r) = \frac{3\lambda Mr + Mr + 6M^2 - \omega^2 r^4}{r(r-2M)(\lambda r + 3M)}. \tag{2.3.56}$$

At last, for the source term

$$j_1 = \frac{1}{i\omega}\frac{\lambda r + 2M}{\lambda r + 3M} 8\pi \tilde{s}^{Rt} - \frac{32\pi}{r}\tilde{s}^{E2} + \frac{8\pi r A}{\lambda r + 2M}(r\tilde{s}^{L0} + 2\tilde{s}^{E1}), \tag{2.3.57}$$

$$j_2 = \frac{16\pi}{A}\tilde{s}^{Et} + \frac{Mr}{A(\lambda r + 3M)} 8\pi \tilde{s}^{Rt} + i\omega \frac{32\pi}{A}\tilde{s}^{E2} - i\omega \frac{8\pi r^2}{\lambda r + 2M}(r\tilde{s}^{L0} + 2\tilde{s}^{E1}). \tag{2.3.58}$$

It is possible to simplify the system of two first-order equations by introducing a new function $\tilde{Z}(\omega, r)$ (which actually has indices l and m, but they were omitted for simplicity). Instead of solving equation (2.3.51) for $\tilde{H}^{(1)}$ and substituting it into equation (2.3.52), so, rewrite the equations as follows

$$\tilde{Z} = \frac{r^2}{\lambda r + 3M}\tilde{K} + \frac{rA}{i\omega(\lambda r + 3M)}\tilde{H^{(1)}}. \tag{2.3.59}$$

Taking the derivative with respect to r of this equation, and using equations (2.3.51) and (2.3.52), it can be expressed $\partial_r \tilde{Z}$ in terms of $\tilde{K}$, $\tilde{H}^{(1)}$ and source terms. The outcome is the following

$$\partial_r \tilde{Z} = \frac{-\lambda r^2 + 3\lambda M r + 3M^2}{A(\lambda r + 3M)^2}\tilde{K} - \frac{\lambda(\lambda+1)r^2 + 3\lambda M r + 6M^2}{i\omega r(\lambda r + 3M)^2}\tilde{H^{(1)}} + J, \tag{2.3.60}$$

where

$$J = \frac{8\pi r}{i\omega(\lambda r + 2M)}(r\tilde{s}^{L0} + 2\tilde{s}^{E1}). \tag{2.3.61}$$

To express $\tilde{K}$ and $\tilde{H}^{(1)}$ in terms of $\tilde{Z}$ and its derivative, as well as the source term J, it can be started with equations (2.3.59) and (2.3.60), as follows

$$\tilde{K} = \frac{\lambda(\lambda+1)r^2 + 3\lambda M r + 6M^2}{r^2(\lambda r + 3M)}\tilde{Z} + A\partial_r\tilde{Z} - AJ, \tag{2.3.62}$$

$$\tilde{H}^{(1)} = -i\omega\frac{\lambda r^2 - 3\lambda M r - 3M^2}{rA(\lambda r + 3M)}\tilde{Z} - i\omega r\partial_r\tilde{Z} - i\omega r J. \tag{2.3.63}$$

Therefore, given the external source, $\tilde{K}$ and $\tilde{H}^{(1)}$ are determined, once $\tilde{Z}$ is known. The two remaining polar perturbations $\tilde{H}^{(0)}$ and $\tilde{H}^{(2)}$ are then obtained using equations (2.3.45) and (2.3.49). To obtain a differential equation that involves only $\tilde{Z}$, it takes one more derivative of the equation (2.3.60). The expression of the resulting derivatives $\partial_r\tilde{K}$ and $\partial_r\tilde{H}^{(1)}$ in terms of $\tilde{K}$, $\tilde{H}^{(1)}$ using equations (2.3.51) and (2.3.52), and then the resulting terms $\tilde{K}$ and $\tilde{H}^{(1)}$ are written in terms of $\tilde{Z}$ and $\partial_r\tilde{Z}$ using equations (2.3.62) and (2.3.63). This procedure leaves the result as follows

$$\frac{d^2}{dr_*^2}\tilde{Z}_{lm} + \left[\omega^2 - V_l^Z(r)\right]\tilde{Z}_{lm} = \tilde{S}_{lm}^{pol}, \tag{2.3.64}$$

this expression is known as *Zerilli Equation*, where the potential is

$$V_l^Z(r) = A(r)\frac{2\lambda^2(\lambda+1)r^3 + 6\lambda^2 M r^2 + 18\lambda M^2 r + 18M^3}{r^3(\lambda r + 3M)^2}, \tag{2.3.65}$$

with the source term represented by

$$\begin{aligned}\tilde{S}_{lm}^{pol} = A\partial_r(AJ_{lm}) - \frac{16\pi\tilde{s}_{lm}^{Et}}{i\omega}\frac{A\left[\lambda(\lambda+1)r^2 + 3Mr\lambda + 6M^2\right]}{r(\lambda r+3M)^2} \\ - \frac{8\pi\tilde{s}_{lm}^{Rt}}{i\omega}\frac{\lambda r^2 A^2}{(\lambda r+3M)^2} + 8\pi(r\tilde{s}_{lm}^{L0} + 2\tilde{s}_{lm}^{E1})\frac{rA^2}{\lambda r+3M} - \frac{32\pi A}{r}\tilde{s}_{lm}^{E2},\end{aligned} \tag{2.3.66}$$

where

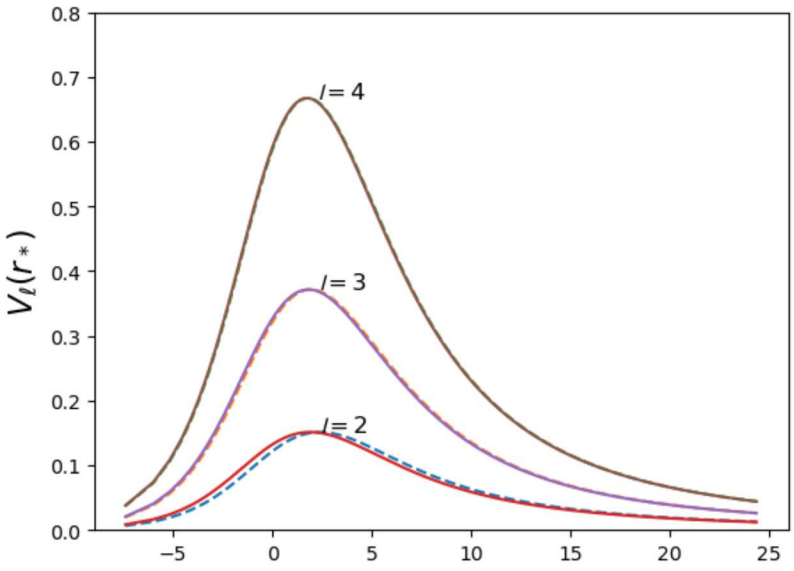
$$J_{lm} = \frac{r}{i\omega(\lambda r+3M)}8\pi(r\tilde{s}_{lm}^{Rt} + 2\tilde{s}_{lm}^{Et}). \tag{2.3.67}$$

Additionally, although the Zerilli potential, $V_l^Z(r)$, has a more complex analytic form, it is numerically nearly identical to the RW potential, particularly for large values of l, as illustrated in Figure 3. Furthermore, both potentials exhibit the same asymptotic behavior at large r

$$V_l^Z(r) \sim V_l^{RW} \sim \frac{l(l+1)}{r^2}, \tag{2.3.68}$$

when $r \to \infty$, and as r approaches R_S (the Schwarzschild radius), both $V_l^Z(r)$ and V_l^{RW} approaches to zero, similar to $A(r)$ (although with different proportionality constants). Additionally, these two potentials share exactly the same spectrum of quasi-normal modes, see more on Section 26 of Chandrasekhar (1983)

Figure 3 – The Zerilli potential, V_l^Z (solid lines), and the RW potential, V_l^{RW} (dashed lines), as functions of r_* for three different values of l. The potential is measured in units of $(GM/c^2)^{-2}$.



Source: plotted by the author

3 Quasi-normal modes

The problem of characterizing Black Hole perturbations has been reduced to solving two differential equations

$$\frac{d^2}{dr_*^2}\tilde{Q}_{lm} + \left[\frac{\omega^2}{c^2} - V_l^{RW}(r)\right]\tilde{Q}_{lm} = \tilde{S}_{lm}^{ax}, \tag{3.0.1}$$

$$\frac{d^2}{dr_*^2}\tilde{Z}_{lm} + \left[\omega^2 - V_l^{Z}(r)\right]\tilde{Z}_{lm} = \tilde{S}_{lm}^{pol}. \tag{3.0.2}$$

These equations describe oscillations of space-time that can be interpreted as a characteristic "ringing" of black holes. The solutions to these equations correspond to the modes of vibration or oscillation of the black hole, analogous to the way a ringing bell produces different tones or frequencies. This phenomenon is often referred to as the "quasinormal mode" of black holes, representing the characteristic vibrational patterns of their event horizons. However, to fully specify the problem that is being studied, boundary conditions must be assigned to these equations. The extra c^2 of equation (3.0.1) is that the coefficients of the superposition of plane waves, i.e. B_{lm}^{out}, of equation (3.0.1) and, A_{lm}^{out}, of equation (3.0.2) have the same dimensions.

3.1 Boundary Conditions

In general, there are various possible ways to choose the boundary conditions for a second-order differential equation defined between $-\infty < r_* < +\infty$, and the appropriate choice depends on the physics of the problem. First and foremost, comes the analysis of the possible asymptotic behaviors of both equations. Considering $r_* \to +\infty$ first, here the analysis will restrict to an energy-momentum tensor that vanishes more rapidly than $1/r^2$, ensuring that the perturbation's energy remains finite when integrated. Both the RW and Zerilli potentials vanish as $1/r^2$ for large r, so in the limit of large r, the RW and Zerilli equations become approximately free equations, i.e. harmonic oscillator solutions. Consequently, the general solution $Z_{lm}(t, r)$ of the Zerilli equation for $r_* \to \infty$ will be a superposition of plane waves (Zerilli, 1970). This implies that the perturbations exhibit a wave-like behavior as they propagate away from the black hole, with each mode characterized by a specific frequency and wavevector. Such as

$$Z_{lm}(t, r_*) \to \int_{-\infty}^{+\infty} d\omega \left[A_{lm}^{out}(\omega)e^{-i\omega(t-r_*/c)} + C_{lm}^{in}(\omega)e^{-i\omega(t+r_*/c)}\right], \tag{3.1.1}$$

where, once $Z_{lm}(t,r)$ is real

$$A^{out}_{lm}(\omega) = [A^{out}_{lm}(-\omega)]^*, \qquad C^{in}_{lm}(\omega) = [C^{in}_{lm}(-\omega)]^*. \tag{3.1.2}$$

The solution that is proportional to $e^{-i\omega(t-r_*/c)}$ represents radiation that escapes to infinity (*purely outgoing*), while $e^{-i\omega(t+r_*/c)}$ describes radiation coming from infinity towards the black hole (*purely incoming*). As mentioned before, the boundary conditions to be imposed will depend on the physics of the problem. Therefore, for a Schwarzschild space-time perturbed by an external agent at an initial time t_0, at this time $Z_{lm}(t_0,r)$ and $Q_{lm}(t_0,r)$ will be non-zero. Thus, a good question is how these perturbations will evolve. In general, part of the perturbation will be propagated to infinity, while another part will be propagated toward the black hole, as shown in Figure 4. Therefore, as $r_* \to +\infty$, will have purely outgoing waves. For the purposes of this work, it is not interesting the case where gravitational radiation is incident upon the black hole from infinity, so it sets $C^{in}_{lm}(\omega) = 0$, on equation (3.1.1) and in Figure 5. So, for $r = +\infty$ (and consequentially $r_* \to +\infty$),

$$Z_{lm}(t,r) \to \int_{-\infty}^{+\infty} d\omega A^{out}_{lm}(\omega) e^{-i\omega(t-r_*/c)}. \tag{3.1.3}$$

Similarly, for the axial perturbation

$$Q_{lm}(t,r) \to \int_{-\infty}^{+\infty} d\omega \, \frac{\omega}{c} \, B^{out}_{lm}(\omega) e^{-i\omega(t-r_*/c)}. \tag{3.1.4}$$

To determine the possible solutions for $r_* \to -\infty$, it is needed to observe that the potentials

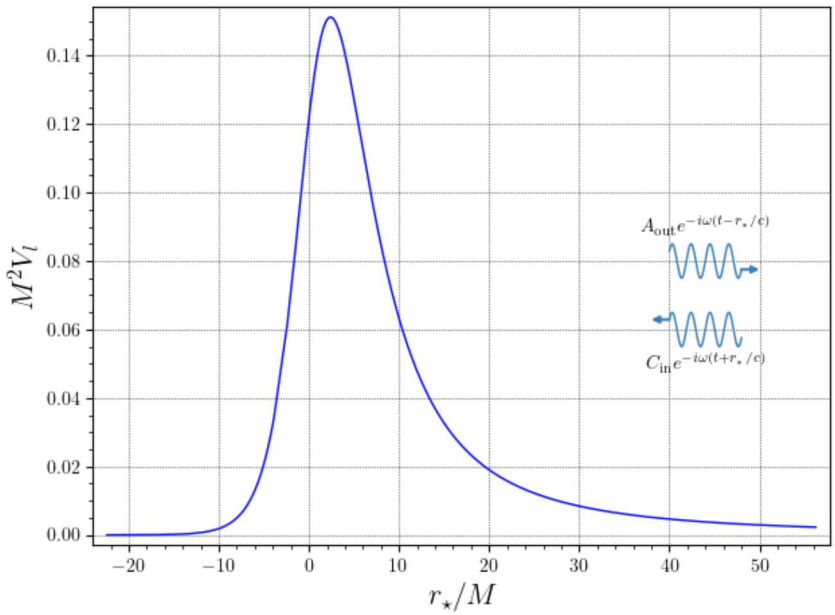
$$V^{RW}_l(r) = A(r)\left[\frac{l(l+1)}{r^2} - \frac{3R_S}{r^3}\right], \tag{3.1.5}$$

$$V^{Z}_l(r) = A(r)\frac{2\lambda^2(\lambda+1)r^3 + 6\lambda^2 M r^2 + 18\lambda M^2 r + 18M^3}{r^3(\lambda r + 3M)^2}, \tag{3.1.6}$$

near the horizon vanish due to $A(r)$, and near the horizon, $r \simeq R_S$. So, the relation between r_* and r becomes

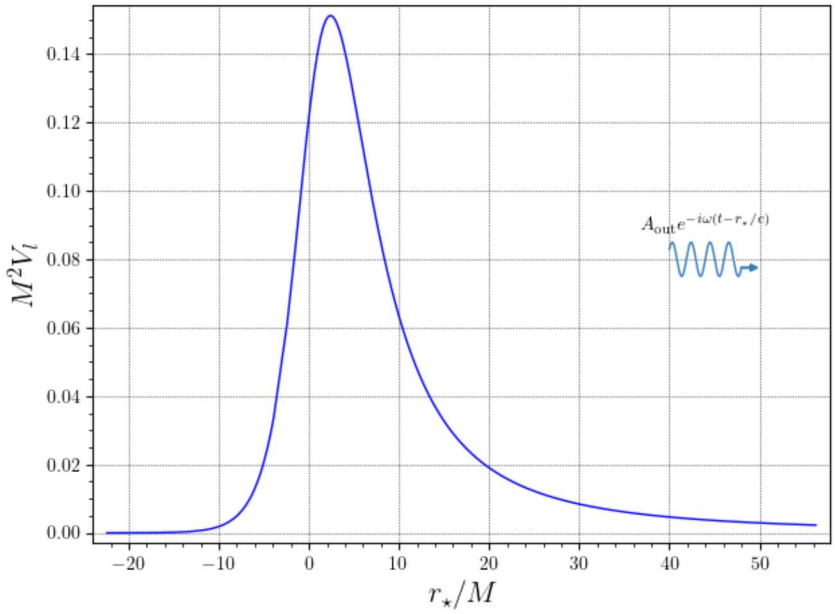
$$r_* \simeq R_S + R_S \log \frac{r - R_S}{R_S}. \tag{3.1.7}$$

Figure 4 – Representation of the superposition of plane waves for $Z_{lm}(t, r_*)$ only for $r_* \to \infty$, with the RW potential.



Source: plotted by the author.

Figure 5 – Representation of the superposition of plane waves for $Z_{lm}(t, r_*)$ only for $r_* \to \infty$, after the assumption of the asymptotic behavior, with the RW potential.



Source: plotted by the author.

Hence, $A(r) \simeq e^{(r_*-R_S)/R_S}$, this equation vanishes as $r_* \to -\infty$. For the limit $r_* \to -\infty$, it follows the same procedure with outgoing and incoming waves, see Figure 6. The incoming waves describe the fact that part of the initial perturbations $Z_{lm}(t_0, r)$ and $Q_{lm}(t_0, r)$

propagate towards the black hole. Here, it is imposed the condition that nothing escapes from the black hole, resulting in purely incoming waves, see Figure 7. Therefore, with the boundary conditions for $r_* \to -\infty$,

$$Z_{lm}(t,r) \to \int_{-\infty}^{+\infty} d\omega A_{lm}^{in}(\omega) e^{-i\omega(t+r_*/c)}, \tag{3.1.8}$$

similarly, for the axial perturbation

$$Q_{lm}(t,r) \to \int_{-\infty}^{+\infty} d\omega \, \frac{\omega}{c} \, B_{lm}^{in}(\omega) e^{-i\omega(t+r_*/c)}. \tag{3.1.9}$$

It is important to note that the values of $A_{lm}^{in,out}(\omega)$ and $B_{lm}^{in,out}(\omega)$ are left unspecified and will be determined by the differential equation itself, given the source term or the initial values $Z_{lm}(t_0,r)$ and $Q_{lm}(t_0,r)$ if studying the evolution of a specific initial perturbation. It is not possible to impose $A_{lm}^{in}(\omega) = A_{lm}^{out}(\omega) = 0$ (and similarly for B_{lm}) because this would implies that the function $\tilde{Z}(\omega,r)$ vanishes as $r_* \to \pm\infty$. The precise values of $A_{lm}^{in,out}(\omega)$ and $B_{lm}^{in,out}(\omega)$ will be determined by the physics of the problem and the specific boundary and initial conditions imposed. In the context of the equivalent Schrödinger equation, the conditions discussed correspond to seeking bound-state solutions. However, it is important to note that both the Zerilli and RW potentials are positive everywhere and do not allow for the existence of bound states, regardless of the value of ω. This implies that the solutions to the differential equations that are considered do not correspond to bound states but rather describe other types of behavior, such as scattering or radiation.

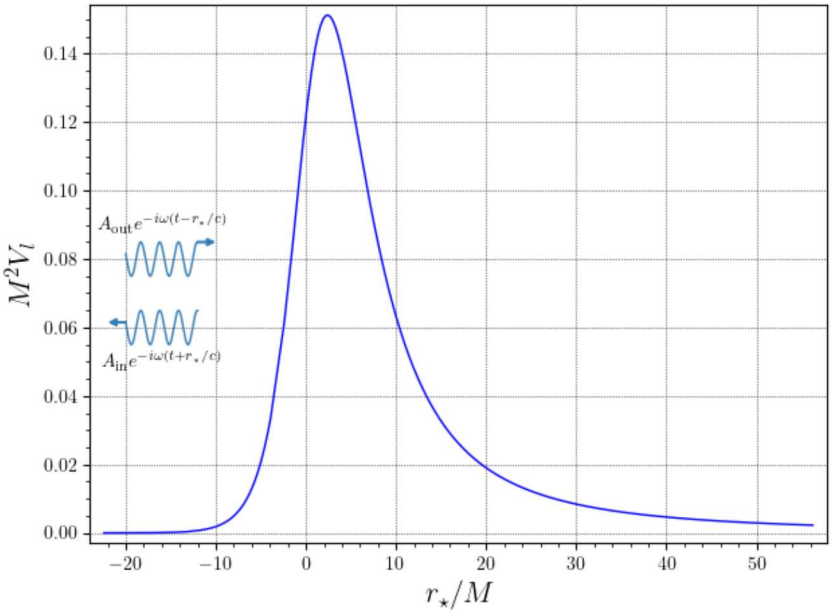
3.2 Waveform

In this section, will be considered the case without a source term and inquire about the evolution of an arbitrary perturbation. So, it is necessary to study an equation in the form

$$\phi''(\omega,x) + [\omega^2 - V(x)]\phi(\omega,x) = 0, \tag{3.2.1}$$

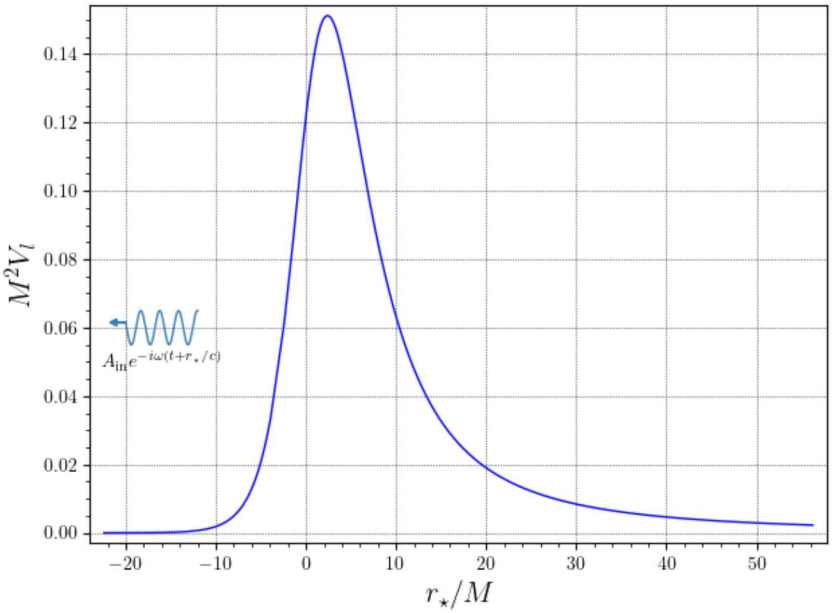
where $x \equiv r_*/c$ ranges from $-\infty$ to $+\infty$, and $\phi(\omega,x)$ represents the Fourier transform. $V(x)$ represents both the RW potential and the Zerilli potential. A useful method for

Figure 6 – Representation of the superposition of plane waves for $Z_{lm}(t, r_*)$ only for $r_* \to -\infty$, with the RW potential.



Source: plotted by the author.

Figure 7 – Representation of the superposition of plane waves for $Z_{lm}(t, r_*)$ only for $r_* \to -\infty$, after the assumption of the asymptotic behavior, with the RW potential.



Source: plotted by the author.

understanding the properties of the system at hand is to examine the evolution of an initial perturbation without the source term. In the case of a resonant bar, the behavior of the system is completely characterized by a set of normal modes, that is, a set of solutions in the form

$$\phi_n(t,x) = e^{-i\omega_n t}\psi_n(x). \tag{3.2.2}$$

By imposing appropriate boundary conditions, it is possible to select a discrete set of frequencies ω_n. Since each normal mode of an one-dimensional string evolves with a simple harmonic dependence, the general evolution of a perturbation takes the form

$$\phi(t,x) = \sum_n a_n e^{-i\omega_n t}\psi_n(x), \tag{3.2.3}$$

with the coefficient a_n determined by the initial form of the perturbation at $t = 0$. Indeed, boundary conditions (3.1.3) and (3.1.9) are crucial in selecting the discrete values of ω that correspond to the normal modes of the black hole perturbation. These conditions ensure that the perturbation exhibits the desired behavior as x approaches $\pm\infty$, resembling an outgoing wave at large positive x and an incoming wave at large negative x. By imposing these appropriate boundary conditions, it effectively restricts the possible solutions of the differential equation to a discrete set of frequencies ω, which correspond to the normal modes of the system. Each normal mode represents a distinct oscillatory pattern or resonance of the black hole perturbation. These quasi-normal modes play a fundamental role in understanding the dynamics of black hole perturbations and the characteristic "ringin" behavior associated with them.

To demonstrate that the boundary conditions indeed select discrete values of ω, it is useful to rewrite equation (3.2.1) as an equivalent formula in the time domain, such as

$$\left[-\frac{\partial^2}{\partial t^2} + \frac{\partial^2}{\partial x^2} - V(x)\right]\phi(t,x) = 0. \tag{3.2.4}$$

Since $V(x)$ approaches zero as $x \to \pm\infty$, in these limits, the above equation reduces to a plane wave moving to the right or left, $e^{-i\omega(t\pm x)}$. For an equivalent scattering problem, consider the situation where a wave packet at $x = -\infty$ propagating to the right, given by

$$\phi_0(t,x) = \int_{-\infty}^{\infty} \frac{d\omega}{2\pi} A_0(\omega) e^{-i\omega(t-x)}. \tag{3.2.5}$$

This wave packet will be partially reflected and partially transmitted by the potential $V(x)$. Therefore, for $x = -\infty$, there will be a wave packet moving to the left, which corresponds to the reflected wave

$$\phi_r(t,x) = \int_{-\infty}^{\infty} \frac{d\omega}{2\pi} A_{\mathrm{r}}(\omega) e^{-i\omega(t+x)}, \qquad (x \to -\infty). \tag{3.2.6}$$

On the other hand, for $x = +\infty$, there will be a wave packet continuing to move to the right, which corresponds to the transmitted wave

$$\phi_{\rm t}(t,x) = \int_{-\infty}^{\infty} \frac{d\omega}{2\pi} A_{\rm t}(\omega) e^{-i\omega(t-x)}. \tag{3.2.7}$$

Thus, in terms of the Fourier-transformed modes $\phi(\omega, x)$, the asymptotic solution for $x = -\infty$ is given by

$$\phi(\omega,x) \simeq A_0(\omega) e^{+i\omega x} + A_{\rm r}(\omega) e^{-i\omega x}, \tag{3.2.8}$$

where $A_0(\omega)$ represents the amplitude of the incident wave, and $A_r(\omega)$ represents the amplitude of the reflected wave. And for $x = +\infty$, it has

$$\phi(\omega,x) \simeq A_{\rm t}(\omega) e^{+i\omega x}, \tag{3.2.9}$$

where the conservation of probability requires that $|A_0(\omega)|^2 = |A_{\rm r}(\omega)|^2 + |A_{\rm t}(\omega)|^2$. In this equivalent one-dimensional scattering problem, the amplitude for reflection is $S(\omega) = A_{\rm r}(\omega)/A_0(\omega)$. The boundary conditions (3.1.3) and (3.1.9) corresponds to $A_0(\omega) = 0$ with $A_{\rm r}(\omega) \neq 0$, and therefore to poles of the scattering amplitude $S(\omega)$. Thus, the imposition of boundary conditions (3.1.3) and (3.1.9) selects discrete values of ω. In the language of scattering theory, these special frequencies are known as resonant frequencies of the system. These special frequency values, denoted as ω_{QNM}, can be expressed as

$$\omega_{QNM} \equiv \omega_R + i\omega_I = \omega_R - i\frac{\gamma}{2}, \tag{3.2.10}$$

where ω_R represents the real part of the frequency and γ represents the damping factor or imaginary part of the frequency. These resonant frequencies correspond to the Quasinormal Modes (QNMs) of the system, which describe the long-lived oscillations or ringing behavior after the initial perturbation. Mathematically, the fact that QNM frequencies are complex can be traced back to the complex nature of the boundary conditions. By drawing a parallel between Equation (3.2.1) and a time-dependent Schrödinger-like equation, it can make use of standard results from quantum mechanics. For example, if imposed as a boundary condition at infinity that the wave function behaves like an outgoing spherical wave (i.e., $\psi \sim (1/r)e^{ikr}$ in three dimensions), then the eigenvalues of the Hamiltonian will be complex. Although physically expected, the form of ω_{QNM} has a peculiar consequence

for the spatial dependence of the function describing a QNM. By definition, in the limit $x \to \pm\infty$, the QNMs satisfy the boundary conditions, which means

$$\phi(\omega, t) \propto e^{i\omega|x|} = e^{i\omega_R|x|}e^{+\gamma|x|/2}. \tag{3.2.11}$$

The exponential term $e^{+\gamma|x|/2}$ indicates the decay or damping of the QNM as it moves away from the perturbed region. This behavior reflects the dissipative nature of the system and accounts for the finite lifetime of the oscillations associated with the QNMs. Since $\gamma > 0$, QNMs diverge exponentially in both the infinite and event horizon limits. Firstly, a QNM cannot represent the physical state of the system at a given moment across all space, as it would carry infinite energy. Instead, a QNM can at most describe the behavior of $\phi(t, x)$ at sufficiently large values of t for a fixed value of x. The larger the value of $|x|$, the longer it takes for the asymptotic behavior to set in. Therefore, the exponential growth factor $e^{+\gamma|x|/2}$ is always compensated by the temporal dependence $e^{-\gamma t/2}$, beside the exponentially damped signal due to QNM, the response of a BH to an external disturbance also has a power-law tail, which dominates the asymptotic behavior as $t \to \infty$. Hence, the correct statement is that QNMs describe the response of the black hole at a fixed location x for intermediate times. These times are large enough for the signal caused by the incoming perturbation to have passed, but not so large that the asymptotic behavior has fully established itself. Another consequence of this spatial dependence is that QNMs generally do not form a complete set. From a mathematical perspective, it is unlikely that a physical perturbation with finite energy, which tends to zero as $x \to \pm\infty$, can be represented as a superposition of wave functions that diverge in those limits and carry infinite energy. Furthermore, it should be noted that boundary conditions (3.1.3) and (3.1.9) are not sufficient to uniquely determine a solution when ω is complex. In other words, considering a solution as follow

$$\phi_1(\omega, x) = e^{i\omega x}\left[1 + O\left(\frac{1}{x}\right)\right] = e^{i\omega_R x}e^{\gamma x/2}\left[1 + O\left(\frac{1}{x}\right)\right], \tag{3.2.12}$$

with the asymptotic behavior of the form ($x \to \pm\infty$), there may exist other solutions satisfying the same boundary conditions. This ambiguity arises due to the complex nature of ω and highlights the non-uniqueness of the QNM solutions. Therefore, the set of QNMs does not constitute a complete basis for representing all possible perturbations. It is important to consider this mathematical subtlety in the definition of QNMs and acknowledge that additional criteria or boundary conditions are needed to uniquely determine a solution within the complex frequency domain. Since equation (3.2.1) is invariant under $\omega \to -\omega$, there must also exist a second solution whose asymptotic behavior is given by

$$\phi_2(\omega, x) = e^{-i\omega x}\left[1 + O\left(\frac{1}{x}\right)\right] = e^{-i\omega_R x}e^{-\gamma x/2}\left[1 + O\left(\frac{1}{x}\right)\right]. \tag{3.2.13}$$

Clearly, any linear combination of the form $\phi_1(\omega, x) + \alpha\phi_2(\omega, x)$, where α is a constant, will still exhibit the same asymptotic behavior as ϕ_1 when $x \to +\infty$. This is because $\phi_2(\omega, x) \propto e^{-\gamma x/2}$ is subleading compared to $\phi_1(\omega, x)$, which is proportional to $e^{+\gamma x/2}$. Hence, imposing the boundary condition $\phi(\omega, x) \propto e^{i\omega x}$ as $x \to +\infty$ is not sufficient to single out a unique solution, and the same holds true for $x \to -\infty$. For this reason, the definition of QNMs in this section, based on the Fourier-transformed equation (3.2.1), is merely heuristic. However, a rigorous treatment that also sheds light on other aspects of QNMs can be obtained using the Laplace transform, as will be discussed next.

3.2.1 Laplace transformation

In order to gain an alternative perspective on Quasinormal Modes (QNMs), it is advantageous to revert to the time-domain formulation of the Regge-Wheeler (RW) and Zerilli equations, expressed as

$$[\partial_x^2 - \partial_t^2 - V(x)]\phi(t, x) = 0. \tag{3.2.14}$$

To further investigate this equation, it will be employed a Laplace transform with respect to the temporal variable. First, it will begin by examining the solution to this equation under specific initial conditions, $\phi(t, x)|_{t=0}$ and $\partial_t\phi(t, x)|_{t=0}$. Subsequently, will be explored the emergence of QNMs within this framework. A Laplace transform $\hat{\phi}(s, x)$ of a function $\phi(t, x)$, with s being a real and positive parameter, is defined as

$$\hat{\phi}(s, x) = \int_0^\infty dt\, e^{-st}\phi(t, x). \tag{3.2.15}$$

If $\phi(t, x)$ possesses a limit, then $\hat{\phi}(s, x)$ has an analytic continuation in the complex half-plane $Re(s) > 0$. The inverse of the aforementioned equation can be expressed as

$$\phi(t, x)\int_{\epsilon-i\infty}^{\epsilon+i\infty}\frac{ds}{2\pi i}e^{st}\hat{\phi}(s, x), \tag{3.2.16}$$

and, from equation (3.2.14), it becomes

$$\int_0^\infty dt\, e^{-st}[\partial_x^2 - \partial_t^2 - V(x)]\phi(t, x) = 0. \tag{3.2.17}$$

In other words,

$$\partial_x^2\hat{\phi}(s,x) - V(x)\hat{\phi}(s,x) - \int_0^\infty dt\, e^{-st}\partial_t^2\phi(t,x) = 0, \tag{3.2.18}$$

which leads to the expression (see Appendix C)

$$[\partial_x^2 - s^2 - V(x)]\hat{\phi}(s,x) = \mathcal{J}(s,x), \tag{3.2.19}$$

where

$$\mathcal{J}(s,x) = -\{s\phi(t,x) + \partial_t\phi(t,x)\}|_{t=0}. \tag{3.2.20}$$

Therefore, the source term depends on the initial conditions at $t = 0$. This should be contrasted with the Fourier transform method, where the equation in Fourier space is homogeneous and does not depend on the initial conditions. This is a key difference compared to the Laplace transform approach, where the source term in the transformed equation depends on the initial conditions at $t = 0$. The Fourier transform provides a different perspective, focusing solely on the frequency domain and the homogeneous equation, while the Laplace transform incorporates both the frequency and initial condition dependencies.

To find the solution of equation (3.2.19), will be necessary to use Green's function formalism. So, let $\hat{G}(s,x,x')$ be any Green's function of Equation (3.2.19), i.e., any solution of

$$[\partial_x^2 - s^2 - V(x)]\hat{G}(s,x,x') = \delta(x-x'). \tag{3.2.21}$$

Thus, the corresponding solution for Equation (3.2.19) will be

$$\hat{\phi}(s,x) = \int_{-\infty}^{\infty} dx'\, \hat{G}(s,x,x')\mathcal{J}(s,x'). \tag{3.2.22}$$

There are many possible Green's functions that, given the initial conditions $\phi(t,x)|_{t=0}$ and $\partial_t\phi(t,x)|_{t=0}$, will completely determine the solution of Equation (3.2.1). The problem is to select an appropriate Green's function for this case. Indeed, a solution

of Green's function can be constructed by considering two linearly independent solutions, $\hat{\phi}_+(s,x)$ and $\hat{\phi}_-(s,x)$, of the homogeneous equation, i.e.

$$[\partial_x^2 - s^2 - V(x)]\hat{\phi}(s,x) = 0. \tag{3.2.23}$$

The Green's function can then be written as

$$\hat{G}(s,x,x') = \frac{1}{W(s)}\Big[\theta(x-x')\hat{\phi}_-(s,x')\hat{\phi}_+(s,x) + \theta(x'-x)\hat{\phi}_-(s,x)\hat{\phi}_+(s,x')\Big], \tag{3.2.24}$$

where $\theta(x)$ is the Heaviside step function and $W(s)$ is the Wronskian of the solutions $\hat{\phi}_+(s,x)$ and $\hat{\phi}_-(s,x)$, given by

$$W(s) = \hat{\phi}_-(s,x)\partial_x\hat{\phi}_+(s,x) - \hat{\phi}_+(s,x)\partial_x\hat{\phi}_-(s,x). \tag{3.2.25}$$

From this definition, and using the fact that $\hat{\phi}_\pm$ are solutions of (3.2.1), it is possible to check that, using Equation (3.2.23),

$$\partial_x W = \hat{\phi}_-\partial_x^2\hat{\phi}_+ - \hat{\phi}_+\partial_x^2\hat{\phi}_- \tag{3.2.26}$$

$$= \hat{\phi}_-(s^2+V)\hat{\phi}_+ - \hat{\phi}_+(s^2+V)\hat{\phi}_- = 0. \tag{3.2.27}$$

This construction ensures that Green's function satisfies the homogeneous equation (3.2.23) and the appropriate boundary conditions. The choice of linearly independent solutions $\hat{\phi}_+(s,x)$ and $\hat{\phi}_-(s,x)$ may vary depending on the specific problem and boundary conditions. The confirmation that equation (3.2.21) indeed yields a Green function can be proven by directly applying the operator $[\partial_x^2 - s^2 - V(x)]$ to it (see Appendix D). Therefore, combining equation (3.2.22) with (3.2.24), the solution to $\hat{\phi}(s,x)$ can be write as

$$\hat{\phi}(s,x) = \frac{1}{W(s)}\hat{\phi}_+(s,x)\int_{-\infty}^{x} dx'\hat{\phi}_-(s,x')\mathcal{J}(s,x') + \frac{1}{W(s)}\hat{\phi}_-(s,x)\int_{x}^{\infty} dx'\hat{\phi}_+(s,x')\mathcal{J}(s,x'). \tag{3.2.28}$$

In the theory of partial differential equations, a theorem states that any Green's function can be written in the form (3.2.24). The choice of the appropriate Green's function for this problem, therefore, lies in selecting the appropriate solutions $\hat{\phi}_-$ and $\hat{\phi}_+$ of

the homogeneous equation. To understand the properties of the solutions $\hat{\phi}_{\pm}$, here will be studied their asymptotic behaviors as $x \to \pm\infty$. In these limits, the Zerilli and RW equations approach zero, as long as $Re(s) \neq 0$. For the dominant order in equation (3.2.23), it can be neglected $V(x)$ compared to s^2. Thus, for $x \to \pm\infty$, (3.2.23) becomes

$$[\partial_x^2 - s^2]\hat{\phi}(s,x) \simeq 0, \tag{3.2.29}$$

an equation that has solutions of the form $e^{\pm sx}$. In other words, it can be chosen two linearly independent solutions of equation (3.2.23) such that, as $x \to +\infty$, one is proportional to e^{+sx} and the other to e^{-sx}. The most general solution of the homogeneous equation, for $(x \to +\infty)$, therefore has the asymptotic form

$$\hat{\phi}_{hom}(s,x) \to a_1(s)e^{sx} + a_2(s)e^{-sx}. \tag{3.2.30}$$

For the limit $x \to -\infty$, the most general solution has the form

$$\hat{\phi}_{hom}(s,x) \to b_1(s)e^{sx} + b_2(s)e^{-sx}. \tag{3.2.31}$$

A generic solution with $a_1 \neq 0$ and $b_1 \neq 0$ diverges exponentially in both limits, as $x \to \pm\infty$, since here is considered $Re(s) > 0$. Given that the linear perturbations of the Schwarzschild space-time are uniformly bounded in x, it is necessary to find a solution $\hat{G}(s,x,x')$ such that the resulting solution obtained from the equation

$$\phi(t,x) = \int_{\epsilon-i\infty}^{\epsilon+i\infty} \frac{ds}{2\pi i} e^{st}\hat{\phi}(s,x), \tag{3.2.32}$$

is well-behaved and does not diverge exponentially as $x \to \pm\infty$. In other words, the Green function $\hat{G}(s,x,x')$ must be chosen in a way that ensures the solution $\hat{\phi}(s,x)$ obtained from it remains bounded and finite as $x \to \pm\infty$ for $Re(s) > 0$. Considering a mathematically simple scenario where the initial perturbation has compact support, such that $\mathcal{J}(s,x')$ in equation (3.2.22) is non-zero only for $x_L < x' < x_R$. Thus, if $x > x_R$, the second integral in (3.2.28) vanishes, and it leaves

$$\hat{\phi}(s,x) = \frac{c_-(s)}{W(s)}\hat{\phi}_+(s,x), \tag{3.2.33}$$

where

$$c_-(s) = \int_{x_L}^{x_R} dx'\, \hat{\phi}_-(s,x')\mathcal{J}(s,x'). \tag{3.2.34}$$

Therefore, the solution $\hat{\phi}(s,x)$ is bounded for $x \to +\infty$ if and only if $\hat{\phi}_+(s,x)$ is bounded for $x \to +\infty$. Similarly, for $x < x_L$,

$$\hat{\phi}(s,x) = \frac{c_+(s)}{W(s)}\hat{\phi}_-(s,x), \tag{3.2.35}$$

where

$$c_+(s) = \int_{x_L}^{x_R} dx'\, \hat{\phi}_+(s,x')\mathcal{J}(s,x'). \tag{3.2.36}$$

Thus, the solution $\hat{\phi}(s,x)$ is only bounded for $x \to -\infty$ if and only if $\hat{\phi}_-(s,x)$ is bounded for $x \to -\infty$. Comparing $\hat{\phi}\pm(s,x)$ with the asymptotic behaviors of $\hat{\phi}_{hom}(s,x)$ for $x \to \pm\infty$, is possible to understand that $\hat{\phi}_+(s,x)$ is uniquely fixed as the particular solution of the homogeneous equation with $a_1(s) = 0$, and $\hat{\phi}_-(s,x)$ is uniquely fixed as the solution with $b_2(s) = 0$. Therefore, their asymptotic behaviors are

$$\hat{\phi}_-(s,x) \simeq \begin{cases} e^{+sx} & (x \to -\infty), \\ a_1(s)e^{sx} + a_2(s)e^{-sx} & (x \to +\infty), \end{cases} \tag{3.2.37}$$

and

$$\hat{\phi}_+(s,x) \simeq \begin{cases} b_1(s)e^{sx} + b_2(s)e^{-sx} & (x \to -\infty), \\ e^{-sx} & (x \to +\infty). \end{cases} \tag{3.2.38}$$

With the previous behaviors and knowing that the Wronskian only depends on s, it can be plugged in $\hat{\phi}_\pm$ into the Wronskian formula and find that, for $x \to -\infty$, $W(s) = -2sb_2(s)$, and for $x \to +\infty$, $W(s) = -2sa_1(s)$. Thus, it is possible to infer that $a_1(s) = b_2(s)$.

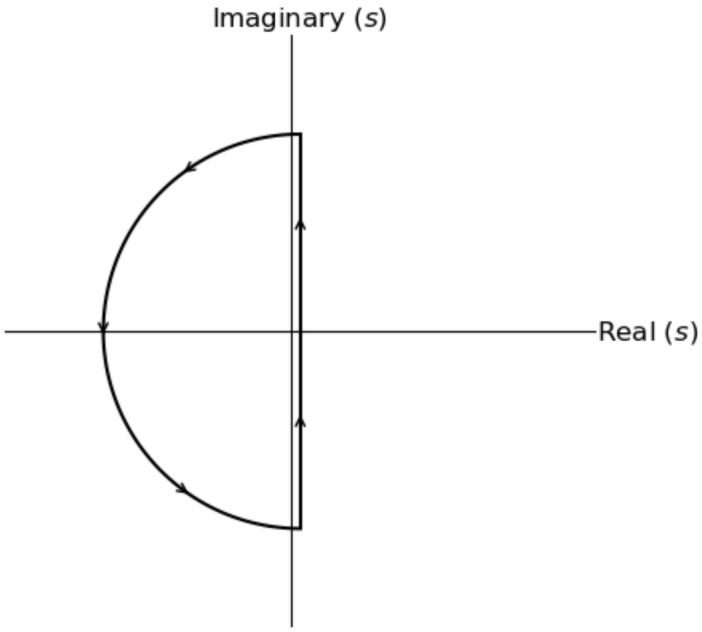
So far, it was seen that Green's function is, in principle, uniquely determined, and therefore, using the equation (3.2.22), the corresponding solution to the given initial data is also, in principle, determined. From here on, it will be provided an explicit form for the solutions $\hat{\phi}_\pm$ for all x. However, it is possible to understand the emergence of QNMs without referring to explicit solutions. For this purpose, it will be examined $\phi(t,x)$, which is obtained from $\hat{\phi}(s,x)$ through the equation (3.2.32). Once again, considering an

initial perturbation with compact support, where $\mathcal{J}(s, x')$ is nonzero only in the interval $x_L < x' < x_R$. By definition, it will be studied the solution $\phi(t, x)$ for $x > x_R$, given by (3.2.33). Thus, for $\phi(t, x)$, it has

$$\phi(t, x) = \frac{1}{2\pi i} \int_{\epsilon - i\infty}^{\epsilon + i\infty} ds\, e^{st} \frac{c_-(s)}{W(s)} \hat{\phi}_+(s, x). \tag{3.2.39}$$

Now, itwill be attempted to close the contour in the complex s plane in order to identify significant contributions to the integral. Since t is positive (remembering that is wanted the solution for $t > 0$, the factor e^{st} diverges on a circle at infinity in the right-half complex plane, where $Re(s) > 0$. Thus, it can only expect to close the contour in the left-half complex plane, where $Re(s) < 0$. This analysis can be seen in the Figure 8 bellow.

Figure 8 – The integration contour in the complex s-plane.



Source: plotted by the author

For now, it will be assumed that the functions $\hat{\phi}_\pm(s, x)$, as well as the source term $\mathcal{J}(s, x)$ that go into $c_-(s)$ are analytic on s, so there are no essential singularities or branch cuts within the boundary. Here it may add that these assumptions turn out to be correct if the potential $V(x)$ has compact support (like a square barrier), or it goes to zero exponentially on both frontiers. Indeed, the assumptions of analyticity and absence of essential singularities or branch cuts within the contour are not generally applicable to potentials such as the Zerilli and Regge-Wheeler potentials, which exhibit power-law behavior at infinity. However, for potentials that do not satisfy these conditions, alternative methods and techniques may be required to analyze their behavior and obtain solutions.

Under the assumptions stated earlier, it will be considered the contribution from the poles of the integrand since $W(s) = 0$. Suppose there is a set of simple zeros in the left half-plane of the complex plane, denoted by $s = s_n$. By applying the residue theorem, the integral can be evaluated as follows

$$\int_{\epsilon-i\infty}^{\epsilon+i\infty} \frac{ds}{2\pi i} e^{st}\hat{\phi}(s,x) = \sum_n \text{Res}\left[e^{st}\hat{\phi}(s,x)\right]_{s=s_n}, \tag{3.2.40}$$

where $\text{Res}[f(s)]_{s=s_n}$ denotes the residue of the function $f(s)$ at the pole $s = s_n$. Since $W(s) = 0$, the denominator in the expression for $\hat{\phi}(s,x)$ has a zero at $s = s_n$, implying that the term $[\partial_x^2 - s^2 - V(x)]\hat{\phi}(s,x)$ in the equation above is regular at $s = s_n$. Therefore, the residue at each pole will contribute to the solution. It is important to note that the specific values of the poles $s = s_n$ and their residues will depend on the particular form of the potential $V(x)$ and the boundary conditions of the problem.

These zeros correspond to the eigenvalues of the problem. In the context of black hole perturbations, these eigenvalues represent the quasinormal frequencies (QNMs) of the system. The presence of these complex eigenvalues is a consequence of the complex nature of the problem and the boundary conditions. The QNMs describe the characteristic oscillations of the perturbations around the black hole, decaying over time due to the dissipative nature of the system. Each complex eigenvalue $s = s_n$ corresponds to a specific QNM mode, characterized by its frequency and damping rate. The real part of s_n corresponds to the oscillation frequency of the mode, while the imaginary part represents the damping rate, determining how fast the perturbation decays over time. The specific values of the complex eigenvalues s_n depend on the details of the problem, such as the black hole geometry, the potential $V(x)$, and the boundary conditions. Finding these eigenvalues often involves solving a complex eigenvalue problem, which can be done numerically or analytically depending on the system's properties.

In the neighborhood of these zeros, it can be written the expression as a Taylor's expansion

$$W(s) = W'(s_n)(s - s_n) + O(s - s_n)^2, \tag{3.2.41}$$

where

$$W'(s_n) \equiv \left.\frac{dW}{ds}\right|_{s=s_n}. \tag{3.2.42}$$

Taking the residues of the poles (and noting that the poles are enclosed counter-clockwise), it is possible to obtain

$$\begin{aligned}\phi(t,x) &= \sum_n e^{s_n t}\frac{c_-(s_n)}{W'(s_n)}\hat{\phi}_+(s_n,x)\\ &\equiv \sum_n c_n u_n(x) e^{s_n t},\end{aligned} \tag{3.2.43}$$

where

$$c_n \equiv \frac{c_-(s_n)}{W'(s_n)} = \frac{1}{W'(s_n)}\int_{x_L}^{x_R} dx'\,\hat{\phi}_-(s_n,x')\mathcal{J}(s_n,x'), \tag{3.2.44}$$

and

$$u_n(x) \equiv \hat{\phi}_+(s_n,x). \tag{3.2.45}$$

The sum over n represents a superposition of terms, each associated with a specific pole $s = s_n$. The functions $u_n(x)$ correspond to the spatial dependence associated with each pole, and they can be obtained by solving the equation (3.2.23). These functions determine the spatial behavior of the solution at each pole $s = s_n$. It is important to recap that the coefficients c_n, the values of s_n, and the corresponding functions $u_n(x)$ depend on the specific form of the potential $V(x)$ and the boundary conditions of the problem. It is valid to observe that under the assumptions that were made, $\phi(t,x)$ is expressed as a sum over a discrete set of terms. Note: To simplify the mathematics, here it was assumed that $\mathcal{J}(s_n,x')$ has compact support. However, as saw previously in the equation for $\hat{\phi}_-(s,x)$, when $Re(s_n) < 0$, $\hat{\phi}_-(s_n,x)$ diverges exponentially as $x \to \pm\infty$. Therefore, removing the assumption of compact support is not trivial, see more in Sun and Price (1988). To bridge the gap between these discrete contributions and the QNMs, observes that the condition $W(s_n) = 0$ when integrated, this equation yields

$$\hat{\phi}_+(s_n,x) = c(s_n)\hat{\phi}_-(s_n,x), \tag{3.2.46}$$

where $c(s_n)$ is a constant coefficient. Indeed, for $s = s_n$, the two solutions of the homogeneous equation, $\hat{\phi}_\pm(s,x)$, are no longer independent. Instead, the solution will have the following form

$$\hat{\phi}_+(s_n,x) \propto \hat{\phi}_-(s_n,x) \equiv \hat{\phi}_*(s_n,x). \tag{3.2.47}$$

As seen before, $\hat{\phi}_{\pm}(s,x) \to e^{\mp sx}$ as $x \to \pm\infty$. Therefore,

$$\hat{\phi}_{*}(s_n,x) \propto e^{-s_n|x|}, \qquad (x \to \pm\infty). \tag{3.2.48}$$

Recapping the analysis that was conducted for the behavior of $\hat{\phi}_{\rm hom}$, it starts with a solution proportional to e^{sx} as $x \to -\infty$, when it evolves too large positive x, the solution will correspond to a mixture of e^{sx} and e^{-sx}. Hence, the values of s_n will be the special values of s for which the solution with $b_2 = 0$ as $x \to -\infty$ matches the solution with $a_1 = 0$ as $x \to +\infty$.
To establish a clear connection with QNMs, it is convenient to express $s = -i\omega$, where $\omega = \omega_R + i\omega_I$ is a complex variable. This substitution allows the introduction of the notation

$$\hat{u}^{in}(\omega,x) \equiv \hat{\phi}_{-}(-i\omega,x), \tag{3.2.49}$$

$$\hat{u}^{up}(\omega,x) \equiv \hat{\phi}_{+}(-i\omega,x). \tag{3.2.50}$$

Here, $\hat{u}^{in}(\omega,x)$ represents the inward-traveling mode, and $\hat{u}^{up}(\omega,x)$ represents the upward-traveling mode in the context of QNMs, as $\hat{u}^{in}(\omega,x)$ and $\hat{u}^{up}(\omega,x)$ correspond to the QNMs of the black hole system. The determination of these modes and their properties is a key aspect in the study of black hole physics and the behavior of perturbations nearby the event horizon. In these notations, the equations for $\hat{\phi}_{\pm}(s,x)$ become

$$\hat{u}^{in}(\omega,x) \simeq \begin{cases} e^{-i\omega x} & (x \to -\infty), \\ A_1(\omega)e^{-i\omega x} + A_2(\omega)e^{+i\omega x} & (x \to +\infty), \end{cases} \tag{3.2.51}$$

and

$$\hat{u}^{up}(\omega,x) \simeq \begin{cases} B_1(\omega)e^{-i\omega x} + B_2(\omega)e^{+i\omega x} & (x \to -\infty), \\ e^{+i\omega x} & (x \to +\infty), \end{cases} \tag{3.2.52}$$

where $A_{1,2}(\omega) \equiv a_{1,2}(-i\omega)$ and $B_{1,2}(\omega) \equiv b_{1,2}(-i\omega)$. Recalling that the time dependence is given by $e^{i\omega t}$, is possible to see that $\hat{u}^{in}$ describes a wave that, near the horizon, is falling into the black hole (purely incoming), while $\hat{u}^{up}$ describes a wave that is moving away from the black hole, towards future null infinity (purely outgoing). In terms of the Wronskian, it has the following expression

$$W = 2i\omega A_1(\omega), \tag{3.2.53}$$

with $A_1(\omega) = B_2(\omega)$. Similarly, by calculating the Jacobian between the "in" and "up" solutions, as $x \to +\infty$, and comparing it with the value as $x \to -\infty$, it is obtained $B_1(\omega) = -A_2^*(\omega)$. These relations highlight the connection between the coefficients of the "in" and "up" solutions, and they play a crucial role in understanding the behavior of the wave solutions near the black hole. Writing $s_n = -i\omega_n$ and $u_*(\omega_n, x) \equiv \phi_*(s_n = -i\omega_n, x)$, the equation for $\hat{\phi}_*(s_n, x)$ becomes

$$u_*(\omega_n, x) \simeq e^{+i\omega_n|x|}, \qquad (x \to \pm\infty). \tag{3.2.54}$$

These are precisely the boundary conditions satisfied by the solutions of the Fourier-transformed Zerilli or RW equations, which is referred to as QNMs. On the other hand, under the substitution $s = -i\omega$, the homogeneous equation in Laplace space

$$[\partial_x^2 - s^2 - V(x)]\hat{\phi}_*(s, x) = 0, \tag{3.2.55}$$

becomes identical to the equation in Fourier space

$$\phi''(\omega, x) + [\omega^2 - V(x)]\phi(\omega, x) = 0, \tag{3.2.56}$$

so the solutions of the former must transform into the solutions of the latter. Indeed, if one observes that the solutions $\hat{\phi}_*(s_n, x)$ correspond precisely to the QNMs expressed in the language of Laplace transform. By writing $\omega_{I,n} = -\gamma_n/2$, it is obtained that

$$s_n = \omega_{I,n} - i\omega_{R,n} \tag{3.2.57}$$

$$= -\frac{\gamma_n}{2} - i\omega_{R,n}. \tag{3.2.58}$$

Thus, the equation for $\phi(t, x)$ can be expressed as

$$\phi(t, x) = \sum_n c_n u_n(x) e^{i\omega_n t} \tag{3.2.59}$$

$$= \sum_n c_n u_n(x) e^{i\omega_{R,n} t} e^{-\gamma_n t/2}. \tag{3.2.60}$$

Since the poles s_n within the contour of integration have $Re(s_n) < 0$, it has $\gamma_n > 0$. Therefore, this solution represents a superposition of damped oscillations. Each term in the summation corresponds to a specific QNM, characterized by its eigenfrequency $\omega_{R,n}$

and damping rate γ_n. The coefficients c_n determine the amplitude and phase of each QNM in the overall solution. As time progresses, the amplitude of the oscillations diminishes, reflecting the dissipative nature of the system.

In terms of the spatial behavior, however, the fact that $Re(s_n) < 0$ implies that the QNM waveform $u_n(x)$ diverges exponentially both at spatial infinity and at the event horizon, given by $e^{\gamma_n|x|/2}$. The analytical result obtained from the resulting expression can be compared with direct numerical integration of the differential equation. By performing the comparison for a scalar wave equation given by

$$[\partial_*^2 - \partial_t^2 - V_l(r)]u_{lm}(t, r) = 0, \tag{3.2.61}$$

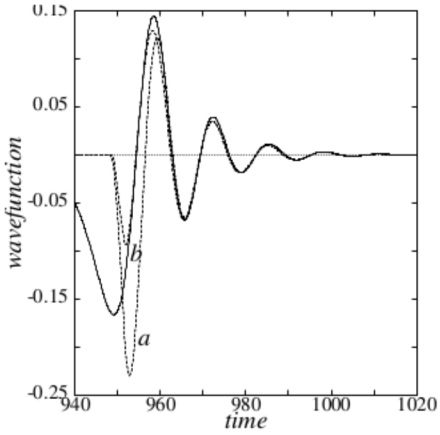
with

$$V_l(r) = A(r)\left[\frac{l(l+1)}{r^2} + \frac{R_S}{r^3}\right], \tag{3.2.62}$$

where $A(r)$ is a radial function and R_S represents the Schwarzschild radius, one can evaluate the agreement between the analytical and numerical solutions. This provides a way to validate the accuracy and effectiveness of the QNM approach in describing the behavior of waveforms in black hole systems. The specific details and methodology of the numerical integration depend on the chosen numerical scheme and the specific form of the potential $V_l(r)$. The accuracy of the numerical results can be improved by increasing the resolution and employing appropriate numerical techniques for solving the differential equation. Comparing the analytical and numerical solutions helps in understanding the behavior and properties of QNMs, as well as their relevance in black hole physics. The Figure 9 illustrates a comparison between the numerical integration of the scalar wave equation for a specific case with angular momentum quantum number $l = 2$ (represented by the solid line) and the approximate contribution from the first $l = 2$ QNMs. The dashed lines in the figure represent two different cases, (a) The first dashed line corresponds to the contribution from the slowest damped QNM. This mode exhibits a slower decay rate compared to the other modes, leading to a longer-lasting oscillatory behavior in the solution, (b) The second dashed line represents the sum of the contributions from the first six QNMs. By including multiple modes, the oscillatory behavior of the solution becomes more pronounced and exhibits a complex pattern determined by the interplay of the individual modes. It is important to note that the QNMs provide an approximate representation of the behavior of the scalar wave equation, capturing the dominant features of the system. However, the numerical integration of the equation provides a more accurate and comprehensive description, taking into account the full dynamics and any additional

effects beyond the QNMs. The comparison between the numerical integration and the QNMs highlights the utility of the QNMs in understanding the qualitative behavior of the system and provides a valuable approximation for analyzing and interpreting the solutions of the scalar wave equation with a specific angular momentum quantum number (Andersson, 1997).

Figure 9 – Comparison of the numerical integration of the scalar wave equation with the approximate contribution from the first QNMs.



Source: (Andersson, 1997)

4 Radial infall into a spherically symmetric black hole

Now, the goal here is to explore how QNMs can be excited by external disturbances. This section will examine the scenario of a test mass falling radially into a Schwarzschild black hole and calculate the GWs emitted during this process, taking into account the contribution from the QNMs. In the simpler context of a particle moving on a radial Newtonian trajectory, it is possible to utilize the quadrupole formula to calculate the emitted gravitational radiation. This approach is sufficient for computing the low-frequency portion of the energy spectrum of the radiation. This is because it is emitted when the infalling particle is located at large distances from the black hole, where these assumptions are appropriate. However, it's important to note that the quadrupole formula represents only the first term of an expansion derived within a flat background space. Consequently, it does not incorporate any information about QNMs. To obtain the complete spectrum of the emitted radiation, including the contribution from QNMs, it must instead utilize the formalism that will be developed in this chapter.

4.1 Energy-momentum tensor

The expression for the energy-momentum tensor of a point particle with mass m is given by

$$T^{\mu\nu} = \frac{1}{\sqrt{-g}} m\gamma \frac{dx^\mu}{dt}\frac{dx^\nu}{dt}\delta^{(3)}(\mathbf{x} - \mathbf{x}_0(t)), \tag{4.1.1}$$

where $\gamma = \frac{dt}{d\tau}$ represents the Lorentz factor in the general relativistic case. In the specific case of the Schwarzschild metric in polar coordinates, the determinant of the metric, $\sqrt{-g}$, can be expressed as

$$\sqrt{-g} = r^2|\sin\theta|. \tag{4.1.2}$$

Now, it will be considered a particle moving along a generic trajectory, given by $x_0^\mu(t) = (t,\, r_0(t),\, \theta_0(t),\, \phi_0(t))$. In this case, it has been chosen the particle to move exclusively along the z-axis. At $t \to -\infty$, the particle is located at $z = +\infty$ with zero initial velocity. This initial condition ensures that the particle starts from rest at infinity along the z-axis. The trajectory of the particle will be determined by the functions $r_0(t)$,

$\theta_0(t)$, and $\phi_0(t)$, which specify its radial distance, polar angle, and azimuthal angle as functions of time, respectively. This setup makes it possible to study the gravitational radiation emitted as the particle moves toward the black hole, incorporating the effects of both the general relativistic dynamics and the background metric described by the Schwarzschild solution. So, equation (4.1.1) can be written as

$$\begin{aligned} T^{\mu\nu} &= \frac{1}{r^2|\sin\theta|} m\gamma \frac{dx_0^\mu}{dt}\frac{dx_0^\nu}{dt}\delta[r-r_0(t)]\delta[\theta-\theta_0(t)]\delta[\phi-\phi_0(t)] \\ &= m\gamma \frac{dx_0^\mu}{dt}\frac{dx_0^\nu}{dt}\frac{\delta[r-r_0(t)]}{r^2}\delta[\cos(\theta)-\cos(\theta_0(t))]\delta[\phi-\phi_0(t)] \\ &\equiv m\gamma \frac{dx_0^\mu}{dt}\frac{dx_0^\nu}{dt}\frac{\delta[r-r_0(t)]}{r^2}\delta^{(2)}[\Omega-\Omega_0(t)]. \end{aligned} \tag{4.1.3}$$

The expression for the coefficients s^a_{lm} from the expansion of the energy-momentum tensor in spherical harmonics, can be obtained with the equations (2.2.25) and (2.2.26), together with the orthogonality property (2.2.12) and the redefinition (2.2.17). Which gives

$$\begin{aligned} s^a_{lm} &= \epsilon_a[c^a(r)]^2 \int d\Omega\, \eta^{\mu\rho}\eta^{\nu\sigma}[\mathbf{t}^a_{lm}(\Omega)]^*_{\mu\nu}T_{\rho\sigma}(\Omega) \\ &= \epsilon_a[c^a(r)]^2 m\gamma \frac{\delta[r-r_0(t)]}{r^2}[\mathbf{t}^a_{lm}(\Omega_0)]^*_{\mu\nu}\eta^{\mu\rho}\eta^{\nu\sigma}g_{\rho\rho'}g_{\sigma\sigma'}\frac{dx_0^{\rho'}}{dt}\frac{dx_0^{\sigma'}}{dt}, \end{aligned} \tag{4.1.4}$$

where α and β represent space-time indices, and $(\boldsymbol{t}^a_{lm})_{\alpha\beta}$ are the tensor harmonics. In order to obtain $\tilde{s}^a_{lm}(\omega, r)$, it is needed to perform the Fourier transform. The result of the transformations reveals that, due to the cylindrical symmetry of the problem, both s^{B1}_{lm} and s^{B2}_{lm} vanish, which implies that the axial modes are not excited. Consequently, the focus now remains solely on the polar modes, which are described by the Zerilli equation. It is important to note that the z-axis has been chosen as the direction from which the particle is approaching, establishing the frame of reference for the polar modes. Indeed, the calculation for each of the remaining coefficients of s^a_{lm} is straightforward, such as

$$s^{tt}_{lm}\left(\boldsymbol{t}^{tt}_{lm}\right)_{\alpha\beta} = \int T^{\mathrm{pol}}_{\alpha\beta}(\boldsymbol{x})_{\alpha\beta}\left(\boldsymbol{t}^{tt}_{lm}\right)^{\alpha\beta}\sqrt{-g}d^3x, \tag{4.1.5}$$

similarly, for s^{Rt}_{lm} and $(\mathbf{t}^{Rt}_{lm})_{\alpha\beta}$

$$s^{Rt}_{lm}\left(\boldsymbol{t}^{Rt}_{lm}\right)_{\alpha\beta} = \int T^{\mathrm{pol}}_{\alpha\beta}(\boldsymbol{x})_{\alpha\beta}\left(\boldsymbol{t}^{Rt}_{lm}\right)^{\alpha\beta}\sqrt{-g}d^3x. \tag{4.1.6}$$

The calculations for s^{L0}_{tt}, s^{T0}_{lm}, s^{Et}_{lm}, s^{E1}_{lm} and s^{E2}_{lm} follow a similar pattern. Therefore, for the

source in the Zerilli equation, $\tilde{S}^{a}_{l,m=0}$, defined in terms of $\tilde{s}^{a}_{lm}(\omega, r)$, is

$$\tilde{S}^{pol}_{lm} = A\partial_r(AJ_{lm}) - \frac{16\pi\tilde{s}^{Et}_{lm}}{i\omega}\frac{A\left[\lambda(\lambda+1)r^2+3Mr\lambda+6M^2\right]}{r(\lambda r+3M)^2} \tag{4.1.7}$$

$$- \frac{8\pi\tilde{s}^{Rt}_{lm}}{i\omega}\frac{\lambda r^2A^2}{(\lambda r+3M)^2} + 8\pi(r\tilde{s}^{L0}_{lm}+2\tilde{s}^{E1}_{lm})\frac{rA^2}{\lambda r+3M} - \frac{32\pi A}{r}\tilde{s}^{E2}_{lm}, \tag{4.1.8}$$

where

$$J_{lm} = \frac{r}{i\omega(\lambda r+3M)}8\pi(r\tilde{s}^{Rt}_{lm}+2\tilde{s}^{Et}_{lm}). \tag{4.1.9}$$

Taking into consideration the cylindrical symmetry of the problem ($\theta_0(t) = 0$), it is possible to make and repeat some observations. First, due to the symmetry, the spherical harmonics $Y_{lm}(\theta, \phi)$ will only have nonzero values when the index m is equal to zero. This means that only the coefficients s^{L0}_{lm}, s^{tt}_{lm}, s^{Rt}_{lm}, and s^{T0}_{lm} will have non-zero contributions. Furthermore, it is important to note that the quantities s^{B1}_{lm} and s^{B2}_{lm}, which play a role in the source terms of the Regge-Wheeler equation, actually vanish. This implies that the axial QNMs are not excited in this scenario. For the polar modes, only the coefficients $\tilde{s}^{a}_{l,m=0}(\omega, r)$ will have non-zero values. This simplifies the problem by reducing the number of coefficients that need to be considered. Lastly, among the remaining coefficients, only s^{L0}_{lm} and s^{Rt}_{lm} appear in the expression for $\tilde{S}^{\rm pol}_{lm}$. These coefficients specifically contribute to the source term in the Zerilli equation. Finally, the expression for the source term will be

$$\tilde{S}_l(\omega, r) = -4m\sqrt{2\pi}\left(l+\frac{1}{2}\right)^{1/2}\frac{A(r)}{\lambda r+3M}\left[\left(\frac{r}{R_S}\right)^{1/2} - \frac{2i\lambda}{\omega(\lambda r+3M)}\right]e^{i\omega T(r)}, \tag{4.1.10}$$

where

$$T(r) = R_S\left[-\frac{2}{3}\left(\frac{r}{R_S}\right)^{3/2} - 2\left(\frac{r}{R_S}\right)^{1/2} + \log\frac{(r/R_S)^{1/2}+1}{(r/R_S)^{1/2}-1}\right]. \tag{4.1.11}$$

In the limit of large r, the equation reduces to the Newtonian trajectory, which is expected. However, if $r \to R_S$, where R_S is the Schwarzschild radius, the coordinate time t required to reach the horizon becomes infinite, indicating that it takes an infinite amount of time to reach the black hole's horizon. This divergence is a consequence of the strong gravitational effects near the event horizon.

4.2 Integration of the Zerilli Equation

The procedures carried out so far will lead to obtaining the following equation

$$\frac{d^2}{dx^2}\tilde{Z}_l(\omega,x)+\left[\omega^2-V_l^Z(r)\right]\tilde{Z}_l(\omega,x)=\tilde{S}_l^{pol}(\omega,r), \tag{4.2.1}$$

where $\tilde{Z}_l(\omega,x)=\tilde{Z}_{l,m=0}(\omega,x)$. This equation can be integrated with Green's function technique, there will be considered two solutions of the homogeneous equation, $\hat{u}_l^{\rm in}(\omega,x)$ e $\hat{u}_l^{\rm up}(\omega,x)$, given by

$$\frac{d^2}{dx^2}\hat{u}_l+\left[\omega^2-V_l^Z(r)\right]\hat{u}_l=0, \tag{4.2.2}$$

with must satisfy both conditions that follow

$$\hat{u}^{\rm in}(\omega,x)\simeq\begin{cases} e^{-i\omega x} & (x\to-\infty),\\ A_1(\omega)e^{-i\omega x}+A_2(\omega)e^{+i\omega x} & (x\to+\infty),\end{cases} \tag{4.2.3}$$

$$\hat{u}^{\rm up}(\omega,x)\simeq\begin{cases} B_1(\omega)e^{-i\omega x}+B_2(\omega)e^{+i\omega x} & (x\to-\infty),\\ e^{+i\omega x} & (x\to+\infty).\end{cases} \tag{4.2.4}$$

To solve equation (4.2.2) is needed to construct the Wronskian, as

$$W_l(\omega)=\hat{u}_l^{\rm in}(\omega,x)\partial_x\hat{u}_l^{\rm up}(\omega,x)-\hat{u}_l^{\rm up}(\omega,x)\partial_x\hat{u}_l^{\rm in}(\omega,x), \tag{4.2.5}$$

with the Green's function

$$\hat{G}_l(\omega,x,x')=\frac{1}{W_l(\omega)}\left[\theta(x-x')\hat{u}_l^{\rm in}(\omega,x')\hat{u}_l^{\rm up}(\omega,x)+\theta(x'-x)\hat{u}_l^{\rm in}(\omega,x)\hat{u}_l^{\rm up}(\omega,x')\right]. \tag{4.2.6}$$

The solution of equation (4.2.2) can be express as

$$\begin{aligned}\tilde{Z}_l(\omega,x)=&\frac{1}{W_l(\omega)}\hat{u}_l^{\rm up}(\omega,x')\int_{-\infty}^{x}dx'\,\hat{u}_l^{\rm in}(\omega,x')\tilde{S}_l(\omega,x')\\&+\frac{1}{W_l(\omega)}\hat{u}_l^{\rm in}(\omega,x')\int_{x}^{+\infty}dx'\,\hat{u}_l^{\rm up}(\omega,x')\tilde{S}_l(\omega,x').\end{aligned} \tag{4.2.7}$$

in the limit of $x\to\infty$ the second integral will vanishes, while $\hat{u}_l^{\rm up}(\omega,x)$ will be proportional

to $e^{i\omega x}$. Therefore, for $x \to \infty$,

$$\tilde{Z}_l(t,r) \to \frac{e^{i\omega x}}{W_l(\omega)} \int_{-\infty}^{+\infty} dx' \hat{u}_l^{\text{in}}(\omega, x') \tilde{S}_l(\omega, x'). \tag{4.2.8}$$

Comparing with 3.1.8, it is clear that

$$A_l^{\text{out}} = \frac{1}{W_l(\omega)} \int_{-\infty}^{\infty} dx' \hat{u}_l^{\text{in}}(\omega, x') \tilde{S}_l(\omega, x'). \tag{4.2.9}$$

So, now it is possible to solve the equation (4.2.1), the strategy is to solve numerically the homogeneous equation 4.2.2, for a given ω, imposing the boundary condition $\hat{u}_l(\omega, x) \to e^{-i\omega x}$ at $x \to -\infty$. In practice, the numerical integration starts from a large but finite negative value, so it is better to include corrections in powers of $1/|x|$ to the asymptotic behavior. These can be computed analytically in terms of a recursion relation, see in more detail in Chandrasekhar and Detweiler (1975).

4.3 The energy spectrum

Following the literature, the results of the numerical analysis for the energy spectrum are depicted in Figure 10 for the multipoles $l = 2$ and $l = 3$. Given that the source term $\tilde{S}_l(\omega, r)$ in the Zerilli equation is proportional to the mass m of the test particle, as noted in equation 4.1.10, the amplitude $A_l^{\text{out}}(\omega)$ derived from equation 4.2.9 is likewise proportional to m, and hence the radiated energy scales with m^2. Consequently, in Figure 10, it is ploted the dimensionless quantity $(c/Gm^2)dE_l/d\omega$, which is independent of the mass m, for $l = 2$ and $l = 3$.

It is evident that the energy spectrum for $l = 2$ is significantly larger than that for $l = 3$. In the limit where $\omega R_S/c \ll 1$, the result for the mode $l = 2$ can be derived using the quadrupole formula, with the trajectory determined by the Newtonian equation of motion. In this regime, it is possible to find that

$$\frac{dE_{l=2}}{d\omega} \simeq 0.177 \frac{Gm^2}{c} \left(\frac{\omega R_S}{c}\right)^{4/3}. \tag{4.3.1}$$

In Figure 10, this approximation is also plotted. It can be observed that this approximation accurately reflects the $l = 2$ energy spectrum only for very low values of ω, specifically for $\omega R_S/c \lesssim 0.1$. This is expected, as the Newtonian radial trajectory for a particle falling into a point-like mass M is a reasonable approximation to the actual geodesic in

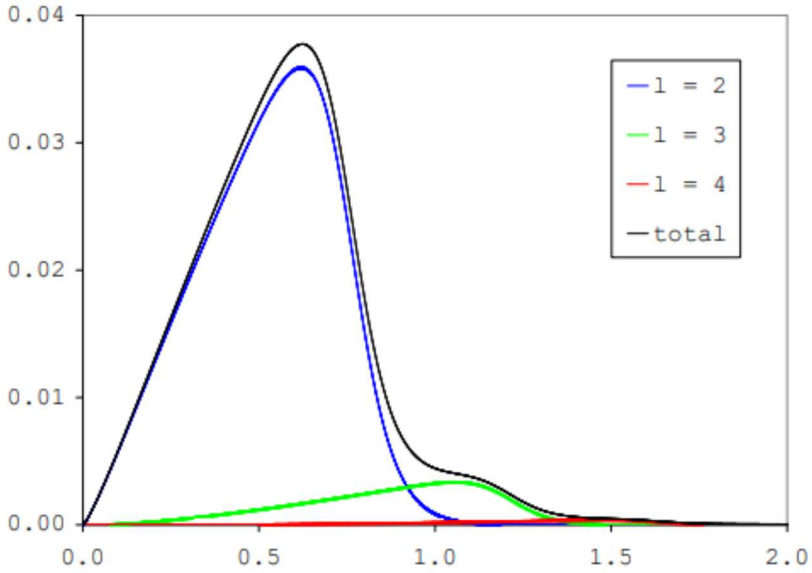


Figure 10 – The energy spectrum $(c/Gm^2)dE_l/d\omega$ as a function of $\omega R_S/c$, for $l = 2, 3, 4$.(Mitsou, 2011).

the Schwarzschild metric only at distances significantly larger than R_S, specifically for $r/R_S \gtrsim \mathcal{O}(10)$. The spectrum exhibits an exponential cutoff beyond a critical value of $\omega R_S/c = \mathcal{O}(1)$. As shown in the figure, for $l = 2$, the peak occurs around $\omega R_S/c \simeq 0.64$. The $l = 3$ mode (represented by the green line in Figure 10) contributes much less, with its peak occurring at higher frequencies, around $\omega R_S/c \simeq 1.1$. It is evident that the spectrum peak is at a frequency similar to ω_R for the least-damped ($n = 1$) QNM, for both $l = 2$ and $l = 3$. Contributions from higher multipoles are not discernible on the linear scale of Figure 10. In Figure 11, it is ploted the spectrum contributions from modes $l = 2$ to $l = 6$ on a logarithmic scale. As l increases, the spectrum's peak shifts towards higher ω, and the maximum value of $dE_l/d\omega$ decreases monotonically with l. Integrating over the frequency, the total radiated energy is found to be

$$\Delta E_{\rm rad} \simeq 0.0104 \left(\frac{m}{M}\right) mc^2. \tag{4.3.2}$$

Now, turning to the waveform analysis. In the radiation zone, the waveform in the TT gauge is described by the functions $u_{lm}(t-r/c)$ and $v_{lm}(t-r/c)$. For radial infall into a Schwarzschild black hole, only the polar modes with $m = 0$ are non-zero, i.e., the functions $u_l(t-r/c) \equiv u_{l,m=0}(t-r/c)$. These functions are obtained by Fourier transforming $A_l^{\rm out}(\omega)$. In Figure 12 to Figure 14, $u_l(t)$ is shown as a function of time for a fixed large value of $r \gg R_S$, for $l = 2, 3$, and 4, respectively. With increasing l, the waveform exhibits more oscillations. Note the change in vertical scale among the figures. The latter part of the waveform displays damped oscillations, which can be well approximated using the least-damped QNMs.

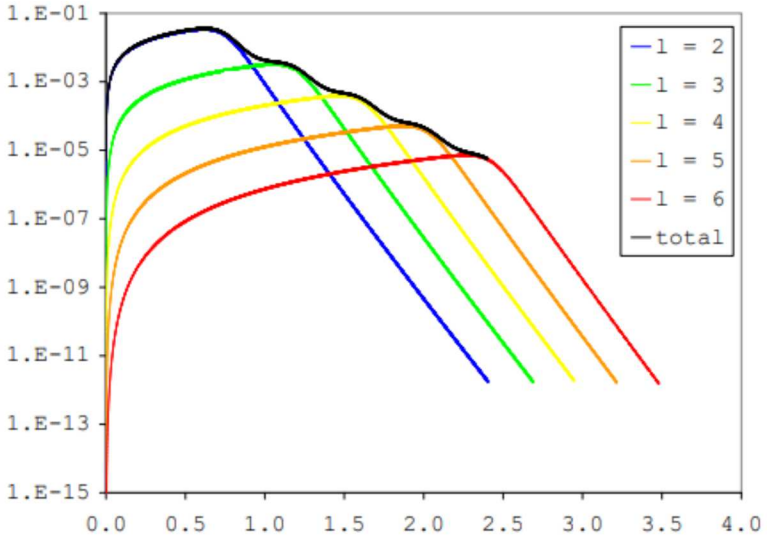
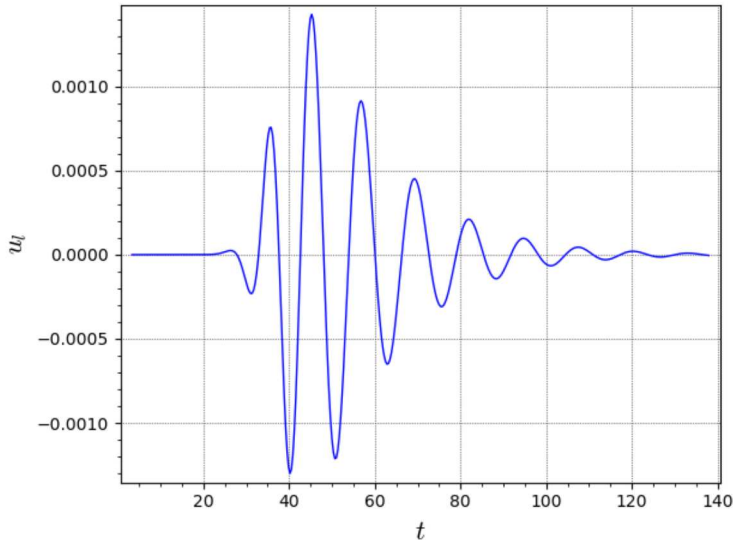


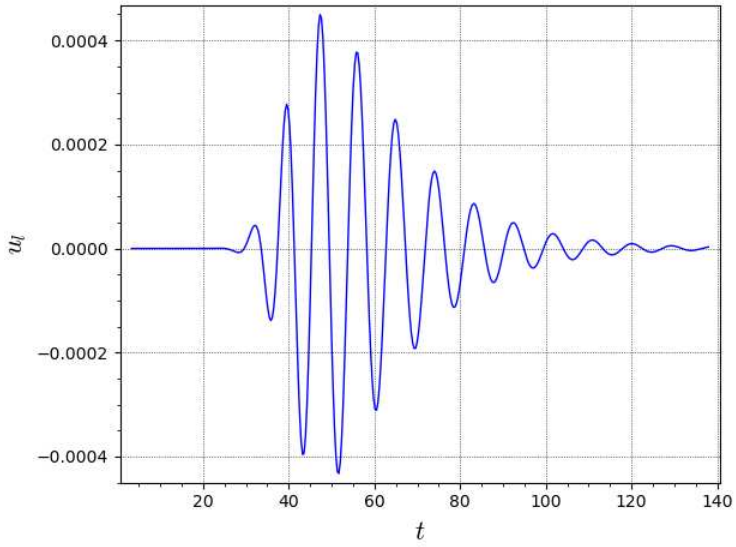
Figure 11 – The energy spectrum $(c/Gm^2)dE_l/d\omega$ as a function of $\omega R_S/c$, for $l = 2, 3, 4, 5, 6$, on a logarithmic vertical scale.(Mitsou, 2011).

Figure 12 – The gravitational waveform $u_l(t)$ with $l = 2$ (in units $G = c = 1$).



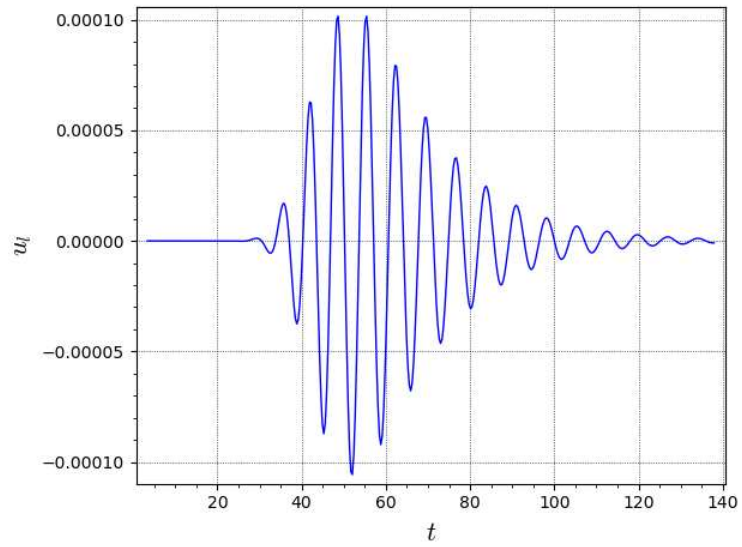
Source: plotted by the author

Figure 13 – The gravitational waveform $u_l(t)$ with $l = 3$ (in units $G = c = 1$).



Source: plotted by the author

Figure 14 – The gravitational waveform $u_l(t)$ with $l = 4$ (in units $G = c = 1$).



Source: plotted by the author

5 Gavitational self-force in general relativity

The detection of gravitational waves stemming from binary black-hole mergers by the LIGO-Virgo Collaboration signifies the commencement of an era where the dynamics of general relativity, in its most extreme manifestation, are directly accessible to observation. In the future, planned (space-based) observatories operating in the millihertz band will capture intricate gravitational-wave signals produced during the inspiral of compact objects into massive black holes situated in galactic centers. These inspiral events serve as highly effective probes of black-hole geometries, providing unparalleled precision tests of General Relativity within its most extreme regime.
Over the past two decades, this prospect has spurred a program dedicated to establishing an accurate theoretical model of strong-field radiative dynamics in a two-body system with a small mass ratio. This issue naturally lends itself to a perturbative treatment, relying on a systematic expansion of the field equations based on the small mass ratio. At the foremost order, there exists a pointlike particle orbiting a large black hole in a geodesic manner. Subsequent orders involve the particle's interaction with its own gravitational perturbation, resulting in an effective 'self-force' propelling the radiative evolution of the orbit. The effects of this force can be systematically accounted for according to the mass ratio.

5.1 Perturbative approaches in extreme-mass-ratio-inspiral

A computation of the local gravitational self-force (GSF) exerted on the smaller object within an extreme-mass-ratio-inspiral (EMRI) system constitutes merely the initial step, albeit a crucial one, in the effort to model the long-term orbital dynamics and emitted gravitational waves. A comprehensive approach must be devised that utilizes the GSF data to construct a sufficiently precise depiction of the evolving orbit and the emitted radiation. In this section, will be provided an overview of the formulation of such an approach, relying on a systematic perturbative expansion that leverages the adiabatic nature of the inspiral process.
However, before delving into this methodology, it is imperative to examine some of the relevant characteristics of bound geodesic orbits within the Kerr geometry. The subsequent subsection succinctly outlines the fundamental aspects of the "orbital mechanics" governing the behavior of test particles in Kerr space. Subsequently will proceed to discuss the challenge of the orbit's evolution under the influence of the gravitational self-force

5.1.1 Geodesic Orbits Around a Kerr Black Hole

In classical mechanics, the motion of a test mass in a spherically symmetric gravitational potential is characterized by conserved energy E and angular momentum $\mathbf{L}$, ensuring planar, periodic orbits. In General Relativity (GR), similar principles apply to Schwarzschild black holes, but deviations from Keplerian dynamics occur due to relativistic effects, such as perihelion precession, where the epicyclic period T_r exceeds the azimuthal period T_φ.

For Kerr black holes, rotational asymmetry disrupts the conservation of total angular momentum $\mathbf{L}$, resulting in non-planar, complex orbits. The Carter constant Q, a fourth integral of motion, accounts for this asymmetry and, alongside E, L_z, and mass m, parametrizes all geodesic orbits. Resonant orbits, where ω_r/ω_θ forms a rational ratio, exhibit precise periodicity and are pivotal for understanding gravitational wave emissions in Extreme Mass-Ratio Inspirals (EMRIs).

A notable feature of GR dynamics is the innermost stable circular orbit (ISCO). For Schwarzschild black holes, the ISCO is located at $r = 6M$. In Kerr black holes, the ISCO radius depends on spin, decreasing for co-rotating motion and increasing for counter-rotating orbits.

The geodesic equations in Kerr spacetime, expressed in terms of Carter's time parameter λ, simplify to:

$$\frac{dt_p}{d\lambda} = \mathcal{T}_r(r_p) + \mathcal{T}_\theta(\theta_p), \tag{5.1.1}$$

$$\frac{dr_p}{d\lambda} = \pm\sqrt{R(r_p)}, \tag{5.1.2}$$

$$\frac{d\theta_p}{d\lambda} = \pm\sqrt{\Theta(\cos\theta_p)}, \tag{5.1.3}$$

$$\frac{d\varphi_p}{d\lambda} = \Phi_r(r_p) + \Phi_\theta(\theta_p), \tag{5.1.4}$$

where the functions depend on E/m, L/m, Q/m, and the black hole's spin.

Geodesic motion in Kerr spacetime is integrable, described using action-angle variables $J_\alpha = \{E, L, Q, m\}$ and $q^\alpha = \{q^t, q^r, q^\theta, q^\phi\}$. Resonances, where radial and longitudinal frequencies are commensurate, and ISCOs play a key role in the study of EMRIs.

5.1.2 Long-term orbital evolution

The long-term inspiral of compact objects under gravitational self-force (GSF) is characterized by gradual inward spiraling due to dissipative effects. This process can be approximated as adiabatic, with the trajectory evolving slowly through a sequence of background geodesics. However, this gradual progression presents mathematical challenges,

as the constants of motion, E, L_z, and Q, evolve on a large time scale, $t_{\rm rr} \sim M^2/m$, requiring advanced perturbative techniques like matched expansions.

To accurately describe the inspiral, the perturbation of the spacetime metric is expressed as a series expansion, with terms dependent on the object's worldline. This approach, known as the self-consistent approximation, solves the coupled field and motion equations iteratively, mitigating errors from earlier perturbative methods. Despite its advantages, this approximation does not fully capture the adiabatic nature of Extreme Mass-Ratio Inspiral (EMRI) systems or the slow evolution of the black hole's mass and spin due to energy and angular momentum absorption.

A more tailored method is the multiscale expansion, which separates the problem into "fast"and "slow"time variables. This allows the motion to be analyzed as snapshots of geodesic orbits over short timescales while tracking the gradual evolution of orbital parameters over long timescales. This approach has been pivotal for understanding phase evolution in EMRIs, essential for accurate waveform modeling.

Recent developments have extended this framework to field equations, addressing limitations such as infrared divergences at large distances or near the black hole horizon. Complementary expansions are employed in these regions and integrated with the multiscale method via matched asymptotic expansions, enhancing its applicability to the intricate dynamics of EMRIs.

5.1.3 Transient resonances

Transient orbital resonances pose a significant challenge in the multiscale expansion approach. Typically, outside resonances, oscillatory modes average out over the radiation-reaction time, leaving only the constant modes to drive long-term evolution. However, near a resonance, certain modes become nearly stationary, causing additional terms in the evolution of the action variables J_α. These terms induce an order-$\sqrt{\eta}$ shift in orbital frequencies, leading to cumulative phase changes of $\sim 1/\sqrt{\eta}$ after the resonance.

The emergence of a new timescale, $M/\sqrt{\eta}$, near resonances disrupts the multiscale approximation, necessitating alternative schemes to handle these dynamics. Resonances also introduce phase errors, which can accumulate with successive resonant crossings, further complicating the modeling of Extreme Mass-Ratio Inspirals (EMRIs).

Pronounced resonant effects occur only when resonance integers $k_A^{\rm res}$ are small, allowing coherent accumulation of forcing terms. While most astrophysical EMRIs encounter at least one strong resonance, studies suggest that their impact on LISA detections will reduce detection rates by no more than $\sim 4\%$.

5.2 Dissipative effects and orbital evolution

The examination of concrete outcomes from numerical Generalized Self-Force (GSF) computations in Extreme Mass Ratio Inspiral (EMRI) systems. It has been assembled two compilations of such findings. The first, elucidated in the current section, delves into the radiative ramifications of the GSF and their influence on orbital dynamics. The focus here primarily revolves around two approximation schemes employed to delineate the evolution. While these methods stand apart from the two-timescale expansion delineated above, one can evaluate their precision within the two-timescale framework. The subsequent collection of outcomes, to be expounded upon in the next subsection, encompasses computations pertaining to various specific conservative physical manifestations of the GSF (alongside other quantities derived from $h^R_{\mu\nu}$).

5.2.1 Balance laws and adiabatic evolution

The adiabatic evolution of inspiraling orbits under Generalized Self-Force (GSF) follows balance laws for energy and angular momentum. Dissipative effects cause orbital energy and angular momentum to decrease, counterbalanced by gravitational wave emission to infinity and the black hole's horizon. These balance relations are expressed as:

$$\langle \dot{E} \rangle = -\langle \dot{\mathcal{E}}_\infty \rangle - \langle \dot{\mathcal{E}}_\mathcal{H} \rangle, \tag{5.2.1}$$

$$\langle \dot{L} \rangle = -\langle \dot{\mathcal{L}}_\infty \rangle - \langle \dot{\mathcal{L}}_\mathcal{H} \rangle. \tag{5.2.2}$$

These equations allow the evolution of orbital parameters without directly calculating the GSF. Computational techniques using Teukolsky's perturbation formalism simplify the calculation of asymptotic fluxes, enabling the modeling of adiabatic inspirals in Extreme Mass-Ratio Inspirals (EMRIs).

For generic Kerr orbits, the Carter constant Q must also evolve. While $\dot{Q}$ cannot be directly related to asymptotic fluxes, practical formulas derived by Mino and collaborators combine asymptotic radiation with local integrals, allowing full adiabatic modeling without explicit GSF calculations.

The balance laws serve as benchmarks for testing GSF codes and second-order perturbation methods. Recent advances validate these relations for various orbital configurations, ensuring accuracy in EMRI evolution modeling. Ongoing research extends these frameworks to higher-order calculations and more complex systems.

5.3 Inspiral Orbits with Gravitational Self-Force

The leading-order, adiabatic, flux-based calculations account for the primary dissipative effect of the first-order gravitational self-force (GSF) but neglect its conservative component and subleading dissipative effects, which emerge at the first post-adiabatic order. These effects, crucial for modeling Extreme Mass Ratio Inspiral (EMRI) systems, influence the secular phase evolution and must be incorporated.

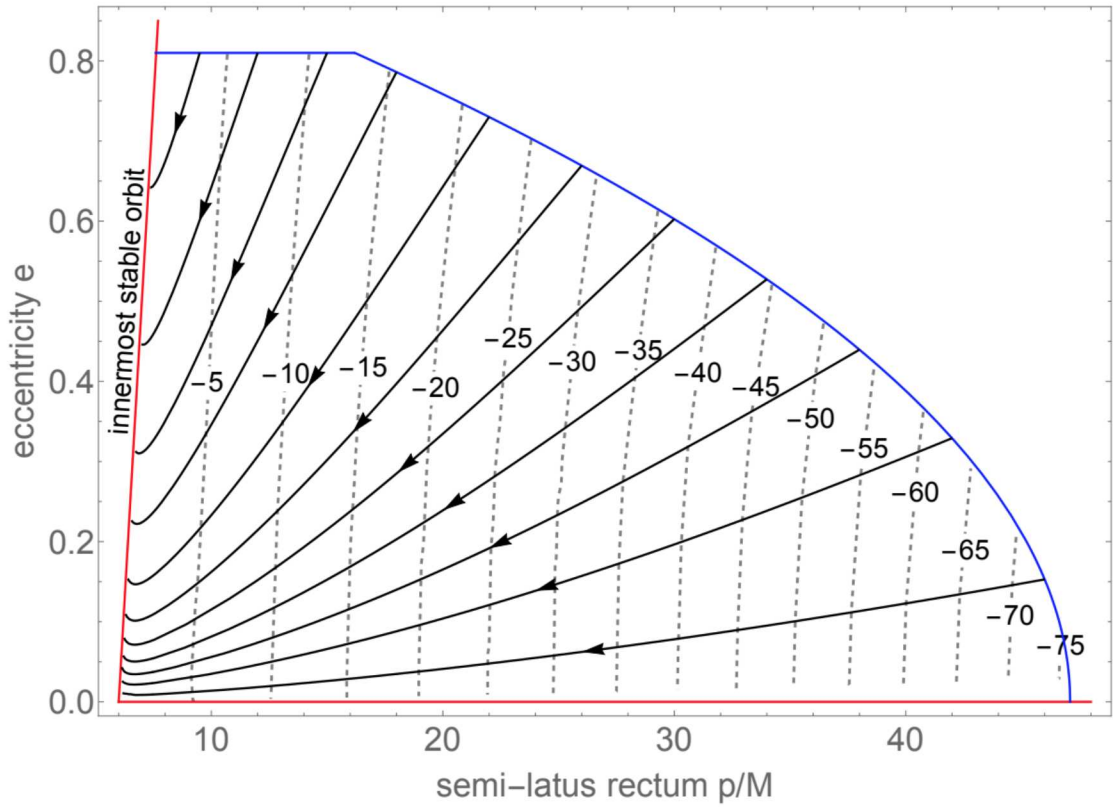
The osculating-geodesics method offers a practical approach, reconstructing inspirals as evolving geodesics with dynamic orbital elements. At each instant, the GSF is approximated using a geodesic tangent to the evolving orbit, determining the rate of change of both principal and positional elements. This contrasts with adiabatic models, which overlook the conservative GSF's influence. While the method introduces numerical errors from using "geodesic"GSF data, these errors scale with the square of the mass ratio and are comparable to neglecting the second-order GSF (Pound and Poisson, 2008).

In practice, the GSF is precomputed for a database of geodesic parameters, enabling interpolation for orbit evolution. Early implementations (Warburton et al., 2012; Osburn et al., 2016) focused on Schwarzschild spacetime, where the GSF was computed for bound orbits and interpolated over phase space. Results showed radiation reaction driving orbits to circularize while revealing phase errors from neglecting the conservative GSF. Figure 15 illustrates this evolution, with orbits evolving from high eccentricity to the last stable orbit, highlighting the importance of conservative effects.

Despite its success, the method faces computational challenges. Resolving forcing terms over orbital timescales is slow, requiring hours per trajectory for small mass ratios. A near-identity transformation (van de Meent and Warburton, 2018) mitigates this by averaging out orbital-scale oscillations, significantly improving efficiency.

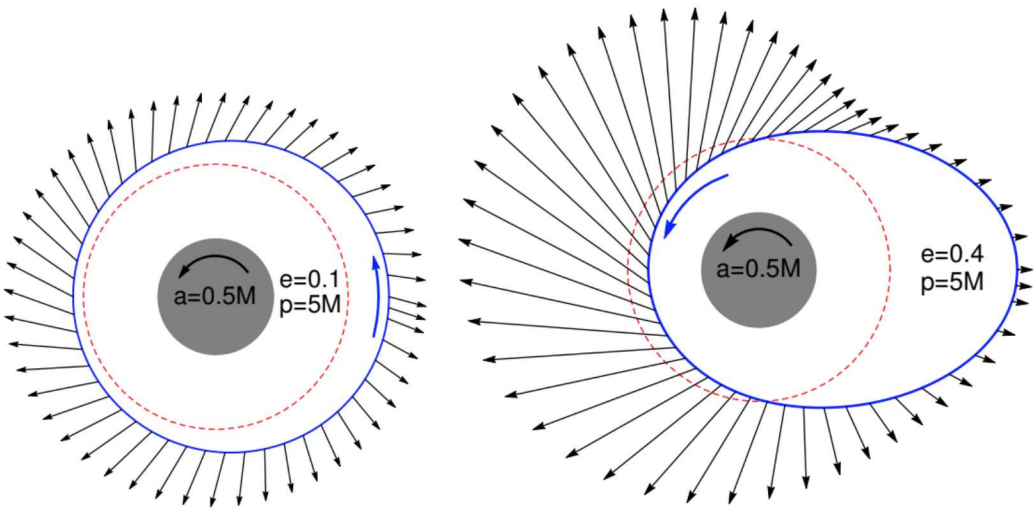
Extensions to Kerr spacetime (van de Meent, 2016, 2018) expand the method's applicability. Figures 16 and 17 show GSF computations for eccentric orbits in the Kerr equatorial plane. Challenges remain, including populating the 3D Kerr parameter space with sufficient GSF data and extending near-identity transformations. Ongoing work aims to refine these methods, addressing resonant crossings and incorporating two-timescale expansions for greater efficiency (Fujita et al., 2017; Pound, 2015).

Figure 15 – Sample inspiral orbits around a Schwarzschild black hole, as calculated by Osburn et al. (2016) for a mass ratio $\eta = 10^{-5}$.



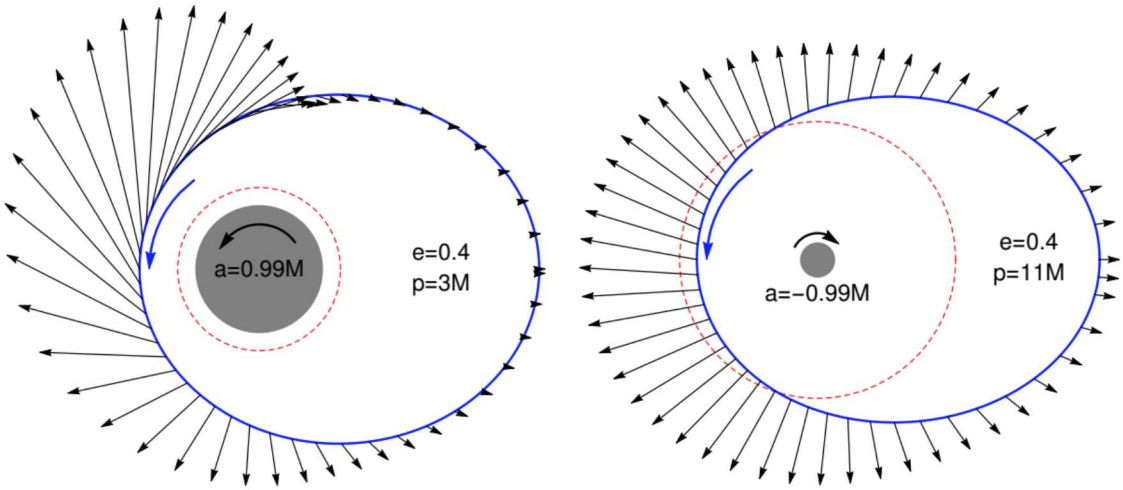
Source: (Barack and Pound, 2018)

Figure 16 – Sample output from van de Meent's code (van de Meent, 2016), showing the first-order GSF along eccentric geodesic orbits in the equatorial plane of a Kerr black hole.



Source: (Barack and Pound, 2018)

Figure 17 – Central hole spinning at 99% of the maximal allowable rate.



Source: (Barack and Pound, 2018)

5.4 Research in progress

The self-force program illustrates the progress in theoretical physics driven by experimental advancements. The renewed interest in this longstanding problem in classical relativity and the significant progress made over the past two decades is largely due to the potential for detecting gravitational waves from Extreme Mass Ratio Inspirals (EMRIs). The primary goal remains developing an accurate theoretical model of astrophysical EMRIs to identify and interpret EMRI signals within the LISA datastream. Much work is needed to achieve this, and this section reviews the principal outstanding issues, both foundational and computational, and the research that is being done.

The foundations of self-force theory are well-developed. For a small, compact object, an algorithm using matched asymptotic expansions exists to derive the metric (up to the smooth vacuum perturbation $h^R_{\mu\nu}$) in the object's local vicinity to any order in perturbation theory. This local metric can be represented as a singular puncture in spacetime, effectively reducing the object to a point-particle-like entity characterized by its multipole moments. The puncture's position represents the object's "position"with its equation of motion determined by the vacuum Einstein field equations and a condition aligning it with the object's center of mass. The physical field outside the object, an effective field within it, and its average motion can all be computed (up to the second perturbative order) from the coupled equations, such as the field and geodesic equations. At the first perturbative order, this framework simplifies to a point particle interacting with the Detweiler-Whiting free radiation field $h^{R(1)}_{\mu\nu}$.

Recent works have focused on improving and extending the theoretical frameworks and

computational methods for self-force calculations. (Grant, 2024) extend the flux-balance law (relationships between the average evolution - capturing the dissipative dynamics - and the values of the field far away from the body) to linear order in spin, in the context of an arbitrary black hole spacetime, and in a way that directly relates the average rates of change to the flux of a conserved current through the horizon and to infinity. They also show that, to linear order in spin, most, but not all, constants of motion at linear order in spin appear to possess flux-balance laws. (Long et al., 2024) calculate numerically the divergence coefficient of the self-force correction to the scattering angle, and then use this to inform a resummation of the post-Minkowskian expansion for the scattering angle, demonstrating that the resummed series agrees remarkably well with numerical self-force results even in the strong-field regime. (Albertini et al., 2024) present the first comparison of waveforms evaluated using the effective-one-body (EOB) approach and gravitational self-force (GSF) theory for inspiralling black hole binaries with a nonspinning primary and a spinning secondary. The frequency-domain analysis is particularly useful in confirming that the gyro-gravitomagnetic functions in the new chosen gauge bring the EOB spin contribution at 1st post-adiabatic order closer to the GSF one. (Feng and Yang, 2024) show that the gravitational back-reaction (i.e., the "self-force") of a point mass moving around a non-rotating, compact star on a circular orbit, compared with the case of a point mass orbiting a Schwarzschild black hole, can be well characterized by a universal frequency-dependent function multiplied by the (dynamical) tidal deformability of the compact star. This finding provides the foundation for building the waveform model for an extreme mass-ratio inspiral system around a star-like black hole mimicker, which is relevant for testing General Relativity and exotic compact objects with space-borne gravitational wave detectors.

6 Conclusions

This dissertation investigated the gravitational perturbations emitted by a spherically symmetric black hole, utilizing both analytical and numerical techniques. Throughout the work, the properties of these perturbations were explored, providing a detailed understanding of the dynamics and characteristics of black holes. Initially, a thorough analysis of spherical harmonics was conducted, with a particular focus on spin-2 tensor harmonics, which are essential for constructing the waveforms of these perturbations. The study of the Zerilli tensor and the Regge-Wheeler gauge facilitated the formulation of the corresponding equations, which are fundamental for describing the axial and polar perturbations of the system. The dissertation also delved into the study of quasinormal modes (QNMs), which are crucial for understanding the damped oscillations that occur when a black hole is perturbed. The application of the Laplace transform proved to be a useful tool for analyzing the frequency response of these modes, enriching the understanding of the characteristics of the associated gravitational waves. The investigation of radial infall into black holes highlighted the importance of the energy-momentum tensor and the integration of the Zerilli equation, elucidating the evolution of perturbations during this process. Finally, the analysis of the gravitational self-force (GSF) in extreme mass ratio inspirals (EMRIs) showed how this force affects the long-term dynamics of orbits, influencing radiative evolution and providing a rigorous test of general relativity in its most extreme regime.
This work significantly contributes to the understanding of gravitational perturbations in spherically symmetric black holes, offering profound insights into their properties and impacts on theoretical physics. Future perspectives suggest continued research in this area, with an emphasis on precise modeling of orbital evolution and emitted gravitational waves, thereby extending the scope of the study presented here.

References

A. Albertini, A. Nagar, J. Mathews, and G. Lukes-Gerakopoulos. Comparing second-order gravitational self-force and effective-one-body waveforms from inspiralling, quasi-circular black hole binaries with a non-spinning primary and a spinning secondary, 2024. URL https://arxiv.org/abs/2406.04108.

N. Andersson. Evolving test fields in a black-hole geometry. *Physical Review D*, 55(2): 468–479, 1997. doi: 10.1103/physrevd.55.468.

L. Barack and C. Cutler. Using lisa extreme-mass-ratio inspiral sources to test off-kerr deviations in the geometry of massive black holes. *Physical Review D*, 75(4), 2007. doi: 10.1103/physrevd.75.042003.

L. Barack and A. Pound. Self-force and radiation reaction in general relativity. *Reports on Progress in Physics*, 82(1), 2018. doi: 10.1088/1361-6633/aae552.

L. Barack and N. Sago. Gravitational self-force on a particle in circular orbit around a schwarzschild black hole. *Phys. Rev. D*, 75:064021, 2007.

B. Carter. Global structure of the kerr family of gravitational fields. *Physical Review*, 174: 1559–1571, 1968.

S. Chandrasekhar. *The Mathematical Theory of Black Holes*. The International Series of Monographs on Physics, 1983.

S. Chandrasekhar and S. Detweiler. The quasi-normal modes of the schwarzschild black hole. *Royal Society*, 344(1639), 1975. doi: 10.1098/rspa.1975.0112.

X. Feng and H. Yang. Universal gravitational self-force for a point mass orbiting around a compact star, 2024. URL https://arxiv.org/abs/2406.02101.

R. Fujita, S. Isoyama, A. L. Tiec, H. Nakano, N. Sago, and T. Tanaka. Hamiltonian formulation of the conservative self-force dynamics in the kerr geometry. *Classical and Quantum Gravity*, 34(13):134001, jun 2017.

A. M. Grant. Flux-balance laws for spinning bodies under the gravitational self-force, 2024. URL https://arxiv.org/abs/2406.10343.

M. Katz and S. Larson. Evaluating black hole detectability with lisa. *Monthly Notices of the Royal Astronomical Society*, 483:3108–3118, 2019. doi: 10.1093/mnras/sty3321.

R. P. Kerr. Gravitational field of a spinning mass as an example of algebraically special metrics. *Phys. Rev. Lett.*, 11:237–238, 1963. doi: 10.1103/PhysRevLett.11.237.

O. Long, C. Whittall, and L. Barack. Black hole scattering near the transition to plunge: Self-force and resummation of post-minkowskian theory, 2024.

M. Maggiore. *Gravitational Waves: Theory and Experiments*, volume 1. Oxford University Press, Oxford, Oxfordshire - England, 2007.

M. Maggiore. *Gravitational Waves: Astrophysics and cosmology*, volume 2. Oxford University Press, Oxford, Oxfordshire - England, 2018.

K. Martel and E. Poisson. Gravitational perturbations of the schwarzschild spacetime: A practical covariant and gauge-invariant formalism. *Physical Review D*, 71(10), 2005. doi: 10.1103/physrevd.71.104003.

E. Mitsou. Gravitational radiation from radial infall of a particle into a schwarzschild black hole: A numerical study of the spectra, quasinormal modes, and power-law tails. *Physical Review D*, 83(4), 2011. ISSN 1550-2368.

R. Monteiro. Classical and thermodynamic stability of black holes. Other thesis, 2010.

E. T. Newman, R. Couch, K. Chinnapared, A. Exton, A. Prakash, and R. Torrence. Metric of a rotating, charged mass. *J. Math. Phys.*, 6:918–919, 1965. doi: 10.1063/1.1704351.

G. Nordström. On the mass of a material s.stem according to the gravitation theory of einstein. *KNAW, Proceedings*, pages 1076–1091, 1918.

J. R. Oppenheimer and H. Snyder. On continued gravitational contraction. *Phys. Rev.*, 56:455–459, 1939.

T. Osburn, N. Warburton, and C. R. Evans. Highly eccentric inspirals into a black hole. *Physical Review D*, 93, Mar. 2016. ISSN 2470-0029.

A. Pound. Second-order perturbation theory: Problems on large scales. *Physical Review D*, 92(10), Nov. 2015.

A. Pound and E. Poisson. Osculating orbits in schwarzschild spacetime, with an application to extreme mass-ratio inspirals. *Physical Review D*, 77(4), Feb. 2008.

T. . Regge and J. Wheeler. Stability of a schwarzschild singularity. *Phys. Rev.*, 108: 1063–1069, Nov 1957. doi: 10.1103/PhysRev.108.1063.

H. Reissner. Uber die eigengravitation des elektrischen feldes nach der einsteinschen theorie. *Annalen Phys.*, 355(9):106–120, 1916. doi: 10.1002/andp.19163550905.

K. Schwarzschild. On the gravitational field of a mass point according to einstein's theory. *Sitzungsber. Preuss. Akad. Wiss. Berlin (Math. Phys.)*, pages 189–196, 1916.

Y. Sun and R. H. Price. Excitation of quasinormal ringing of a schwarzschild black hole. *Phys. Rev. D*, 38:1040–1052, 1988. doi: 10.1103/PhysRevD.38.1040.

K. S. Thorne. Multipole expansions of gravitational radiation. *Reviews of Modern Physics*, 52(2), 1980. doi: 10.1103/RevModPhys.52.299.

M. van de Meent. Gravitational self-force on eccentric equatorial orbits around a kerr black hole. *Physical Review D*, 94(4), 2016. ISSN 2470-0029.

M. van de Meent. Gravitational self-force on generic bound geodesics in Kerr spacetime. *Phys. Rev. D*, 97(10):104033, 2018. doi: 10.1103/PhysRevD.97.104033.

M. van de Meent and N. Warburton. Fast self-forced inspirals. *Classical and Quantum Gravity*, 35(14):144003, jun 2018. doi: 10.1088/1361-6382/aac8ce.

N. Warburton, S. Akcay, L. Barack, J. R. Gair, and N. Sago. Evolution of inspiral orbits around a schwarzschild black hole. *Physical Review D*, 85(6), Mar. 2012.

F. J. Zerilli. Gravitational field of a particle falling in a scharzschild geometry analyzed in tensor harmonics. *Physical Review D*, 2(10), 1970. doi: doi.org/10.1103/PhysRevD.2.2141.

APPENDIX A – Coefficients of pure-spin $\mathbf{s = 2}$ spherical harmonics

Coefficients that are in the definition of the pure-spin $s = 2$ tensor spherical harmonics with, given by (Thorne, 1980)

$$a_{11} = + \left(\frac{(j+1)(j+2)}{(2j+1)(2j+3)} \right)^{1/2}, \qquad a_{12} = - \left(\frac{2j(j+1)}{3(2j-1)(2j+3)} \right)^{1/2}, \tag{A.0.1}$$

$$a_{13} = + \left(\frac{j(j-1)}{(2j-1)(2j+1)} \right)^{1/2}, \qquad a_{21} = - \left(\frac{2j(j+2)}{(2j+1)(2j+3)} \right)^{1/2}, \tag{A.0.2}$$

$$a_{22} = - \left(\frac{3}{(2j-1)(2j+3)} \right)^{1/2}, \qquad a_{23} = + \left(\frac{2(j-1)(j+1)}{(2j-1)(2j+1)} \right)^{1/2}, \tag{A.0.3}$$

$$a_{31} = + \left(\frac{j(j-1)}{2(2j+1)(2j+3)} \right)^{1/2}, \qquad a_{32} = + \left(\frac{3(j-1)(j+2)}{(2j-1)(2j+3)} \right)^{1/2}, \tag{A.0.4}$$

$$a_{33} = + \left(\frac{(j+1)(j+2)}{2(2j-1)(2j+1)} \right)^{1/2}, \qquad b_{11} = + \left(\frac{j+2}{2j+1} \right)^{1/2}, \tag{A.0.5}$$

$$b_{12} = - \left(\frac{j-1}{2j+1} \right)^{1/2}, \qquad b_{21} = - \left(\frac{j-1}{2j+1} \right)^{1/2}, \tag{A.0.6}$$

$$b_{22} = - \left(\frac{j+2}{2j+1} \right)^{1/2}. \tag{A.0.7}$$

APPENDIX B – Non-zero terms of the Christoffel symbols in the Schwarzschild metric

In terms of $A(r) = 1 - R_S/r$, the non-zero terms of $\bar{\Gamma}^{\gamma}_{\alpha\beta}$ for the Schwarzschild metric are

$$\bar{\Gamma}^{r}_{rr} = -\frac{R_S}{2r^2 A(r)}, \qquad \bar{\Gamma}^{r}_{\theta\theta} = -rA(r),$$
$$\bar{\Gamma}^{r}_{\phi\phi} = -rA(r)\sin^2\theta, \qquad \bar{\Gamma}^{r}_{tt} = \frac{A(r)R_S}{2r^2},$$
$$\bar{\Gamma}^{\theta}_{r\theta} = \frac{1}{r}, \qquad \bar{\Gamma}^{\theta}_{\phi\phi} = -\sin^2\theta\cos\theta,$$
$$\bar{\Gamma}^{\phi}_{r\phi} = \frac{1}{r}, \qquad \bar{\Gamma}^{\phi}_{\theta\phi} = \theta,$$
$$\bar{\Gamma}^{t}_{tr} = \frac{R_S}{2r^2 A(r)},$$

besides those ones obtained by $\bar{\Gamma}^{\gamma}_{\alpha\beta} = \bar{\Gamma}^{\gamma}_{\beta\alpha}$.

APPENDIX C – Laplace transform for Zerilli and Regge-Wheeler homogeneous equations

A Laplace transform $\hat{\phi}(s,x)$ of a function $\phi(t,x)$, with s being a real and positive parameter, is defined as

$$\hat{\phi}(s,x) = \int_0^\infty dt\, e^{-st}\phi(t,x).$$

Then, equation (3.2.14) can be express as

$$\int_0^\infty dt\, e^{-st}[\partial_x^2 - \partial_t^2 - V(x)]\phi(t,x) = 0.$$

If one expands the expression, the equation can be write as bellow

$$\partial_x^2\hat{\phi}(s,x) - V(x)\hat{\phi}(s,x) - \int_0^\infty dt\, e^{-st}\partial_t^2\phi(t,x) = 0.$$

Here, the simplification of the equation above can be achieve simplify by doing the chain rule twice. Just focusing in the terms inside the integral, it can be express with the chain rule as

$$\partial_t(e^{-st}\partial_t\phi) = -se^{-st}\partial_t\phi + e^{-st}\partial_t^2\phi,$$

where the far right term is the one in the integral, so

$$\int_0^\infty dt\, e^{-st}\partial_t^2\phi = \int_0^\infty dt\, \left[\partial_t(e^{-st}\partial_t\phi) + se^{-st}\partial_t\phi\right].$$

The first term on the right will just be $e^{-st}\partial_t\phi$ defined at $t=0$ and at $t=\infty$, since the integral of the derivative of a function is simply the function at the integration limits. Since e^{-st} at $t=\infty$ is zero and $e^{-st}=1$ at $t=\infty$,

$$\int_0^\infty dt\, e^{-st}\partial_t^2\phi = -\{\partial_t\phi\}|_{t=0} + s\int_0^\infty dt\, e^{-st}\partial_t\phi.$$

The same procedure will be done for the far right term, as follows

$$\partial_t(e^{-st}\phi) = -se^{-st}\phi + e^{-st}\partial_t\phi,$$

substituting again in the integral,

$$\int_0^\infty dt\, e^{-st}\partial_t^2\phi = -\{\partial_t\phi\}|_{t=0} + s\int_0^\infty dt\, \left[\partial_t(e^{-st}\phi) + se^{-st}\phi\right].$$

Again, the same steps done before with the function and the limits leads to

$$\int_0^\infty dt\, e^{-st}\partial_t^2\phi = -\{\partial_t\phi\}|_{t=0} - \{s\phi\}|_{t=0} + s^2\int_0^\infty dt\, e^{-st}\phi,$$

and the last term is simply the definition of $\hat{\phi}$ multiplied by s^2. So, returning the expression above to the first equation,

$$\partial_x^2\hat{\phi}(s,x) - V(x)\hat{\phi}(s,x) + \{\partial_t\phi + s\phi\}|_{t=0} - s^2\hat{\phi} = 0,$$

that finally leads to

$$[\partial_x^2 - V(x) - s^2]\hat{\phi}(s,x) = -\{\partial_t\phi(t,x) + s\phi(t,x)\}|_{t=0}.$$

APPENDIX D – The Green's function and the homogeneous equation of $\hat{\phi}(\mathbf{s}, \mathbf{x})$

To prove that the equation

$$[\partial_x^2 - s^2 - V(x)]\hat{G}(s, x, x') = \delta(x - x'),$$

is true, by applying the operator $[\partial_x^2 - s^2 - V(x)]$ to the Green's function, it is first necessary to recover some equations. Such as, the Green's function for the problem

$$\hat{G}(s, x, x') = \frac{1}{W(s)}\Big[\theta(x - x')\hat{\phi}_-(s, x')\hat{\phi}_+(s, x) + \theta(x' - x)\hat{\phi}_-(s, x)\hat{\phi}_+(s, x')\Big],$$

and the Wronskian of the solutions $\hat{\phi}_+(s, x)$ and $\hat{\phi}_-(s, x)$

$$W(s) = \hat{\phi}_-(s, x)\partial_x\hat{\phi}_+(s, x) - \hat{\phi}_+(s, x)\partial_x\hat{\phi}_-(s, x).$$

So, applying the operator,

$$[\partial_x^2 - s^2 - V(x)]\hat{G}(s, x, x') = \frac{[\partial_x^2 - s^2 - V(x)]}{W(s)}\Big[\theta(x - x')\hat{\phi}_-(s, x')\hat{\phi}_+(s, x) + \theta(x' - x)\hat{\phi}_-(s, x)\hat{\phi}_+(s, x')\Big],$$

or, more explicitly

$$[\partial_x^2 - s^2 - V(x)]\hat{G}(s, x, x') = \frac{[\partial_x^2]}{W(s)}\Big[\theta(x - x')\hat{\phi}_-(s, x')\hat{\phi}_+(s, x) + \theta(x' - x)\hat{\phi}_-(s, x)\hat{\phi}_+(s, x')\Big] + \frac{[-s^2 - V(x)]}{W(s)}\Big[\theta(x - x')\hat{\phi}_-(s, x')\hat{\phi}_+(s, x) + \theta(x' - x)\hat{\phi}_-(s, x)\hat{\phi}_+(s, x')\Big].$$

First, we will focus only in the derivative part, the reason will be clear latter. So

$$[\partial_x^2]\hat{G}(s,x,x') = \frac{[\partial_x^2]}{W(s)}\Big[\theta(x-x')\hat{\phi}_-(s,x')\hat{\phi}_+(s,x) + \theta(x'-x)\hat{\phi}_-(s,x)\hat{\phi}_+(s,x')\Big],$$

applying the operator, we will have

$$[\partial_x^2]\hat{G}(s,x,x') = \frac{\hat{\phi}_-(s,x')}{W(s)}\Big[\partial_x^2\left(\theta(x-x')\hat{\phi}_+(s,x)\right)\Big] + \frac{\hat{\phi}_+(s,x')}{W(s)}\Big[\partial_x^2\left(\theta(x'-x)\hat{\phi}_-(s,x)\right)\Big].$$

Here, $\hat{\phi}_-(s,x')$ and $W(s)$ don't depended of x, so they don't get affected by the derivative. To continue the procedure, it is important to define a couple of equations that will be necessary to this demonstration. For a differentiable function $f(x)$,

$$\begin{aligned}\partial_x^2\left[\theta(x-x')f(x)\right] &= \partial_x\left[\delta(x-x')f(x) + \theta(x-x')f'(x)\right]\\ &= \delta'(x-x')f(x) + 2\delta(x-x')f'(x) + \theta(x-x')f''(x)\\ &= \delta(x-x')f'(x) + \theta(x-x')f''(x),\end{aligned}$$

where $\partial_x\theta(x-x') = \delta(x-x')$ and using one of the defining properties of the Dirac delta, $\delta'(x-x')f(x) = -\delta(x-x')f'(x)$. Similarly for the $\theta(x'-x)$ and knowing that $\theta(x'-x) = 1-\theta(x-x')$,

$$\begin{aligned}\partial_x^2\left[\theta(x'-x)f(x)\right] &= \partial_x\left[-\delta(x-x')f(x) + \theta(x'-x)f'(x)\right]\\ &= -\delta'(x-x')f(x) - 2\delta(x-x')f'(x) + \theta(x'-x)f''(x)\\ &= -\delta(x-x')f'(x) + \theta(x'-x)f''(x),\end{aligned}$$

So, returning to the equation of the operator on Green's function, we have

$$\begin{aligned}[\partial_x^2]\hat{G}(s,x,x') = &\frac{\hat{\phi}_-(s,x')}{W(s)}\Big[\delta(x-x')\partial_x\hat{\phi}_+(s,x) + \theta(x-x')\partial_x^2\hat{\phi}_+(s,x)\Big]\\ &+ \frac{\hat{\phi}_+(s,x')}{W(s)}\Big[-\delta(x-x')\partial_x\hat{\phi}_-(s,x) + \theta(x'-x)\partial_x^2\hat{\phi}_-(s,x)\Big].\end{aligned}$$

Since we already know that $\partial_x^2\hat{\phi} = -[-s^2 - V(x)]\hat{\phi}$, and including the rest of the operator applied on $\hat{G}(s,x,x')$,

$$
\begin{aligned}
[\partial_x^2 - s^2 - V(x)]\hat{G}(s,x,x') = &\frac{\hat{\phi}_-(s,x')}{W(s)}\Big[\delta(x-x')\partial_x\hat{\phi}_+(s,x) - \theta(x-x')[-s^2-V(x)]\hat{\phi}_+(s,x)\Big] \\
&+ \frac{\hat{\phi}_+(s,x')}{W(s)}\Big[-\delta(x-x')\partial_x\hat{\phi}_-(s,x) - \theta(x'-x)[-s^2-V(x)]\hat{\phi}_-(s,x)\Big] \\
&+ \frac{[-s^2-V(x)]}{W(s)}\Big[\theta(x-x')\hat{\phi}_-(s,x')\hat{\phi}_+(s,x) + \theta(x'-x)\hat{\phi}_-(s,x)\hat{\phi}_+(s,x')\Big].
\end{aligned}
$$

It is clear that the terms that are multiplied by $[-s^2-V(x)]$ cancel with each other. Which left us with

$$
\begin{aligned}
[\partial_x^2 - s^2 - V(x)]\hat{G}(s,x,x') &= \frac{1}{W(s)}\Big[\delta(x-x')\hat{\phi}_-(s,x')\partial_x\hat{\phi}_+(s,x) - \delta(x-x')\hat{\phi}_+(s,x')\partial_x\hat{\phi}_-(s,x)\Big] \\
&= \frac{\delta(x-x')}{W(s)}\Big[\hat{\phi}_-(s,x')\partial_x\hat{\phi}_+(s,x) - \hat{\phi}_+(s,x')\partial_x\hat{\phi}_-(s,x)\Big],
\end{aligned}
$$

the term inside the square brackets is clearly the definition of $W(s)$, which finally leads to

$$
[\partial_x^2 - s^2 - V(x)]\hat{G}(s,x,x') = \delta(x-x').
$$

APPENDIX E – Trajectory equations in the Kerr spacetime

The equations of motion for test particles in the Kerr spacetime are governed by four constants of motion. The first is the invariant mass $m$of the test particle, defined by the relation $-m^2 = p^\alpha g_{\alpha\beta} p^\beta$, where p^α is the four-momentum of the particle. Furthermore, there are two constants of motion given by the time translation and rotation symmetries of Kerr spacetime, the energy $E = -p_t$, and the component of the orbital angular momentum parallel to the spin of the black hole $L_z = p_\varphi$. Using Hamilton–Jacobi theory, (Carter, 1968) showed that there exists a fourth constant of motion, Q, now referred to as the Carter constant. It is related to the total angular momentum of the particle and is given by

$$Q = p_\theta^2 + \cos^2\theta \left(a^2(m^2 - E^2) + \left(\frac{L_z}{\sin\theta} \right)^2 \right)$$

Since there are four (independent) constants of motion for degrees of freedom, the equations of motion for a test particle in Kerr spacetime are integrable. Using these constants of motion, the trajectory equations for a test particle can be written (using natural units of $G = M = c = 1$),

$$\begin{aligned}
\Sigma \frac{dt}{d\lambda} &= -a(aE\sin^2\theta - L_z) + \frac{r^2 + a^2}{\Delta} P(r) \\
\Sigma \frac{dr}{d\lambda} &= \pm\sqrt{R(r)} \\
\Sigma \frac{d\theta}{d\lambda} &= \pm\sqrt{\Theta(\theta)} \\
\Sigma \frac{d\varphi}{d\lambda} &= -\left(aE - \frac{L_z}{\sin^2\theta} \right) + \frac{a}{\Delta} P(r)
\end{aligned}$$

with

$$\begin{aligned}
\Theta(\theta) &= Q - \cos^2\theta \left(a^2(m^2 - E^2) + \frac{L_z^2}{\sin^2\theta} \right) \\
P(r) &= E(r^2 + a^2) - aL_z \\
R(r) &= P(r)^2 - \Delta(m^2 r^2 + (L_z - aE)^2 + q)
\end{aligned}$$

where λ is an affine parameter such that $dx^\alpha/d\lambda = p^\alpha$. In particular, when $m > 0$ the affine parameter λ, is related to the proper time τ through $\lambda = \tau/m$.

Because of the frame-dragging-effect, a zero-angular-momentum observer (ZAMO) is co-rotating with the angular velocity Ω which is defined with respect to the bookkeeper's coordinate time t. The local velocity v of the test-particle is measured relative to a probe co-rotating with Ω. The gravitational time-dilation between a ZAMO at fixed r and a stationary observer far away from the mass is

$$\frac{t}{\tau} = \sqrt{\frac{(a^2+r^2)^2 - a^2\Delta\sin^2\theta}{\Delta\Sigma}}$$

In Cartesian Kerr–Schild coordinates, the equations for a photon are

$$\begin{aligned}
\ddot{x} + i\ddot{y} &= 4iMa\frac{r}{\Sigma^2}W\left[\dot{x} + i\dot{y} - \frac{x+iy}{r}\dot{r}\right] - M(x+iy)\left(\frac{4r^2}{\Sigma} - 1\right)\frac{C - a^2W^2}{r\Sigma^2} \\
\ddot{z} &= -Mz\left(\frac{4r^2}{\Sigma} - 1\right)\frac{C}{r\Sigma^2}
\end{aligned}$$

where C is analogous to Carter's constant and W is a useful quantity

$$\begin{aligned}
C &= p_\theta^2\left(aE - \frac{L_z}{\sin^2\theta}\right)^2 \\
W &= \dot{t} - a\sin^2\theta\dot{\varphi}
\end{aligned}$$

If we set $a = 0$, the Schwarzschild geodesics are restored. Here,

$$\begin{aligned}
a &= \frac{J}{Mc}, \\
\Sigma &= r^2 + a^2\cos^2\theta, \\
\Delta &= r^2 - R_S r + a^2.
\end{aligned}$$

where J represents the spin angular momentum.